MECHANISTIC DISSECTION OF PHOSPHORYLATION-DEPENDENT REGULATION OF ETS-1 DNA BINDING

by

Charles Ashley Meeker

A dissertation submitted to the faculty of
The University of Utah
in partial fulfillment of the requirements for the degree of

Doctor of Philosophy

Department of Oncological Sciences

The University of Utah

May 2011

The University of Utah Graduate School

STATEMENT OF DISSERTATION APPROVAL

The dissertation of **Charles Ashley Meeker**

has been approved by the following supervisory committee members:

Barbara J. Graves	, Chair	**8/2/2010** Date Approved
Donald E. Ayer	, Member	**8/2/2010** Date Approved
Katharine S. Ullman	, Member	**8/2/2010** Date Approved
Matthew K. Topham	, Member	**8/2/2010** Date Approved
Michael S. Kay	, Member	**8/2/2010** Date Approved

and by **Barbara J. Graves**, Chair of the Department of **Oncological Sciences**

and by Charles A. Wight, Dean of The Graduate School.

ABSTRACT

Intrinsically unstructured protein (IUP) regions and conformational disorder are increasingly recognized for their prevalence in the eukaryotic genome and functional importance in disease-related proteins and biological regulatory processes. The dynamic molecular motions inherent in these regions, as well as those found in structured protein regions, are proving to be important targets of regulation. The autoregulation of DNA binding in the transcription factor Ets-1 provides an example of how a flexible, unstructured region can modulate the activity of a structured, regulatable unit by affecting the dynamic character of the protein.

This thesis explores the mechanism of phosphorylation-dependent regulation of Ets-1 DNA binding. The serine-rich region (SRR) of Ets-1 is shown to be predominantly unstructured before and after Ca^{2+}-dependent phosphorylation. Phosphorylation of the SRR is shown to stabilize the regulatable unit, which is composed of domains responsible for DNA binding and autoinhibition, and to reduce the DNA-binding affinity of an Ets-1 fragment that is amenable to spectroscopic analysis. NMR-based experiments further determine that phosphorylation partially dampens the fast timescale mobility of the SRR and enhances its localization to the regulatable unit. Aromatic residues adjacent to the phosphor-acceptor sites are found to be required for the reported 100-fold decrease in binding affinity and inhibitory structural alterations. The juxtaposition of phospho-acceptor site and aromatic residue are shown to form a functional unit within the SRR which can be artificially amplified to further increase aromatic residue-dependent,

phosphorylation-induced inhibition of Ets-1. We conclude the discovery of a new mechanism whereby phosphorylation of an IUP region enhances a transient hydrophobic interaction, modulating the activity of a structured unit without adopting a structured conformation.

TABLE OF CONTENTS

LIST OF FIGURES

ACKNOWLEDGEMENTS

I would like to thank my advisor, Dr. Barbara Graves, for her commitment to my training as a scientist. Words can not fully express the appreciation I have for her dedication to her students and research lab. I would like to express my gratitude for members of the Graves' lab, both past and present, for support in times success and disappointment. I would like to acknowledge Dr. Lawrence McIntosh and members of his lab involved in this thesis. To members of my thesis committee; Don Ayer, Katie Ullman, Matt Topham, and Michael Kay - your attention to detail and sincere interest in this project provided an enjoyable, yet challenging forum for scientific training. I am truly indebted to those involved behind the scientific scenes; Barb Saffel, Tami Brunson, Dee Dalponte, Jessica Hampton, and Sarah Weiland - Thank you for everything you do and are.

To my parents, Bill and Marilyn Meeker, I express my love and appreciation for a lifetime of faith and support. To my family, I express gratitude and love for all the encouragement and help you have been over the years. To my loving children Cayden, Emma, and Grace, who bring the sunshine back into my life when discouragement has turned things dark, I love you. And to Amberly, my soul mate and best friend, my life would be worth nothing without you. I love, cherish, and appreciate you with all my heart.

CHAPTER 1

INTRODUCTION

The true nature of proteins: structured vs. disordered / rigid vs. dynamic

To use a picture, I would like to say that enzyme and glucoside have to fit to each other like a lock and key in order to exert a chemical effect on each other. -- Emil Fischer, 1852-1919 (Lemieux and Spohr, 1994).

Over a century ago, Emil Fischer used the analogy of a "lock and key" to explain the amazing specificity found among different types of similar enzymes, all of which participate in hydrolysis of glucoside multimers. Whereas one enzyme could hydrolyze α- but not β-glycosidic bonds, another could hydrolyze β- but not α-glycosidic bonds (Lemieux and Spohr, 1994). In his analogy, the enzyme is a lock, whose active site is comparable to a key-hole. The enzyme's substrate, of course, is the key. Just like the unique shape and size of a key allows it to fit the key-hole of its lock, Fischer hypothesized that only a substrate of the correct shape and size can fit into the active site of a particular enzyme.

Studies like those performed by Emil Fischer have led to the widely-accepted belief that the three-dimensional (3-D) structure of a given protein is the major determinant of that protein's function. The understanding that amino acid sequence determines the tertiary fold of a protein gave birth to the widely accepted sequence-structure-function paradigm in molecular and cellular biochemistry (Anfinsen and Redfield, 1956). Further support came in 1965 when the 3-D structure of lysozyme, which had co-crystallized with its bound inhibitor, showed that catalysis was almost certainly facilitated by the precise locations of amino acids within its active site (Blake et al., 1965). Since that time, 66,212 structures of proteins and protein complexes, solved by X-ray crystallography and nuclear magnetic resonance (NMR) spectroscopy, have been deposited into the Protein Data Bank (PDB; www.pdb.org). Though not intended,

the beautiful molecular graphics of these molecules has reinforced the static, rigid view of functional protein structure.

Functional importance of being intrinsically unstructured / disordered

Although the existence of a disordered element to proteins has long been acknowledged, a recent paradigm shift has arisen with the recognition that over 50% of the eukaryotic proteome can be classified as intrinsically unstructured or disordered (Dunker et al., 2000). Thus, advances in experimental characterization and computational prediction of unstructured proteins and protein regions have severely challenged the classic dogma of structure-function (Dunker et al., 2008). To qualify as intrinsically unstructured, a protein needs to contain at least one region that is >30 residues in length which displays an unstructured, disordered profile. According to this definition, a striking 25-30% of eukaryotic proteins contain more residues in a disordered conformation than in one of order (Oldfield et al., 2005). Interestingly, these intrinsically unstructured proteins (IUPs) are noticeably overrepresented in disease-related proteins. Close to 75% of known cancer-related proteins, 70% of signaling proteins, and an astonishing 94% of transcription factors are predicted to have one or more regions of intrinsic disorder (Iakoucheva et al., 2002; Liu et al., 2006; Midic et al., 2009). Regions of intrinsic disorder are often characterized by their low sequence complexity, low content of bulky amino acids (Phe, Trp, Tyr, Met, Val, Leu, and Ile), and high occurrence of certain polar and charged amino acids (Ser, Pro, Lys, Gln, Glu, and sometimes Gly and Ala) (Obradovic et al., 2003; Romero et al., 2001). For this reason, IUP regions remain unstructured in isolation, as they are unable to sufficiently bury the hydrophobic core required to fold spontaneously (Dyson and Wright, 2005).

The role of conformational disorder is widely recognized for its importance at sites of posttranslational modification and ligand binding, and in modular proteins, as a flexible linker sequences between two structural domains (Iakoucheva et al., 2004; Uversky and Dunker, 2010). An excellent example is the flexible, unstructured N-terminal tail of histones which are bound and modified by enzymes which add or remove methyl, acetyl, or phospho-marks, allowing for the recruitment of chromatin remodelers and other DNA-associated proteins (Segal and Widom, 2009). It has also been noted that upon ligand binding or other molecular event, IUP sequences often go through an induced transition from a disordered conformation to one of structured order (Dyson and Wright, 2005). The intrinsically disordered KID domain of the transcription factor CREB, for instance, is folded into two α-helices following phosphorylated and subsequent interaction with the KIX domain of the co-activator p300 (Sugase et al., 2007).

Inherently functional IUP regions, however, have only recently been recognized and reported as having a significant role in biology (Wright and Dyson, 1999). These regions have a direct role in regulatory processes while remaining in an unstructured state; in other words, they require a disordered conformation to perform their function (Mittag et al., 2010). Exactly how these IUPs perform their biological function remains an unsolved problem.

NMR techniques for detecting protein dynamics and conformational mobility

In reality, IUP regions are not the only part of proteins with dynamic character. It is now recognized that structured and unstructured regions alike undergo a wide range of motions in terms of both time and distance scales (Boehr et al., 2006). A variety of

spectroscopic experiments now make it possible to study dynamic motions in proteins over time scales between 10^{-12} and 10^{5} seconds and over distance scales of 0.1 to 2000 Å (Figure 1.1) (Boehr et al., 2006; Liang et al., 2006; Stein et al., 2009). Molecular motion within any of these time frames, which span from bond vibrations to global unfolding transitions, may be functionally significant and directly related to enzymatic catalysis, ligand binding, and/or other forms of molecular recognition (Boehr et al., 2006; Henzler-Wildman et al., 2007).

Slow timescale motions

Slow molecular motions, such as the transient unfolding of one α-helix in the B-domain of protein A, and the amino and carboxyl helices of cytochrome c, occur on a msec-to-sec timescale and are readily observed by hydrogen exchange (HX) experiments with detection by NMR spectroscopy or mass spectrometry (Figure 1.1) (Bai et al., 1997; Bai et al., 1994; Englander and Mayne, 1992). Backbone amides in an unfolded peptide region rapidly exchange hydrogen (protons or deuterons, when applicable) with aqueous solvent (Englander, 1998). Amide protons which are protected by the hydrogen bonding associated with α-helix formation, however, exchange only after local or global fluctuations that disrupt this bonding (Englander, 2000). Amide HX measurement can, therefore, both identify labile regions of structure as they exchange hydrogen with solvent under native and mild-denaturing conditions, indicating the transient unfolding of structural elements, and provide a measure of the rates and free energy changes associated with these conformational fluctuations (Bai et al., 1995; Englander, 2000). Structural reinforcement brought about by a binding event or posttranslational

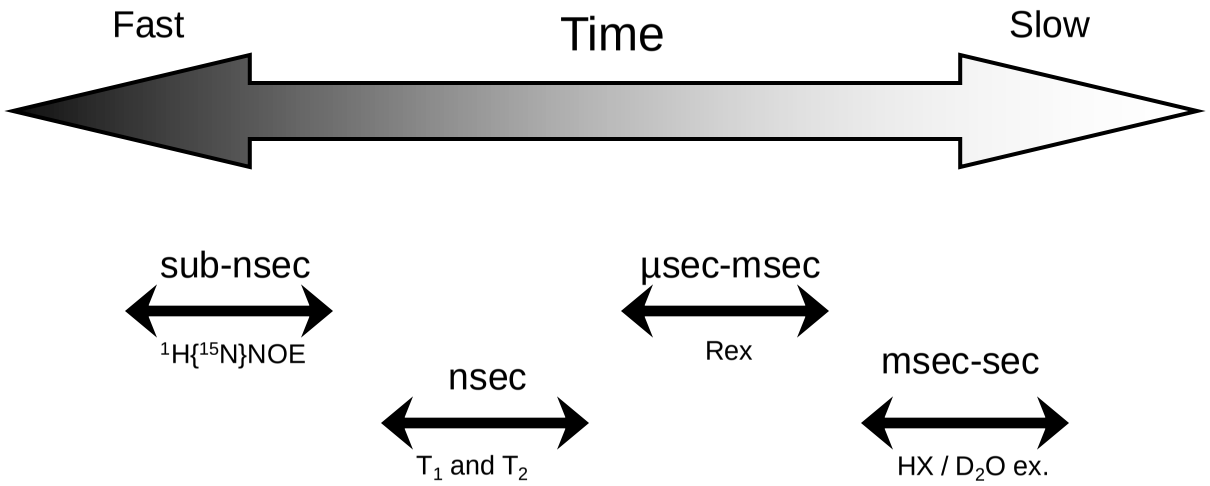

Figure 1.1 Timescales of NMR dynamics. NMR can be useful in measuring the dynamic character of proteins over a wide range of timeframe windows. Fast protein motions in the range from psec to msec are measured by relaxation experiments ($^{1}H\{^{15}N\}$NOE, T_1, T_2, and R_{ex}). Slower molecular motions in the msec to many seconds range can be detected by hydrogen exchange (HX and D_2O exchange).

modification can also be observed as an increase in protection against HX (Amero et al., 2009; Lee et al., 2008).

Intermediate timescale motions

Intermediate amplitude motions, which generally occur on the μsec-to-msec timescale, such as the conformational rearrangement of the SH3 domain of the Drosophila protein drk or the allosteric transitions of aspartate transcarbamoylase, are frequently detected by heteronuclear spin relaxation techniques (Figure 1.1) (Mulder et al., 2001; Tollinger et al., 2001; Velyvis et al., 2007). Exposure to the nuclear spin of neighboring molecules causes conformationally-dynamic nuclei to encounter different chemical and magnetic environments, producing changes in the rate of spin relaxation (Rex). These changes can be quantified using a suite of heteronuclear relaxation or relaxation dispersion experiments (Kay, 1998; Palmer, 2001). Arguably, these motions are most relevant to biological processes, including ligand binding and enzymatic catalysis.

Fast timescale motions

Dynamic peptide backbone mobility on the nsec and sub-nsec timescales, like those observed in loop regions of staphylococcal nuclease, can also be detected by NMR relaxation measurements (Figure 1.1) (Kay et al., 1989; Palmer, 2001; Palmer et al., 2001). These motions are commonly observed for exposed, flexible loop regions of proteins, and have recently gained attention for their prevalence in intrinsically disordered polypeptide sequences. Common techniques for monitoring these motions include spin relaxation experiments which measure spin-spin relaxation (T_2) or spin-lattice relaxation (T_1), or nuclear Overhauser effect ($^1H[^{15}N]NOE$) (Kay et al., 1989).

In instances where dynamic interactions are too transient to be observed by traditional NMR methods, the use of paramagnetic relaxation enhancement (PRE) measurements has been utilized to determine the location and behavior of flexible, unstructured protein regions (Lee et al., 2008). The presence of a paramagnetic metal ion bound with high affinity, or an organic molecule attached covalently, essentially bleaches out the NMR signal of any nuclei that is within its functional proximity. The use of an Amino Terminal Cu^{2+} /Ni^{2+} (ATCUN) binding motif in PRE spectroscopy was pioneered by Dr. Lewis E. Kay as a means of extending the distance restraint limit of ~5 Å for ^{1}H-^{1}H NOEs, to a range of ~10-20 Å (Donaldson et al., 2001). Site-directed spin labels (SDSL), originally developed by Dr. Harden M. McConnell and utilized for PRE in the lab of Dr. Wayne L. Hubbell, has extended the measurable distance of PRE up to ~ 80 Å, making it a powerful technique for studying more distant, transient interactions (Altenbach et al., 1989; Hubbell and McConnell, 1968; Hubbell et al., 1996; Jeschke, 2002).

Ets-1 and the ETS family of transcription factors

This thesis focuses on the ETS protein, Ets-1, and its autoinhibition of DNA binding as a model to study the functional significance of protein dynamics within, and between, structured and unstructured regions. Over the past two decades, the ETS family of regulatory transcription factors has emerged as a model for sequence-specific DNA binding in the field of gene regulation. Identified by a highly conserved ETS DNA binding domain, family members bind a core GGAA/T consensus sequence via direct contact with the phosphate backbone in the major groove (Figure 1.2) (Nye et al., 1992; Wasylyk et al., 1993; Wei et al., 2010). Currently, 27 human members of the ets family

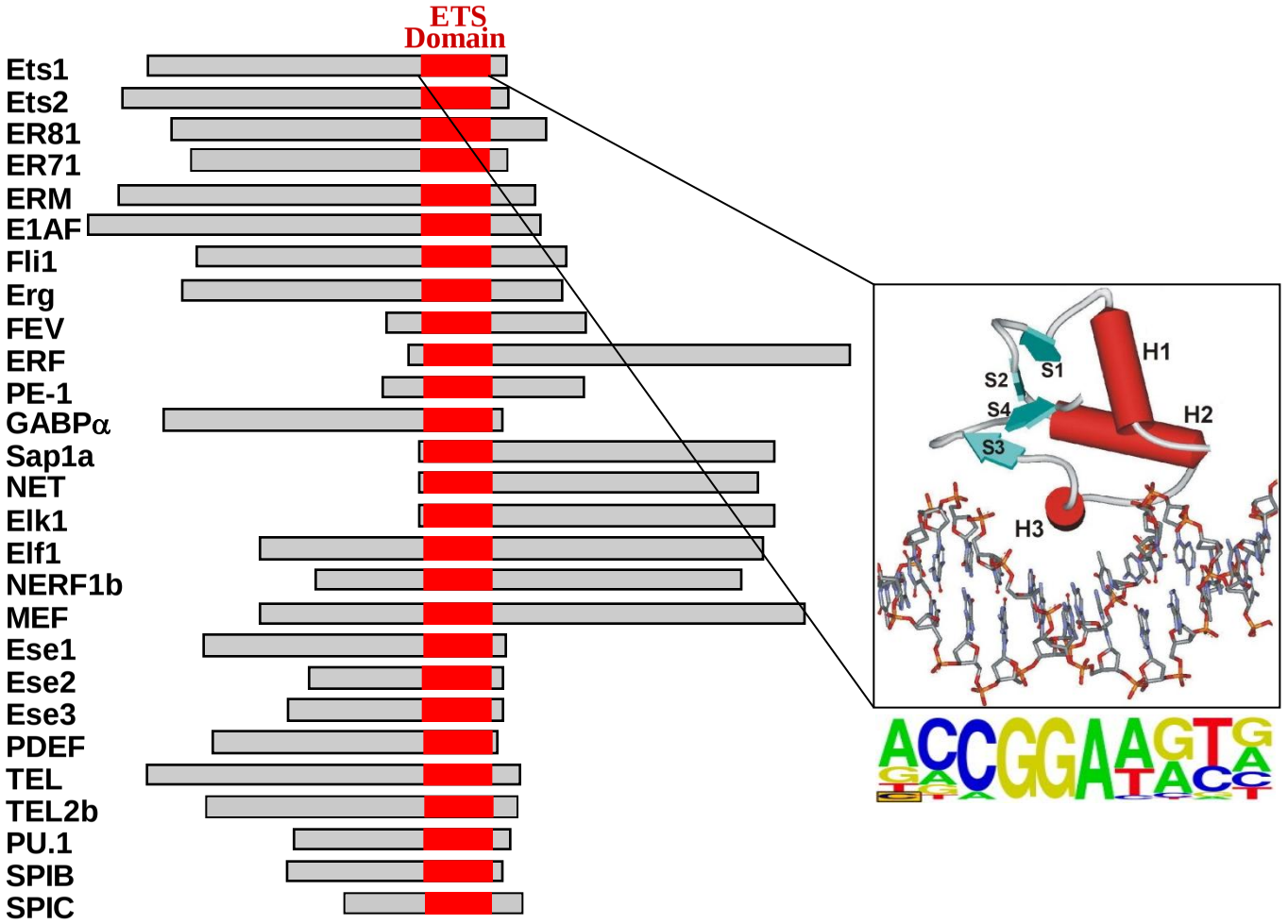

Figure 1.2 The ETS family of regulatory transcription factors. Each of the 27 human members of the ETS family contain a DNA binding ETS domain (red boxes) which binds specifically to DNA sequences containing a core GGA with preference for A or T at the fourth position. Flanking sequences are also highly conserved according to in vitro selection studies (Wei et al., 2010). Also shown is the ETS domain portion of the X-ray crystal structure of Ets-1, which displays a winged-helix-turn-helix motif, bound to DNA (Garvie et al., 2002).

have been identified with ETS domain sequence conservation ranging from 38-97%. Outside the ETS domain, a wide range of sequence and structural differences, including the presence or absence of entire protein domains involved in binding partner recruitment and transcriptional activation, give variety to the family. The sequence specific ETS DNA binding domain, however, remains highly conserved. Once bound, these transcription factors have been shown to regulate a myriad of cellular processes in normal and cancerous human cells through regulation of transcriptional targets (Oikawa and Yamada, 2003). Ets factors are known to bind the promoters and regulate expression of genes as widely recognized as those encoding p53 and BRCA1/2, and as common as RPS26, a "housekeeping" ribosomal protein involved in cellular metabolism (Baker et al., 2003; Hollenhorst et al., 2007; Venanzoni et al., 1996). The presence of mutated ETS family members in human cancer and other diseases illustrates the medical importance of this gene family (Dittmer, 2003; Lincoln and Bove, 2005; Oikawa, 2004).

Ets-1 structural organization

Knowledge of the structural elements of the Ets-1 protein has been a contributing factor in understanding its biological function. Ets-1 is a 50 KDa, multi-domain protein shown to be expressed at high levels in the lung, spleen, and thymus (Hollenhorst et al., 2004) (Figure 1.3). In the C-terminal portion of the Ets-1 protein is the 85-amino acid DNA binding ETS domain; this region of the protein is necessary and sufficient for sequence-specific DNA binding. The ETS domain displays a winged-helix-turn-helix motif that must be structurally intact for DNA binding to occur (Figure 1.3) (Donaldson et al., 1996; Graves et al., 1996). Its N-terminal "Pointed" (PNT) domain, which is only conserved in 1/3 of the family, mediates protein-protein interactions. More especially, in

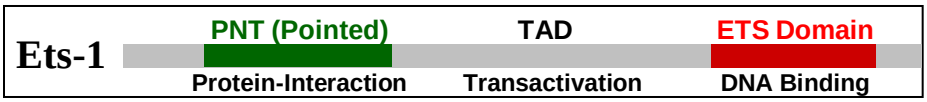

Figure 1.3 Schematic representation of Ets-1. Structured Pointed (PNT) domain (green) and ETS domain (red) are displayed. The transcriptional activation domain (TAD) lies between these two structured domains.

response to receptor tyrosine kinase signaling through the RAS/MAPK signaling pathway, ERK2-phosphorylation of specific threonine/serine residues adjacent to the PNT domain augments recruitment of the transcriptional co-activator CBP/p300 by Ets-1 (Foulds et al., 2004). Intriguingly, the PNT domain serves as both a docking site for ERK2 to enhance phosphorylation of these residues, as well as an interface for binding the TAZ1 domain of CBP/p300. Between these to structural domains is a poorly characterized transcriptional activation domain (TAD) that is thought to synergize with the PNT domain and play a major role in regulating transcriptional activation while acting as an unstructured linker (Gegonne et al., 1993; Yang et al., 1998).

Autoinhibition in Ets-1

Quantitative studies have determined that the DNA-binding activity of Ets-1 is inhibited (Figure 1.4) (Hagman and Grosschedl, 1992; Jonsen et al., 1996; Lim et al., 1992). In vitro electrophoretic mobility shift assay (EMSA) were used to determine the dissociation constant (K_D) of the full-length Ets-1 protein at $2x10^{-10}$ M (Jonsen et al., 1996). Studies attempting to isolate the minimal DNA-binding domain of Ets-1 concluded that deletion of either the N-terminal or C-terminal regions flanking the ETS domain resulted in a 10-fold increase in DNA-binding affinity ($K_D \approx 2x10^{-11}$ M) (Jonsen et al., 1996). The existence of activating mutants of this sort is a defining characteristic of autoinhibition, a regulatory phenomenon that has become both widely accepted and studied over the past 30 years (Cooper et al., 1986; Pufall and Graves, 2002).

Relief and reinforcement of autoinhibition as a regulatory strategy

Autoinhibition can be defined as the negative regulation of the activity associated with one region of a protein through an intramolecular interaction with a separate region

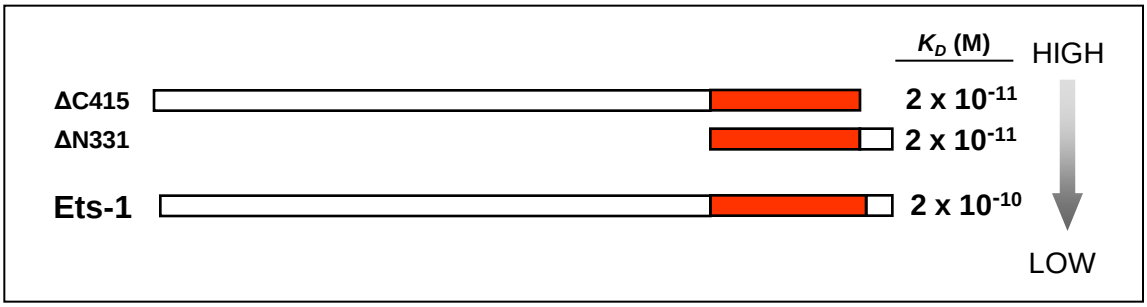

Figure 1.4 Autoinhibition of Ets-1 revealed through deletion mutagenesis and EMSA binding studies. DNA-binding affinities (expressed as equilibrium dissociation constants) for full length Ets-1 and three Ets-1 deletion fragments. Both ΔN331 and ΔC415, as individual truncation mutants, display a DNA binding affinity of approximately 2 x 10^{-11} M (Jonsen et al., 1996) indicating the presence of interacting inhibitory elements in both the N- and C-terminal regions flanking the ETS domain.

of the polypeptide. This intramolecular interaction may be a direct steric effect, like occluding the functional domain from interacting with a ligand, or allosteric in nature, like inducing a conformational change that renders the protein inactive. The repressive effects of an autoinhibitory domain may be imposed upon protein activities ranging from DNA binding and protein-protein interactions to transcriptional activation and enzymatic catalysis (reviewed in Pufall and Graves, 2002a).

Regardless of the nature of the interaction, a means of relieving the autoinhibition is usually also in place as a regulatory strategy. This allows cellular proteins to be held in an off (or attenuated) state until, in response to a specific signaling event, the inhibition is lifted and a higher level of protein activity is observed. A common means of relieving autoinhibition is through the intermolecular binding of a second molecule, which displaces the intramolecular interaction between autoinhibitory and functional domain (Courtneidge, 1985; Misura et al., 2000; Rohatgi et al., 2000). Other general strategies for relieving autoinhibition include proteolytic cleavage of the autoinhibitory domain and posttranslational modifications (Brown et al., 2000; Lin et al., 1999; Simons et al., 1998). On the other hand, some intermolecular binding events and posttranslational modification have been shown to reinforce autoinhibition through stabilizing the intramolecular interaction between the autoinhibitory and functional domains (Courtneidge, 1985; Misura et al., 2000). Thus we see that an autoinhibited protein, with the ability to have this inhibition relieved and/or reinforced, provides a mechanism for fine-tuning protein activity in the cellular environment in response to growth, developmental, or apoptotic signaling. Ets-1 is a prime example of a protein whose autoinhibition can be both reinforced and relieved by separate cellular events.

The autoinhibitory mechanism of Ets-1

Detailed study of Ets-1 deletion fragments, including structural analysis, has determined that the inhibitory sequences flanking the ETS domain of Ets-1 are helical in nature and that the globular fold of the protein allows the two domains to pack together, forming an autoinhibitory module located distal to the DNA-binding interface of the tertiary structure (Figure 1.5) (Lee et al., 2005; Petersen et al., 1995; Skalicky et al., 1996). In the DNA-bound state the protein displays an unfolded inhibitory helix HI-1 (Petersen et al., 1995). Consistent with these findings, structural disruption of the inhibitory module, either through deletion of an inhibitory domain or introduction of a point mutation that induces unfolding of HI-1, causes the DNA-binding affinity to increase 10-fold (Figure 1.4) (Cowley and Graves, 2000; Garvie et al., 2002; Jonsen et al., 1996; Petersen et al., 1995). Additional NMR-based experimentation over the last decade has developed an allosteric model of autoinhibition in Ets-1. In this model, the inhibitory module is intramolecularly connected to the DNA-binding domain through a network of amino acids located in the core of the protein (Figure 1.6) (Pufall et al., 2005). Activating and inhibitory changes to the inhibitory module are communication through the core, down to the DNA-binding interface. The core is comprised of ~25 residues, the majority of which are hydrophobic in nature and display a dynamic character on a μsec-to-msec timescale – meaning they are ordered into predominant secondary and tertiary structure that exhibits substantial internal molecular motions – which we propose is essential for regulating autoinhibition in Ets-1. Dampening of the internal motions of this dynamic core is associated with both a well-structured inhibitory module and a decrease in DNA-binding affinity, leading to an inactive conformation. Fragments of Ets-1 in

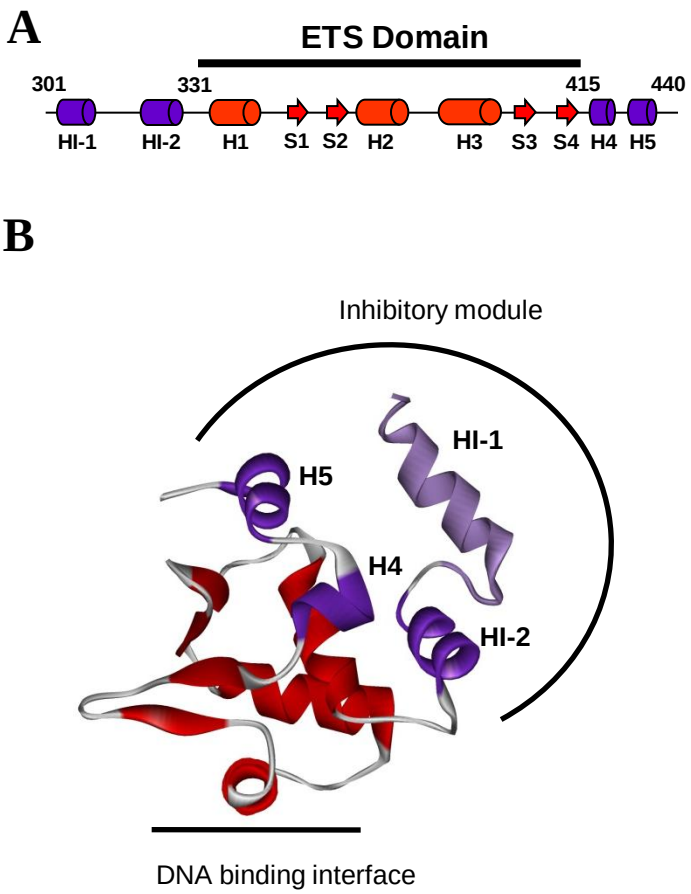

Figure 1.5 Helical inhibitory regions flanking the ETS domain form a module distal to the DNA binding interface. (A) Schematic representation of the secondary structural elements found in residues 301-440 of Ets-1 (α-helix, cylinder [H]; β-sheet, arrow [S]). (B) NMR structure (1R36.pdb) of the ETS domain and inhibitory module of Ets-1 (Pufall et al., 2005).

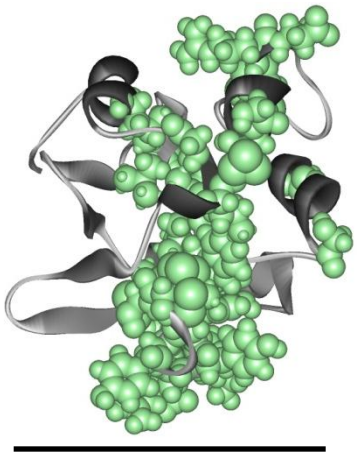

Figure 1.6 NMR structure highlighting the dynamic core of Ets-1. Both the amide ^{1}H-^{15}N chemical shifts and µsec-to-msec timescale dynamics for the ~25 residues (green) comprising the core change progressively from activated to autoinhibited, and from autoinhibited to phospho-inhibited (adapted from Pufall et al., 2005).

which critical inhibitory helices have been deleted, or mutated to cause helical unfolding are representative on the active state, displaying a higher degree of internal molecular motion and binding DNA with 10-fold higher affinity than the full-length, wild-type Ets-1 protein (Cowley and Graves, 2000; Jonsen et al., 1996; Pufall et al., 2005). Additionally, the NMR chemical shifts of dynamic core residues are progressively perturbed as the level of Ets-1 inhibition is increased. This co-linear pattern of inhibitory changes is a hallmark of a molecule in equilibrium between at least two conformational states, where the end points represent the fully active and fully inactive state, respectively (Volkman et al., 2001). Intermediate chemical shifts, rather than an alternative conformation for Ets-1, represent the average state of the population in equilibrium. Together, these findings support an allosteric model in which dynamic conformational sampling within the ETS domain provides Ets-1 with the ability to actively bind DNA with high affinity, while the less dynamic, inactive form of the protein displays reduced DNA-binding affinity. Indeed, recent NMR studies of the *lac* repressor protein have shown that scanning of DNA sequences in search of sequence-specific binding site requires a dynamic DNA-binding domain (Kalodimos et al., 2004).

Ets-1 autoinhibition is regulated by an intrinsically unstructured protein region and phosphorylation of that region

In addition to the inhibitory helices, an IUP region plays a role in Ets-1 autoinhibition. Adjacent to the N-terminal inhibitory domain is a highly flexible, serine-rich region (SRR) that contains no well-defined structure, as evidenced by an NMR secondary-structure propensity score, amide HX measurement, and missing electron density in that region of its X-ray crystal structure (Garvie et al., 2002; Skalicky et al., 1996). The unstructured SRR, however, stabilizes the autoinhibitory module, dampens

the dynamic nature of the core, and reduces DNA-binding affinity an additional 10-fold (Pufall et al., 2005). Phosphorylation of three specific serine residues in the SRR further depresses the internal motion of the molecule and decreases DNA-binding affinity another 50- to 100-fold, while retaining flexibility and peptide backbone conformational mobility (Figure 1.7) (Cowley and Graves, 2000; Pufall et al., 2005). Furthermore, changes in NMR chemical shifts for dynamic core residues shared by Ets-1 fragments containing and lacking an inhibitory SRR are further perturbed, in a co-linear pattern, upon phosphorylation of the SRR (Pufall et al., 2005).

Multi-site phosphorylation of the SRR has been documented in vivo in response to T- and B-cell receptor activation and calcium release and studied in vitro using the Ca^{2+}/Calmodulin-Dependent Protein Kinase II (CamKII) (Cowley and Graves, 2000; Fisher et al., 1991; Pognonec et al., 1988; Pognonec et al., 1989; Pufall et al., 2005). The phosphorylation-induced decrease in DNA-binding affinity leads to a decrease in promoter occupancy in vivo (data not shown), as well as reduced expression of granulocyte macrophage colony stimulating factor (GM-CSF) and stromelysin-1 (MMP-3) (Baillat et al., 2002; Liu and Grundstrom, 2002). Mutation of these serine residues is sufficient to eliminate phosphorylation-induced reinforcement of autoinhibition in vitro and reduce Calcium ionophore-induced repression of reporter activity in vivo (Cowley and Graves, 2000; Liu and Grundstrom, 2002; Pufall et al., 2005). Often, multi-site phosphorylation-induced changes in protein activity are seen as a binary "off/on" switch, in which a threshold is achieved after the addition of a critical number of modifications. Such is the case with nuclear factor of activated T cells (NFAT1) and Sic1 (Okamura et al., 2000; Orlicky et al., 2003; Salazar and Hofer, 2003). Ets-1, however, exhibits

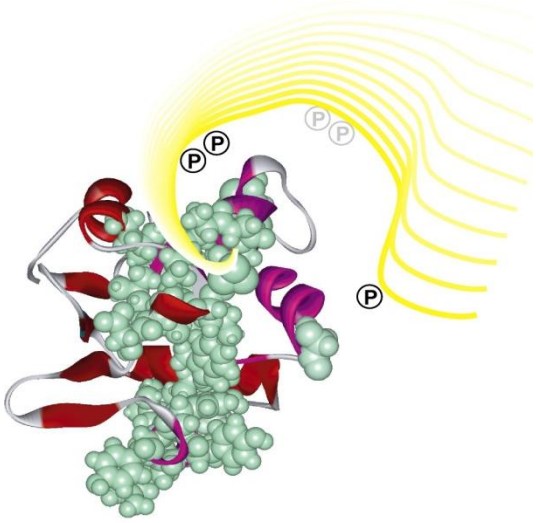

Figure 1.7 Phosphorylated SRR remains dynamic, without secondary structure or a fixed position, while functionally regulating Ets-1 autoinhibition. Phosphorylation of the unstructured SRR (yellow) causes a dampening of the dynamic core of Ets-1 and a 50- to 100-fold decrease in DNA binding affinity (Cowley and Graves, 2000; Pufall et al., 2005).

variable control of DNA binding as progressively increasing levels of phosphorylation progressively reinforce autoinhibition (Pufall et al., 2005).

Ets-1 autoinhibition is relieved through cooperative protein partner binding

Previous studies found of Ets-1 can be counteracted through synergistic DNA binding with the partner protein core-binding factor alpha2 (CBFα2; also known as RUNX1, AML1 or PEBP2) (Figure 1.8) (Goetz et al., 2000; Wotton et al., 1994). Not only does cooperative DNA binding have an activating effect similar in magnitude to the level of repression conferred by autoinhibition, but mutant forms of Ets-1 which are deficient in autoinhibition do not show cooperative DNA binding with RUNX1 (Goetz et al., 2000). These initial studies were performed using either the region of the Mo-MLV enhancer with binding sites for both Ets-1 and RUNX1, or the artificial composite site, SC1/core, which contains the high-affinity Ets-1 binding site, SC1, and the RUNX site from the Mo-MLV enhancer, spaced optimally for co-occupancy. Recent studies performed in the Graves lab using chromatin immunoprecipitation coupled with genome-wide microarray analysis have identified in vivo binding sites for Ets-1 in the Jurkat human T-cell line (Hollenhorst et al., 2007). Binding sites displaying strong ETS consensus binding sequences were found to be redundantly occupied by Ets-1 as well as Elf1 and/or GABPα, two mammalian members of the ets family. However, sites found to be occupied more specifically by only one of the three ets factors displayed weaker ETS binding sites (i.e., ETS binding sequences that vary from the consensus) coupled with a binding site for a cooperative protein partner. For example, the MDSO25 and BTRC promoters both contain a weak ETS binding site and a core RUNX site separated by a single amino acid. These promoters are bound specifically by Ets-1, and not the other

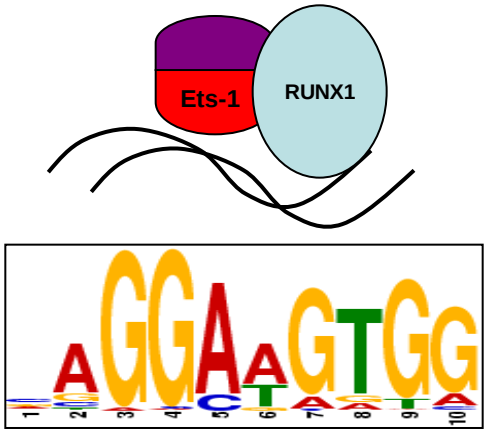

Figure 1.8 Cooperative binding with RUNX1 relieves autoinhibition in Ets-1. DNA-binding affinity of Ets-1, bound cooperatively with RUNX1, is similar to that of an uninhibited fragment (or point mutant) of Ets-1 alone (Goetz et al., 2000). In vivo consensus site from Ets-1 and RUNX1 ChIP-Seq (Hollenhorst et al., 2009).

two ets proteins, in vivo, and also display dual occupancy with RUNX1 (Hollenhorst et al., 2009; Hollenhorst et al., 2007).

Holes in the story: what we do not know about Ets-1 autoinhibition

The biochemical and structural effects of the unstructured SRR on Ets-1 autoinhibition indicates a possibly transient intramolecular interaction with the remainder of the protein. The increased effects observed upon phosphorylation of the SRR may be an indication of an enhanced interaction. However, as I began my thesis work, a number of unanswered questions remained about the functional significance and mechanism of the SRR and its place in the allosteric model. Where is the interface for the proposed interaction between the unstructured SRR and structured regulatable unit? What is the chemical nature of this transient interaction? How does phosphate addition cause the observed inhibitory effects?

Summary

Studies of Ets-1 presented in this thesis report provide insight and answers to questions about the structural and biochemical basis for the autoinhibitory effects of the SRR on Ets-1 DNA-binding affinity. Chapter 2 reports the direct comparison of the autoinhibitory phenomenon with and without SRR phosphorylation of a single Ets-1 species. It details structural changes to the SRR, inhibitory helices, and ETS domain observed upon SRR phosphorylation. It also reveals a previously undetectable interaction interface between the unstructured SRR and structured regulatable unit by means of a recently developed NMR technique. Chapter 3 investigates the chemical forces required for phosphorylation-induced changes to Ets-1 binding affinity and protein structure. We discovered a novel role for aromatic residues in association with

phosphorylation of the SRR and thus extended the mechanistic model of Ets-1 autoinhibition, significantly. The complete thesis not only advances our understanding of autoinhibition in Ets-1, but also gives a great new example of how an IUP region can perform a regulatory function by interacting transiently with a broad interface, while retaining a disordered conformation.

References

Altenbach C, Flitsch SL, Khorana HG, Hubbell WL. 1989. Structural studies on transmembrane proteins. 2. Spin labeling of bacteriorhodopsin mutants at unique cysteines. Biochemistry 28(19):7806-7812.

Amero CD, Byerly DW, McElroy CA, Simmons A, Foster MP. 2009. Ligand-induced changes in the structure and dynamics of Escherichia coli peptide deformylase. Biochemistry 48(32):7595-7607.

Anfinsen CB, Redfield RR. 1956. Protein structure in relation to function and biosynthesis. Advances in protein chemistry 11:1-100.

Bai Y, Karimi A, Dyson HJ, Wright PE. 1997. Absence of a stable intermediate on the folding pathway of protein A. Protein Sci 6(7):1449-1457.

Bai Y, Milne JS, Mayne L, Englander SW. 1994. Protein stability parameters measured by hydrogen exchange. Proteins 20(1):4-14.

Bai Y, Sosnick TR, Mayne L, Englander SW. 1995. Protein folding intermediates: native-state hydrogen exchange. Science (New York, NY 269(5221):192-197.

Baillat D, Begue A, Stehelin D, Aumercier M. 2002. ETS-1 transcription factor binds cooperatively to the palindromic head to head ETS-binding sites of the stromelysin-1 promoter by counteracting autoinhibition. The Journal of biological chemistry 277(33):29386-29398.

Baker KM, Wei G, Schaffner AE, Ostrowski MC. 2003. Ets-2 and components of mammalian SWI/SNF form a repressor complex that negatively regulates the BRCA1 promoter. J Biol Chem 278(20):17876-17884.

Blake CC, Koenig DF, Mair GA, North AC, Phillips DC, Sarma VR. 1965. Structure of hen egg-white lysozyme. A three-dimensional Fourier synthesis at 2 Angstrom resolution. Nature 206(986):757-761.

Boehr DD, Dyson HJ, Wright PE. 2006. An NMR perspective on enzyme dynamics. Chemical reviews 106(8):3055-3079.

Brown MS, Ye J, Rawson RB, Goldstein JL. 2000. Regulated intramembrane proteolysis: a control mechanism conserved from bacteria to humans. Cell 100(4):391-398.

Cooper JA, Gould KL, Cartwright CA, Hunter T. 1986. Tyr527 is phosphorylated in pp60c-src: implications for regulation. Science (New York, NY 231(4744):1431-1434.

Courtneidge SA. 1985. Activation of the pp60c-src kinase by middle T antigen binding or by dephosphorylation. The EMBO journal 4(6):1471-1477.

Cowley DO, Graves BJ. 2000. Phosphorylation represses Ets-1 DNA binding by reinforcing autoinhibition. Genes Dev 14(3):366-376.

Dittmer J. 2003. The biology of the Ets1 proto-oncogene. Mol Cancer 2(1):29.

Donaldson LW, Petersen JM, Graves BJ, McIntosh LP. 1996. Solution structure of the ETS domain from murine Ets-1: a winged helix-turn-helix DNA binding motif. EMBO J 15:125-134.

Donaldson LW, Skrynnikov NR, Choy WY, Muhandiram DR, Sarkar B, Forman-Kay JD, Kay LE. 2001. Structural characterization of proteins with an attached ATCUN motif by paramagnetic relaxation enhancement NMR spectroscopy. Journal of the American Chemical Society 123(40):9843-9847.

Dunker AK, Obradovic Z, Romero P, Garner EC, Brown CJ. 2000. Intrinsic protein disorder in complete genomes. Genome informatics 11:161-171.

Dunker AK, Oldfield CJ, Meng J, Romero P, Yang JY, Chen JW, Vacic V, Obradovic Z, Uversky VN. 2008. The unfoldomics decade: an update on intrinsically disordered proteins. BMC genomics 9 Suppl 2:S1.

Dyson HJ, Wright PE. 2005. Intrinsically unstructured proteins and their functions. Nat Rev Mol Cell Biol 6(3):197-208.

Englander SW. 1998. Native-state HX. Trends in biochemical sciences 23(10):378; author reply 379-381.

Englander SW. 2000. Protein folding intermediates and pathways studied by hydrogen exchange. Annual review of biophysics and biomolecular structure 29:213-238.

Englander SW, Mayne L. 1992. Protein folding studied using hydrogen-exchange labeling and two-dimensional NMR. Annual review of biophysics and biomolecular structure 21:243-265.

Fisher CL, Ghysdael J, Cambier JC. 1991. Ligation of membrane Ig leads to calcium-mediated phosphorylation of the proto-oncogene product, Ets-1. J Immunology 146:1743-1749.

Foulds CE, Nelson ML, Blaszczak A, Graves BJ. 2004. MAPK phosphorylation activates Ets-1 and Ets-2 by CBP/p300 recruitment. Mol Cell Biol 24:10954-10964.

Garvie CW, Pufall MA, Graves BJ, Wolberger C. 2002. Structural analysis of the autoinhibition of Ets-1 and its role in protein partnerships. J Biol Chem 277(47):45529-45536.

Gegonne A, Bosselut R, Bailly R, Ghysdael J. 1993. Synergistic activation of the HTLV1 LTR Ets-responsive region by transcription factors Ets1 and Sp1. EMBO J 12:1169-1178.

Goetz TL, Gu TL, Speck NA, Graves BJ. 2000. Auto-inhibition of Ets-1 is counteracted by DNA binding cooperativity with core-binding factor alpha2. Mol Cell Biol 20(1):81-90.

Graves BJ, Gillespie ME, McIntosh LP. 1996. DNA binding by the ETS domain [letter]. Nature 384(6607):322.

Hagman J, Grosschedl R. 1992. An inhibitory carboxyl terminal domain in Ets-1 and Ets-2 mediates differential binding of ETS family factors to promoter sequences of the *mb-1* gene. Proc Natl Acad Sci USA 89:8889-8893.

Henzler-Wildman KA, Lei M, Thai V, Kerns SJ, Karplus M, Kern D. 2007. A hierarchy of timescales in protein dynamics is linked to enzyme catalysis. Nature 450(7171):913-916.

Hollenhorst PC, Chandler KJ, Poulsen RL, Johnson WE, Speck NA, Graves BJ. 2009. DNA specificity determinants associate with distinct transcription factor functions. PLoS Genetics 5(12):e1000778.

Hollenhorst PC, Jones DA, Graves BJ. 2004. Expression profiles frame the promoter specificity dilemma of the ETS family of transcription factors. Nucleic acids research 32(18):5693-5702.

Hollenhorst PC, Shah AA, Hopkins C, Graves BJ. 2007. Genome-wide analyses reveal properties of redundant and specific promoter occupancy within the ETS gene family. Genes Dev 21(15):1882-1894.

Hubbell WL, McConnell HM. 1968. Spin-label studies of the excitable membranes of nerve and muscle. Proceedings of the National Academy of Sciences of the United States of America 61(1):12-16.

Hubbell WL, McHaourab HS, Altenbach C, Lietzow MA. 1996. Watching proteins move using site-directed spin labeling. Structure 4(7):779-783.

Iakoucheva LM, Brown CJ, Lawson JD, Obradovic Z, Dunker AK. 2002. Intrinsic disorder in cell-signaling and cancer-associated proteins. Journal of molecular biology 323(3):573-584.

Iakoucheva LM, Radivojac P, Brown CJ, O'Connor TR, Sikes JG, Obradovic Z, Dunker AK. 2004. The importance of intrinsic disorder for protein phosphorylation. Nucleic acids research 32(3):1037-1049.

Jeschke G. 2002. Distance measurements in the nanometer range by pulse EPR. Chemphyschem 3(11):927-932.

Jonsen MD, Petersen JM, Xu Q, Graves BJ. 1996. Characterization of the cooperative function of inhibitory sequences of Ets-1. Mol Cell Biol 16(5):2065-2073.

Kalodimos CG, Biris N, Bonvin AM, Levandoski MM, Guennuegues M, Boelens R, Kaptein R. 2004. Structure and flexibility adaptation in nonspecific and specific protein-DNA complexes. Science (New York, NY 305(5682):386-389.

Kay LE. 1998. Protein dynamics from NMR. Biochem Cell Biol 76(2-3):145-152.

Kay LE, Torchia DA, Bax A. 1989. Backbone dynamics of proteins as studied by 15N inverse detected heteronuclear NMR spectroscopy: application to staphylococcal nuclease. Biochemistry 28(23):8972-8979.

Lee GM, Donaldson LW, Pufall MA, Kang HS, Pot I, Graves BJ, McIntosh LP. 2005. The structural and dynamic basis of Ets-1 DNA binding autoinhibition. J Biol Chem 280(8):7088-7099.

Lee GM, Pufall MA, Meeker CA, Kang HS, Graves BJ, McIntosh LP. 2008. The affinity of Ets-1 for DNA is modulated by phosphorylation through transient interactions of an unstructured region. J Mol Biol 382(4):1014-1030.

Lemieux RU, Spohr U. 1994. How Emil Fischer was led to the lock and key concept for enzyme specificity. Advances in carbohydrate chemistry and biochemistry 50:1-20.

Liang B, Bushweller JH, Tamm LK. 2006. Site-directed parallel spin-labeling and paramagnetic relaxation enhancement in structure determination of membrane proteins by solution NMR spectroscopy. Journal of the American Chemical Society 128(13):4389-4397.

Lim F, Kraut N, Frampton J, Graf T. 1992. DNA binding by c-Ets-1, but not v-Ets, is repressed by an intramolecular mechanism. EMBO J 11:643-652.

Lin R, Mamane Y, Hiscott J. 1999. Structural and functional analysis of interferon regulatory factor 3: localization of the transactivation and autoinhibitory domains. Molecular and cellular biology 19(4):2465-2474.

Lincoln DW, 2nd, Bove K. 2005. The transcription factor Ets-1 in breast cancer. Front Biosci 10:506-511.

Liu H, Grundstrom T. 2002. Calcium regulation of GM-CSF by calmodulin-dependent kinase II phosphorylation of Ets1. Mol Biol Cell 13(12):4497-4507.

Liu J, Perumal NB, Oldfield CJ, Su EW, Uversky VN, Dunker AK. 2006. Intrinsic disorder in transcription factors. Biochemistry 45(22):6873-6888.

Midic U, Oldfield CJ, Dunker AK, Obradovic Z, Uversky VN. 2009. Protein disorder in the human diseasome: unfoldomics of human genetic diseases. BMC genomics 10 Suppl 1:S12.

Misura KM, Scheller RH, Weis WI. 2000. Three-dimensional structure of the neuronal-Sec1-syntaxin 1a complex. Nature 404(6776):355-362.

Mittag T, Kay LE, Forman-Kay JD. 2010. Protein dynamics and conformational disorder in molecular recognition. J Mol Recognit 23(2):105-116.

Mulder FA, Skrynnikov NR, Hon B, Dahlquist FW, Kay LE. 2001. Measurement of slow (micros-ms) time scale dynamics in protein side chains by (15)N relaxation dispersion NMR spectroscopy: application to Asn and Gln residues in a cavity mutant of T4 lysozyme. Journal of the American Chemical Society 123(5):967-975.

Nye JA, Petersen JM, Gunther CV, Jonsen MD, Graves BJ. 1992. Interaction of murine Ets-1 with GGA-binding sites establishes the ETS domain as a new DNA-binding motif. Genes Dev 6:975-990.

Obradovic Z, Peng K, Vucetic S, Radivojac P, Brown CJ, Dunker AK. 2003. Predicting intrinsic disorder from amino acid sequence. Proteins 53 Suppl 6:566-572.

Oikawa T. 2004. ETS transcription factors: possible targets for cancer therapy. Cancer Sci 95(8):626-633.

Oikawa T, Yamada T. 2003. Molecular biology of the Ets family of transcription factors. Gene 303:11-34.

Okamura H, Aramburu J, Garcia-Rodriguez C, Viola JP, Raghavan A, Tahiliani M, Zhang X, Qin J, Hogan PG, Rao A. 2000. Concerted dephosphorylation of the transcription factor NFAT1 induces a conformational switch that regulates transcriptional activity. Molecular cell 6(3):539-550.

Oldfield CJ, Cheng Y, Cortese MS, Brown CJ, Uversky VN, Dunker AK. 2005. Comparing and combining predictors of mostly disordered proteins. Biochemistry 44(6):1989-2000.

Orlicky S, Tang X, Willems A, Tyers M, Sicheri F. 2003. Structural basis for phosphodependent substrate selection and orientation by the SCFCdc4 ubiquitin ligase. Cell 112(2):243-256.

Palmer AG, 3rd. 2001. Nmr probes of molecular dynamics: overview and comparison with other techniques. Annual review of biophysics and biomolecular structure 30:129-155.

Palmer AG, 3rd, Kroenke CD, Loria JP. 2001. Nuclear magnetic resonance methods for quantifying microsecond-to-millisecond motions in biological macromolecules. Methods in enzymology 339:204-238.

Petersen JM, Skalicky JJ, Donaldson LW, McIntosh LP, Alber T, Graves BJ. 1995. Modulation of transcription factor Ets-1 DNA binding: DNA-induced unfolding of an alpha helix. Science (New York, NY 269(5232):1866-1869.

Pognonec P, Boulukos KE, Gesquiere JC, Stehelin D, Ghysdael J. 1988. Mitogenic stimulation of thymocytes results in the calcium-dependent phosphorylation of c-*ets*-1 proteins. EMBO J 7:977-983.

Pognonec P, Boulukos KE, Ghysdael J. 1989. The c-ets-1 protein is chromatin associated and binds to DNA in vitro. Oncogene 4:691-697.

Pufall MA, Graves BJ. 2002. Autoinhibitory domains: modular effectors of cellular regulation. Annu Rev Cell Dev Biol 18:421-462.

Pufall MA, Lee GM, Nelson ML, Kang HS, Velyvis A, Kay LE, McIntosh LP, Graves BJ. 2005. Variable control of Ets-1 DNA binding by multiple phosphates in an unstructured region. Science (New York, NY 309(5731):142-145.

Rohatgi R, Ho HY, Kirschner MW. 2000. Mechanism of N-WASP activation by CDC42 and phosphatidylinositol 4, 5-bisphosphate. J Cell Biol 150(6):1299-1310.

Romero P, Obradovic Z, Li X, Garner EC, Brown CJ, Dunker AK. 2001. Sequence complexity of disordered protein. Proteins 42(1):38-48.

Salazar C, Hofer T. 2003. Allosteric regulation of the transcription factor NFAT1 by multiple phosphorylation sites: a mathematical analysis. J Mol Biol 327(1):31-45.

Segal E, Widom J. 2009. What controls nucleosome positions? Trends Genet 25(8):335-343.

Simons PC, Pietromonaco SF, Reczek D, Bretscher A, Elias L. 1998. C-terminal threonine phosphorylation activates ERM proteins to link the cell's cortical lipid bilayer to the cytoskeleton. Biochemical and biophysical research communications 253(3):561-565.

Skalicky JJ, Donaldson LW, Petersen JM, Graves BJ, McIntosh LP. 1996. Structural coupling of the inhibitory regions flanking the ETS domain of murine Ets-1. Prot Science 5:296-309.

Stein A, Pache RA, Bernado P, Pons M, Aloy P. 2009. Dynamic interactions of proteins in complex networks: a more structured view. The FEBS journal 276(19):5390-5405.

Sugase K, Dyson HJ, Wright PE. 2007. Mechanism of coupled folding and binding of an intrinsically disordered protein. Nature 447(7147):1021-1025.

Tollinger M, Skrynnikov NR, Mulder FA, Forman-Kay JD, Kay LE. 2001. Slow dynamics in folded and unfolded states of an SH3 domain. J Am Chem Soc 123(46):11341-11352.

Uversky VN, Dunker AK. 2010. Understanding protein non-folding. Biochimica et biophysica acta 1804(6):1231-1264.

Velyvis A, Yang YR, Schachman HK, Kay LE. 2007. A solution NMR study showing that active site ligands and nucleotides directly perturb the allosteric equilibrium in aspartate transcarbamoylase. Proceedings of the National Academy of Sciences of the United States of America 104(21):8815-8820.

Venanzoni MC, Robinson LR, Hodge DR, Kola I, Seth A. 1996. ETS1 and ETS2 in p53 regulation: spatial separation of ETS binding sites (EBS) modulate protein: DNA interaction. Oncogene 12(6):1199-1204.

Volkman BF, Lipson D, Wemmer DE, Kern D. 2001. Two-state allosteric behavior in a single-domain signaling protein. Science (New York, NY 291(5512):2429-2433.

Wasylyk B, Hahn SL, Giovane A. 1993. The Ets family of transcription factors. Eur J Biochem 211:7-18.

Wei GH, Badis G, Berger MF, Kivioja T, Palin K, Enge M, Bonke M, Jolma A, Varjosalo M, Gehrke AR, Yan J, Talukder S, Turunen M, Taipale M,

Stunnenberg HG, Ukkonen E, Hughes TR, Bulyk ML, Taipale J. 2010. Genome-wide analysis of ETS-family DNA-binding in vitro and in vivo. The EMBO journal.

Wotton D, Ghysdael J, Wang S, Speck NA, Owen MJ. 1994. Cooperative binding of Ets-1 and Core Binding Factor to DNA. Mol Cell Biol 14:840-850.

Wright PE, Dyson HJ. 1999. Intrinsically unstructured proteins: re-assessing the protein structure-function paradigm. J Mol Biol 293(2):321-331.

Yang C, Shapiro LH, Rivera M, Kumar A, Brindle PK. 1998. A role for CREB binding protein and p300 transcriptional coactivators in Ets-1 transactivation functions. Mol Cell Biol 18(4):2218-2229.

CHAPTER 2

THE AFFINITY OF ETS-1 FOR DNA IS MODULATED BY PHOSPHORYLATION THROUGH TRANSIENT INTERACTION OF AN UNSTRUCTURED REGION

This chapter was reprinted with permission from 2008 Elsevier Ltd. J. Mol. Biol. (2008) 382(4), 1014–1030.

The experiments described in this chapter were conducted by current and former members of Dr. Barbara Graves' laboratory, as well as the collaborating laboratory of Dr. Lawrence McIntosh. My contributions were the development of ΔN279 as a new reagent for studying phosphorylation effects in Ets-1, including DNA binding characterization of $\Delta N279^{2p}$. I was also responsible for the expression and purification of all isotopically-labeled proteins for which NMR data is reported.

doi:10.1016/j.jmb.2008.07.064 *J. Mol. Biol.* (2008) **382**, 1014–1030

JMB

Available online at www.sciencedirect.com

ScienceDirect

ELSEVIER

The Affinity of Ets-1 for DNA is Modulated by Phosphorylation Through Transient Interactions of an Unstructured Region

Gregory M. Lee[1]†, Miles A. Pufall[2]†, Charles A. Meeker[2], Hyun-Seo Kang[1], Barbara J. Graves[2]* and Lawrence P. McIntosh[1]*

[1]*Department of Biochemistry and Molecular Biology, Department of Chemistry, and the Michael Smith Laboratories, University of British Columbia, Vancouver, BC, Canada V6T 1Z3*

[2]*Department of Oncological Sciences, Huntsman Cancer Institute, University of Utah, Salt Lake City, UT 84312, USA*

Received 7 June 2008; received in revised form 24 July 2008; accepted 24 July 2008
Available online 29 July 2008

Binding of the transcription factor Ets-1 to DNA is allosterically regulated by a serine-rich region (SRR) that modulates the dynamic character of the adjacent structured DNA-binding ETS domain and its flanking autoinhibitory elements. Multi-site phosphorylation of the flexible SRR in response to Ca^{2+} signaling mediates variable regulation of Ets-1 DNA-binding affinity. In this study, we further investigated the mechanism of this regulation. First, thermal and urea denaturation experiments demonstrated that phosphorylation of the predominantly unstructured SRR imparts enhanced thermodynamic stability on the well-folded ETS domain and its inhibitory module. We next identified a minimal fragment (residues 279–440) that exhibits both enhanced autoinhibition of Ets-1 DNA-binding and allosteric reinforcement by phosphorylation. To test for intramolecular interactions between the SRR and the rest of the fragment that were not detectable by ^{1}H-^{1}H NOE measurements, paramagnetic relaxation enhancements were performed using Cu^{2+} bound to the N-terminal ATCUN motif. Increased relaxation detected for specific amide and methyl groups revealed a preferential interaction surface for the flexible SRR extending from the inhibitory module to the DNA-binding interface. Phosphorylation enhanced the localization of the SRR to this surface. We therefore hypothesize that the positioning of the SRR at the DNA-binding interface and its role in shifting Ets-1 to an inhibited conformation are linked. In particular, transient interactions dampen the conformational flexibility of the ETS domain and inhibitory module required for high-affinity binding, as well as possibly occlude the DNA interaction site. Surprisingly, the phosphorylation-dependent effects were relatively insensitive to changes in ionic strength, suggesting that electrostatic forces are not the dominant mechanism for mediating these interactions. The results of this study highlight the role of flexibility and transient binding in the variable regulation of Ets-1 activity.

Keywords: transcription; allosteric regulation; protein dynamics; NMR spectroscopy; paramagnetic relaxation

Edited by P. Wright

**Corresponding authors.* E-mail addresses: barbara.graves@hci.utah.edu; mcintosh@chem.ubc.ca.

† G.M.L. and M.A.P. contributed equally to this work.

Present addresses: G. M. Lee, Department of Pharmaceutical Chemistry, University of California, San Francisco, CA 94158, USA; M. A. Pufall, Department of Cellular & Molecular Pharmacology, University of California, San Francisco, CA 94158, USA.

Abbreviations used: ATCUN, amino-terminal copper and nickel-binding; EMSA, electrophoretic mobility-shift assay; HSQC, heteronuclear single quantum correlation; HTH, helix-turn-helix; HX, hydrogen exchange; NOE, nuclear Overhauser effect; NOESY, nuclear Overhauser effect spectroscopy; PRE, paramagnetic relaxation enhancement; SRR, serine-rich region (residues 244–301); SRR*, truncated serine-rich region (residues 279–301); Ets-1, fragments are indicated by the boundaries of truncations from the N-terminus of the protein, e.g. ΔN301 is a deletion of residues 1–300 and corresponds to Ets-1(301–440).

Introduction

Regions of intrinsic disorder are being identified with increasing frequency as targets of protein regulation.[1–3] Two general features of these regions have been described: first, they adopt an ordered conformation in order to perform their function; and second, they are often sites of post-translational modifications, which either induce or disrupt the active conformation. For example, the tail of stathmin, which is disordered in its apo form, adopts a stable β-hairpin when bound to tubulin, leading to the disruption of microtubule formation. Phosphorylation of this region abolishes the hairpin, thus disrupting binding and allowing microtubule formation to proceed.[4] Conversely, phosphorylation of the intrinsically disordered KID domain of the DNA-binding transcription factor CREB enhances recognition by the KIX domain of co-activator p300. The phosphorylated KID domain undergoes a disorder-to-order transition upon interaction with the KIX domain, forming two α-helices that provide a stable interface for association with p300 and allowing activation of transcription.[5] In both cases, the change in the physicochemical properties of the modified protein conferred by addition of phosphates has a role in either inducing or disrupting the active structure. In contrast, our recent studies of the transcription factor Ets-1 show that a predominantly unstructured, multiply phosphorylated region acts as an intramolecular allosteric regulator of the well-folded DNA-binding domain.[6] The interplay between the unstructured and structured regions of Ets-1 is the focus of this investigation.

The binding of Ets-1 to DNA is mediated by the ETS domain, which contains three α-helices and a four-stranded β-sheet, and is modulated by flanking regions that fold into an inhibitory module composed of four α-helices (Fig. 1).[7,8] The inhibitory module packs along a surface of the ETS domain at helix H1, opposite the helix (H2)-turn-helix(H3) DNA recognition interface. DNA binding is accompanied by a structural rearrangement that disrupts the inhibitory module, as highlighted most dramatically by the unfolding of the marginally stable N-terminal inhibitory helix HI-1.[8–10] Proper packing of the inhibitory module against the ETS domain is required for autoinhibition, as demonstrated by the higher affinity of variants containing mutations that disrupt the hydrophobic core of the module.[11] The presence of an adjacent disordered serine-rich region (residues 244–300, termed the SRR) accentuates repression of the ETS domain and inhibitory modules (residues 301–440, also termed ΔN301 or the "regulatable unit") and recapitulates binding of the full-length protein.[6] Multi-site phosphorylation of the SRR in response to Ca^{2+} signaling further attenuates DNA binding,[12] with each added phosphate causing progressively increased repression.[6] Protein partnerships, both heterotypic and homotypic, can also counteract autoinhibition, thereby enhancing DNA binding.[13–15] Thus, Ets-1 displays a 1000-fold range in DNA binding affinity, from a state completely activated by deletion or biological partners to a fully phosphorylated, repressed state.

The mechanism of autoinhibition and its reinforcement by phosphorylation was partially elucidated by the discovery of the dynamic nature of the ETS domain and its inhibitory elements, even in the absence of DNA.[6,8] The degree of this internal motion correlates with the DNA-binding affinity of various deletion fragments and phosphorylated forms of Ets-1. Specifically, the presence of the SRR and its phosphorylation reduces the millisecond to microsecond timescale motions of the inhibitory module and ETS domain, as well as imparting its overall stabilization, as shown by increased protection from amide hydrogen exchange (HX).[6] Along with chemical shift perturbation mapping, these NMR-based observations indicated that Ets-1 exists in a conformational equilibrium between at least two states. The active state, which can bind DNA, exhibits conformational mobility within HI-1 and HI-2 of the inhibitory module and, importantly, the DNA recognition helix H3.[6] This led to the model that the dynamic nature of Ets-1 reflects the sampling of conformations necessary to bind to DNA recognition sites with high affinity, and that a reduction in these dynamics shifts the equilibrium to a more rigid, low-affinity state.

The shift between dynamic-active and rigid-inactive states is reminiscent of the classical allosteric transition between the relaxed and tense forms of a protein.[16] However, distinct from this model, the phosphorylation-dependent exchange between the two states of Ets-1 is not all-or-none. Progressive mutation of phosphoacceptor sites within the SRR yielded species with progressively decreasing inhibition, indicating that the affinity of Ets-1 for DNA can be fine-tuned *in vitro*[6] and *in vivo*[17] by multi-site phosphorylation. Importantly, each added phosphate also shifts the equilibrium toward the inhibited conformation, further bolstering the idea that decreasing the active state population is the mode for reducing DNA affinity. Surprisingly, the phosphorylated SRR directs this conformational transition despite being predominantly unstructured and flexible on the sub-nanosecond timescale.[6]

To further our understanding of the mechanism of Ets-1 autoinhibition and to determine how structured and unstructured protein segments interact, we investigated several unresolved features of the allosteric model. Does the SRR interact directly with the ETS domain and inhibitory helices to mediate its stabilizing effect? Does this change upon phosphorylation? What is the physicochemical nature of this interaction between an unstructured, flexible region and a dynamic structured region? In particular, are electrostatic forces involved due to the addition of negative charges upon phosphorylation? To address these questions, we demonstrate that SRR phosphorylation increases the global thermodynamic stability of an

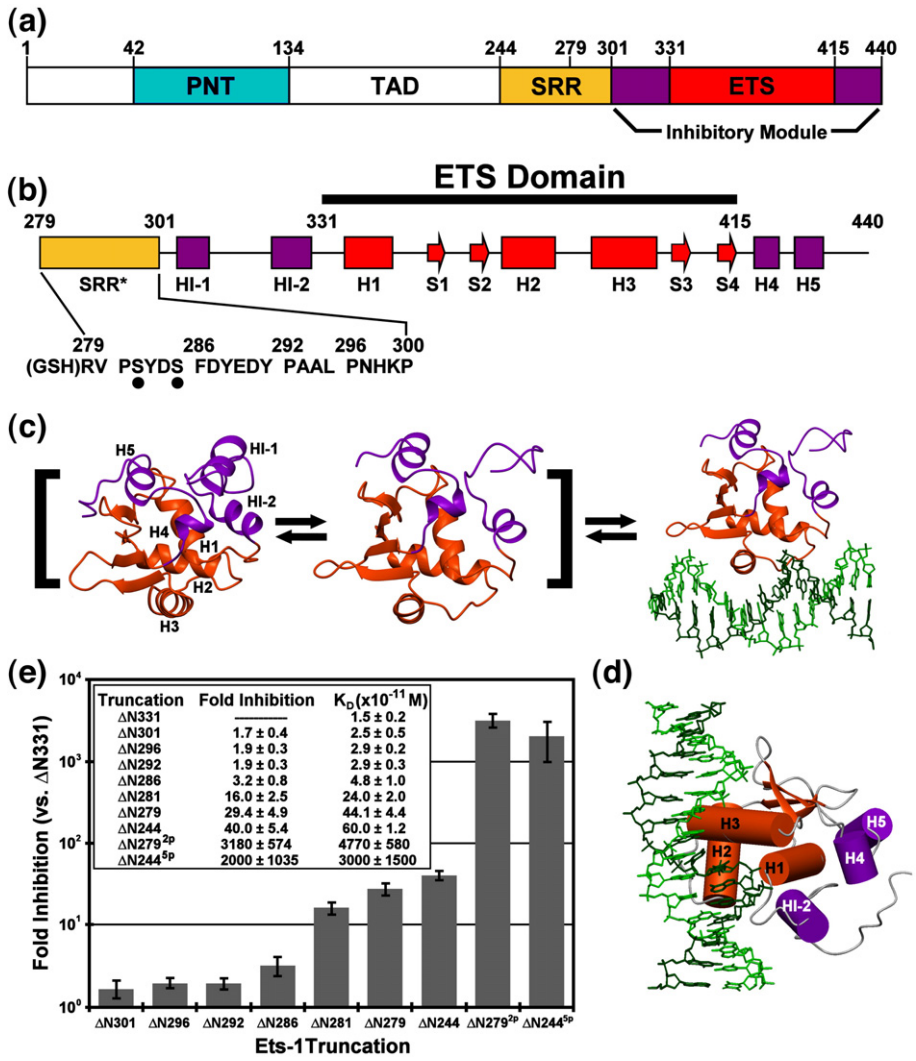

Fig. 1. (a) The structural organization of Ets-1, showing the protein interaction PNT domain (cyan), transactivation domain (TAD, white), and serine-rich region (SRR, yellow), along with the regulatable unit, composed of the DNA-binding ETS domain (red), and inhibitory module (purple). (b) The secondary structural elements of ΔN279 (α-helix, H; β-strand, S) and sequence of residues 279–300 of the truncated SRR*, including sites of Ca^{2+}-dependent kinase phosphorylation (S282 and S285; dots) and a Gly-Ser-His motif resulting from thrombin cleavage of an N-terminal His_6-tag. (c) Allosteric model of autoinhibition in which free Ets-1 exists in equilibrium between rigid-inactive and flexible-active states, the latter characterized most conspicuously by the unfolding of HI-1. The structures shown are for isolated ΔN301 (left, *1R36*.pdb), DNA-bound ΔN280 (right, *1MDM*.pdb), and a proposed DNA-free state with HI-1 unfolded (middle). (d) A view of DNA-bound ΔN280, oriented as in the cylinder model in Figs. 6c and 7d. (e) A summary of the EMSAs of DNA binding by Ets-1 truncation constructs, showing the equilibrium dissociation constants, K_D, and the fold inhibition relative to ΔN331, the completely de-repressed fragment of Ets-1. The shorter fragments (ΔN301, ΔN296, ΔN292, and ΔN286) have modest effects, whereas the longer constructs have a higher level of inhibition. Phosphorylation of S282 and S285 (ΔN279^{2p}) represses DNA binding significantly relative to unmodified state ΔN279. This recapitulates the behavior of ΔN244.[6] ΔN281 results from deletion of V280 from ΔN280 during *E. coli* expression, and ΔN279 and ΔN279^{2p} have an N-terminal Gly-Ser-His motif.

Ets-1 fragment. Using NMR spectroscopy, we also show that the SRR is predominantly unstructured both before and after phosphorylation. However, addition of phosphates to the SRR subtly dampens its fast timescale motions detected by ^{15}N relaxation, as well as restricting the conformational dynamics of the regulatable unit, as shown by reduced amide HX. Importantly, paramagnetic relaxation enhancement (PRE) measurements revealed that the flexible SRR localizes to a surface that extends from the inhibitory module to the DNA-binding interface, and that this localization is more persistent upon phosphorylation. These observations suggest that transient intramolecular interactions can affect the dynamic nature of the ETS domain and its inhibitory elements, thus supporting an allosteric mechanism of autoinhibition. The location of the SRR near the DNA-binding surface might also augment autoinhibition through a steric mechanism.

Results

SRR phosphorylation thermodynamically stabilizes the regulatable unit

We focused our investigation on the interaction between the flexible, unstructured SRR (residues 244–300) and the structured, but dynamic, regulatable unit (residues 301–440). The motions of this unit, composed of the DNA-binding ETS domain and its flanking inhibitory module, are dampened in the presence of the SRR and more so in response to multi-site phosphorylation.[6] To test whether this effect is detectable as a change in global thermodynamic stability, CD spectroscopy was used to monitor thermal- and urea-induced denaturation of ΔN244 and $\Delta N244^{5P}$ (the ΔN244 variant phosphorylated at S251, S270, S273, S282, and S285). The secondary structure of ΔN244 and $\Delta N244^{5P}$ remained essentially identical, as indicated by their equivalent molar ellipticities (Fig. 2a). However phosphorylation shifted the midpoint temperature of denaturation (T_m) dramatically from ~55 °C to >90 °C (Fig. 2b). Similarly, phosphorylation increased the midpoint urea denaturation concentration ($[urea]_{1/2}$) from ~4.8 M for ΔN244 to ~5.6 M for $\Delta N244^{5P}$ (Fig. 2c). Thus, without any change in helical content, SRR phosphorylation stabilizes the regulatable unit substantially. Unfortunately, calculation of the free energy of this stabilization was unreliable due to poorly defined baselines for the urea-unfolded proteins.

ΔN279 is a minimally sized fragment that exhibits phosphorylation-enhanced autoinhibition

We previously used fragments ΔN301, ΔN280, and $\Delta N244^{5P}$ to investigate autoinhibition and the effect of phosphorylation on the regulatable unit of Ets-1 by NMR spectroscopic analyses.[6,8,18] This experimental design was necessary due to limited solubility of the non-phosphorylated ΔN244 (~100 μM) under NMR sample conditions. We sought to define a smaller fragment of Ets-1 that recapitulated both the autoinhibition and phosphorylation effects, and was more amenable to NMR spectroscopic analysis in the unmodified state. ΔN280, previously characterized by NMR methods, displays autoinhibition levels comparable to that of native, unmodified full-length Ets-1.[9,18,19] Importantly, two phosphoacceptor sites, S282 and S285, which act additively with the more N-terminal sites

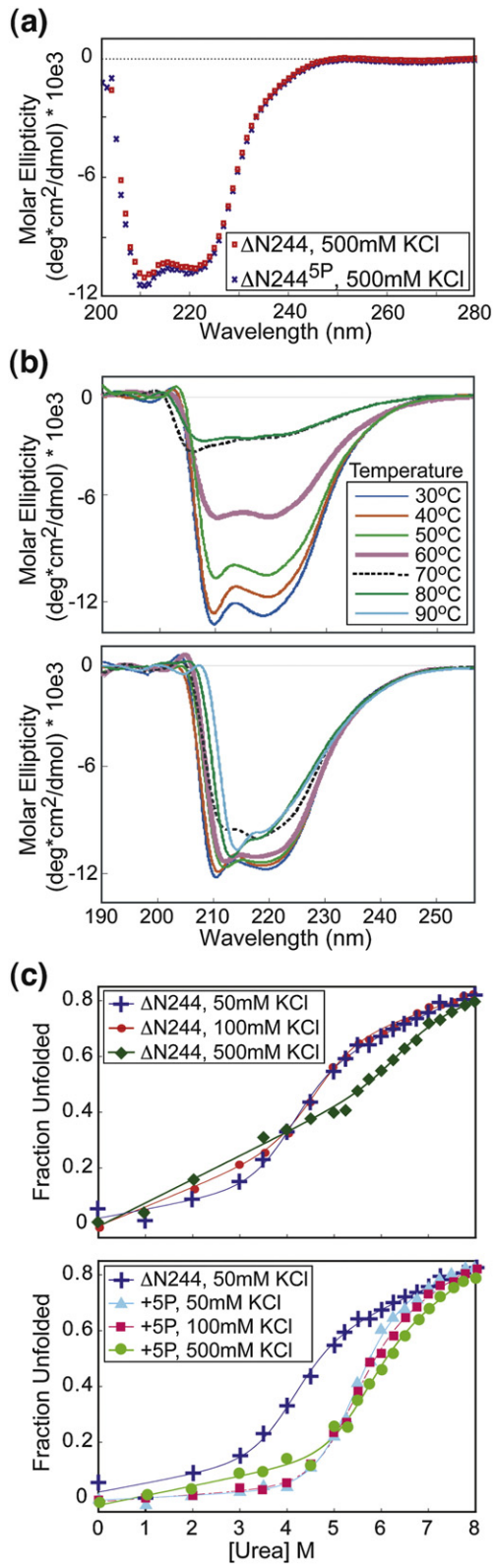

Fig. 2. Phosphorylation stabilizes Ets-1. (a) The CD spectra of ΔN244 and $\Delta N244^{5P}$ are essentially superimposable, indicating that phosphorylation does not alter the secondary structure of the Ets-1 fragment. (b) Signal-averaged CD spectra of ΔN244 and $\Delta N244^{5P}$ recorded with increasing temperature in 10 °C intervals. ΔN244 had a midpoint unfolding temperature of ~55 °C, whereas $\Delta N244^{5P}$ remained well folded at 90 °C. (c) Urea denaturation of ΔN244 *versus* $\Delta N244^{5P}$ in the presence of 50 mM, 100 mM, and 500 mM KCl. Lines show the data fit (see Methods). Phosphorylation elevated the $[urea]_{1/2}$ from ~4.8 M to ~5.6 M in 50 mM KCl. Increasing ionic strength reduced the co-operativity of ΔN244 unfolding, but did not markedly change the stability of $\Delta N244^{5P}$. Samples were in 25 mM potassium phosphate, pH 7.9, and 100 mM KCl at 25 °C unless stated otherwise.

in ΔN244, are retained in ΔN280. In addition, although all residues of the $\Delta N244^{5P}$ SRR are conformationally dynamic,[6] a Lipari-Szabo model-free analysis[20] of their amide ^{15}N T_1, T_2, and heteronuclear $^{1}H\{^{15}N\}$-nuclear Overhauser effect (NOE) parameters showed non-uniform mobility. Specifically, residues 280–300 have restricted fast timescale motions relative to the remaining N-terminal portion of the SRR (Supplementary Data Figs. S1 and S2). Accordingly, we chose to focus on the former region, and developed an Ets-1 species spanning residues 279–440. This fragment is preceded by a short tripeptide (Gly-Ser-His) resulting from the proteolytic cleavage of a His_6 tag. For simplicity, we denote this as ΔN279 (Fig. 1b).

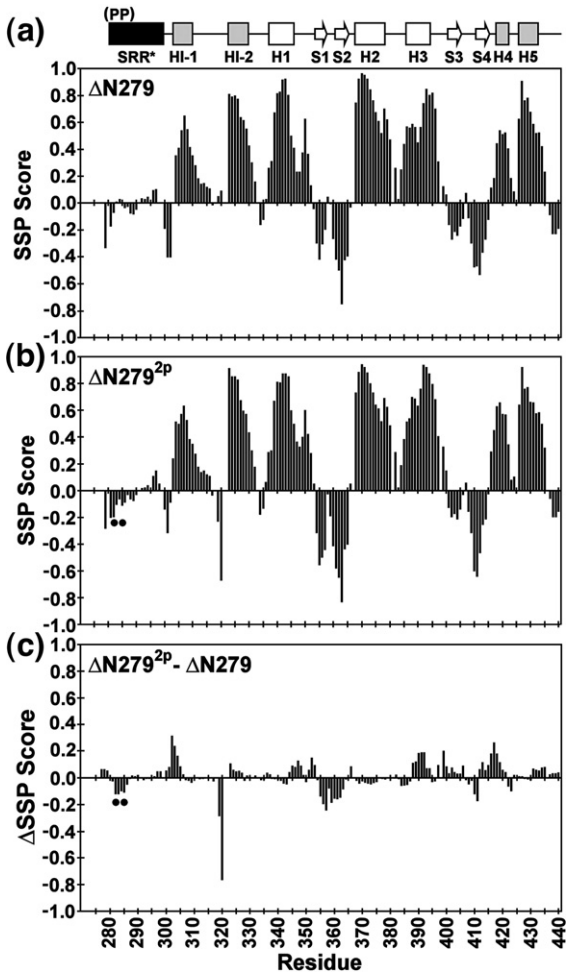

Fig. 3. The SRR* of ΔN279 and $\Delta N279^{2P}$ lack any predominant secondary structure, and phosphorylation does not alter the secondary structure of the inhibitory module or ETS domain. Shown are the secondary structural propensity (SSP) scores for ΔN279 (a) and $\Delta N279^{2P}$ (b), along with ΔSSP (c), the change upon phosphorylation, derived from available main chain ^{1}H, ^{13}C, and ^{15}N chemical shifts (and using random coil phosphoserine chemical shifts[25]). Values approaching +1 and −1 are indicative of well defined α-helices and β-strands, respectively.[24] The phosphoserines are indicated by dots, and missing data points correspond to residues with unassigned NMR signals.

To ensure that ΔN279, containing the minimally sized SRR* (residues 279–300), retained both the autoinhibition and phosphorylation effects, we measured the DNA-binding activity of a series of N-terminal truncations by quantitative electrophoretic mobility-shift assays (EMSAs) and compared these data to the affinity of unrepressed ΔN331 to assess the level of autoinhibition (Fig. 1e). All deletions exhibited reduced autoinhibition, indicating that residues 279–300 are necessary for full repression. Importantly, mass spectrometry and gel electrophoresis confirmed the efficient phosphorylation of ΔN279 at S282 and S285 (data not shown). The resulting $\Delta N279^{2P}$ exhibited a K_D of $\sim 5 \times 10^{-8}$ M, representing a ~100-fold reduction relative to unmodified ΔN279. Thus, ΔN279 recapitulated both autoinhibition and phosphorylation effects. The signals from backbone amide and sidechain nuclei of ΔN279 and $\Delta N279^{2P}$ were assigned using a suite of heteronuclear NMR experiments (Supplemental Figs. S3 and S4).[8] We confirmed by chemical shift analyses that the secondary structure elements of the inhibitory module and ETS domain were the same as observed in previous X-ray crystallographic and NMR spectroscopic studies of various Ets-1 fragments (Fig. 3 and Supplementary Data Fig. S2).[8,10] Therefore, we were poised to study the effects of phosphorylation of the SRR using a single well-characterized species, ΔN279. To distinguish the full-length SRR of ΔN244 from the truncated one in ΔN279, we designate the latter as SRR*.

SRR* is unstructured and dynamic

Previous biophysical comparison of $\Delta N244^{5P}$ and ΔN280 indicated that the SRR was unstructured and suggested that there were no losses or gains of structural elements upon phosphorylation (Supplementary Data Fig. S2).[6,18] These findings were re-investigated with the better-behaved ΔN279 species, thus enabling more complete assignment and a detailed assessment of any changes within the same species upon SRR* phosphorylation. Secondary structure elements were identified by analyzing the $^{1}H^{\alpha}$, $^{13}C^{\alpha}$, $^{13}C^{\beta}$, and ^{13}CO chemical shifts with the CSI,[21] RCI,[22] TALOS,[23] and SSP[24] algorithms. By all these criteria, and in contrast to the well-structured regulatable unit, the SRR* residues exhibited random coil chemical shifts in ΔN279 and $\Delta N279^{2P}$ (Fig. 3). Thus, the SRR* lacks any predominant secondary structure in both its unmodified and phosphorylated states. The possible presence of structural elements was tested also by amide HX using a combination of ^{1}H-^{1}H magnetization transfer and ^{1}H-^{2}H exchange experiments. In both ΔN279 and $\Delta N279^{2P}$, the SRR* exhibited amide HX rates within a factor of ~5 of those predicted for a random coil polypeptide of the same sequence (Fig. 4a and c). These data sets confirmed that the truncated SRR* does not adopt a predominant conformation in either the unmodified or phosphorylated states of ΔN279. Finally, ^{15}N- and

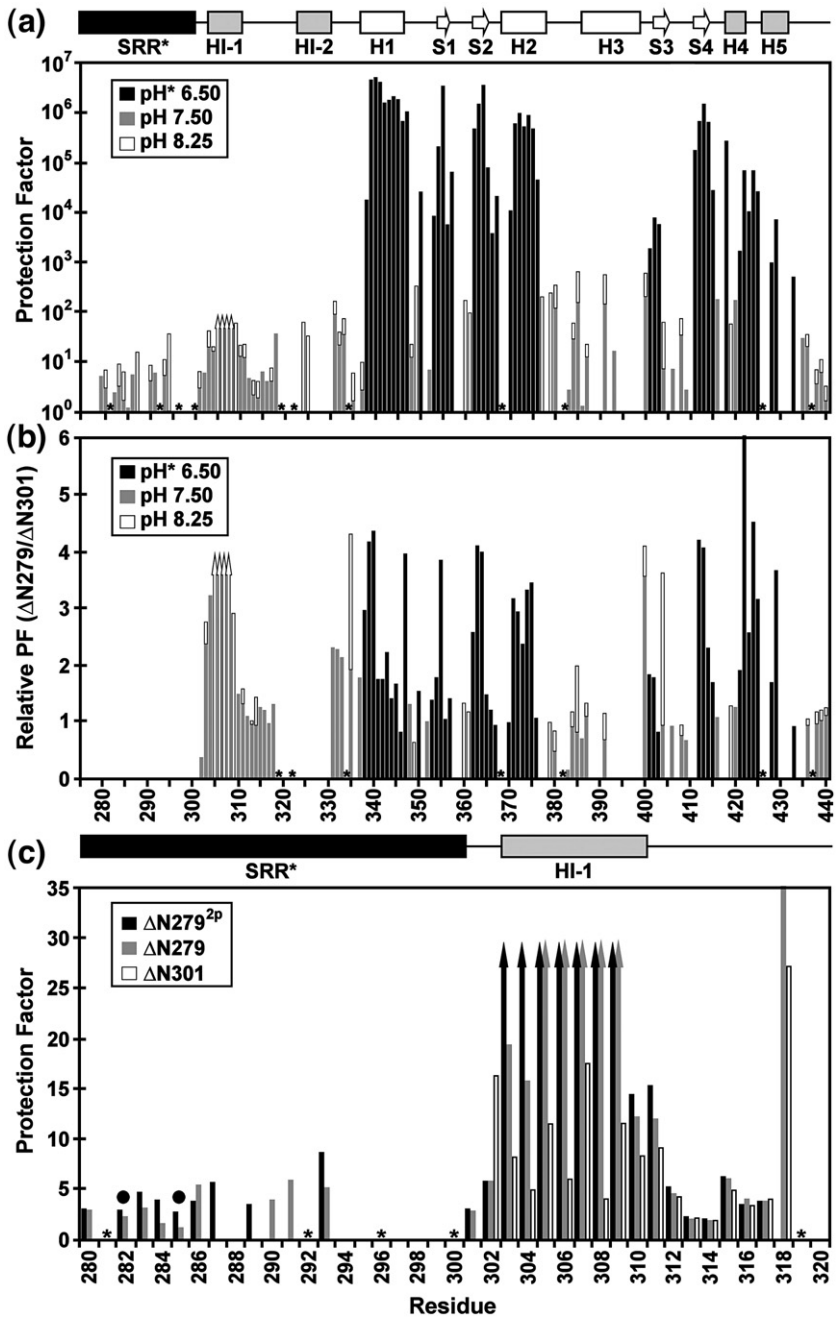

Fig. 4. Amide HX measurements provide insights into the structure, stability, and dynamics of the Ets-1 deletion fragments (500 mM NaCl, 28 °C). (a) The comprehensive backbone amide HX protection factors of ΔN279, determined from slow H_2O-^2H_2O exchange (pH* 6.50, black) and fast H_2O-H_2O CLEANEX (pH 7.50, gray; pH 8.25, white) measurements. Residues 305–308 exchanged too slowly to be characterized by CLEANEX, yet too fast to be detected after transfer into ^2H_2O buffer, and thus their protection factors fall within the range of ~30 to 200 (up arrows). The SRR* is predominantly unstructured, showing little protection against HX. The inhibitory helices HI-1 and H1-2, as well as the DNA recognition helix H3, undergo relatively facile HX. (b) However, the presence of the SRR* stabilizes the inhibitory module and ETS domain against HX by up to ~4-fold. The relative protection factors for ΔN279 *versus* ΔN301, obtained from H_2O-^2H_2O exchange (pH* 6.5, black) and/or CLEANEX measurements (pH 7.5, gray; pH 8.25, white) are shown. (c) Phosphorylation of S282 and S285 further stabilizes the N-terminal inhibitory helix of ΔN279 against amide HX. The amide protection factors of residues 280–320 in $\Delta N279^{2P}$ (black), ΔN279 (gray), and ΔN301 (white), acquired from CLEANEX exchange experiments at pH 7.5 are shown. Up arrows indicate minimal estimated values. Filled circles indicate the phosphoacceptor serines, and missing data correspond to prolines (*) or amides with weak or overlapping NMR signals. Slow amide HX kinetics, which require measurements over many months, were not determined for $\Delta N279^{2P}$.

^{13}C-edited nuclear Overhauser effect spectroscopy-heteronuclear single quantum correlation (NOESY-HSQC) spectra were recorded to determine if any persistent inter-residue contact was detectable either within the SRR* or between the SRR* and the regulatable unit. Only intra- and nearest-neighbor inter-residue ^1H-^1H NOE interactions were observed within the SRR*, and no long-range NOE was detected between the SRR* and the regulatable unit in ΔN279 or $\Delta N279^{2P}$ (data not shown). Together, these assays yielded no evidence of any persistent structural element within either form of the SRR*, nor any long-lived interaction between the SRR* and the regulatable unit.

Phosphorylation partially dampens the flexibility of the unstructured SRR*

Earlier analysis of $\Delta N244^{5P}$ indicated that SRR was conformationally dynamic,[6] but no direct test of phosphorylation effects on the same species was possible. Thus, ^{15}N relaxation experiments were performed with ΔN279 in its unmodified and phosphorylated states. Amides within the regulatable unit of ΔN279 exhibited average T_1, T_2, and ^1H {^{15}N}-NOE values of 883±74 ms, 54±8 ms, and 0.82±0.08, respectively (500 mM NaCl, 28 °C). In contrast, amides within the SRR* displayed markedly different relaxation properties with average T_1, T_2, and ^1H

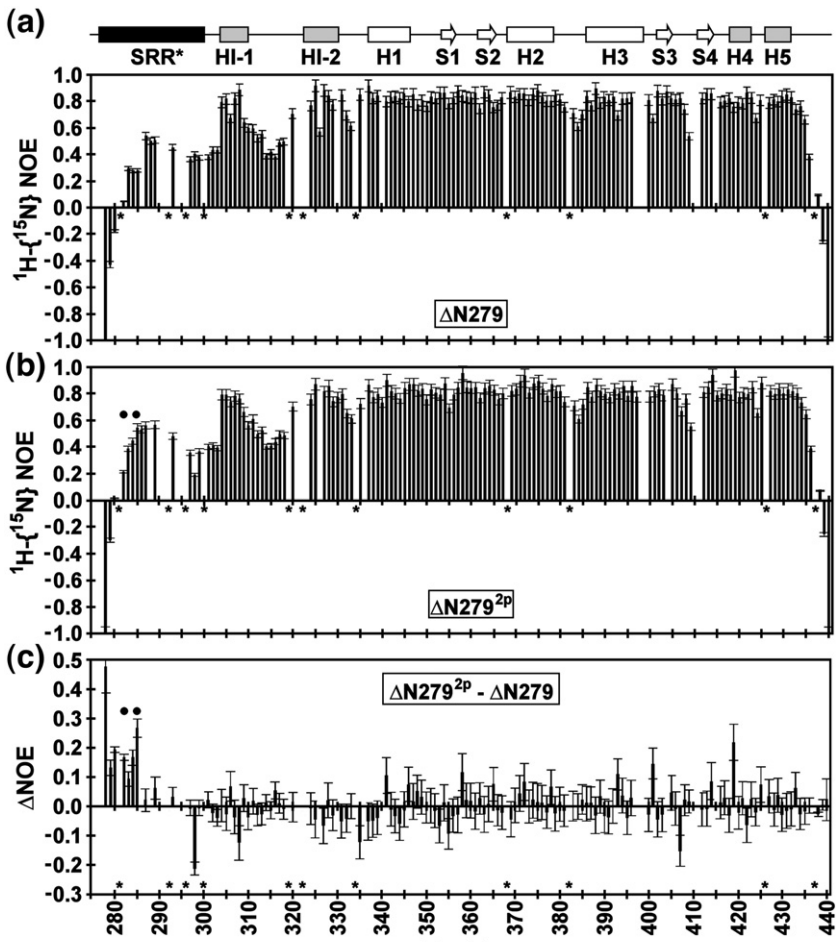

Fig. 5. The heteronuclear ^{1}H{^{15}N}-NOE values of ΔN279 (a), ΔN279^{2p} (b), and (c) the difference, ΔNOE = NOE (ΔN279^{2p}) – NOE (ΔN279), recorded in 500 mM NaCl at 28 °C. The uniformly high NOE ratios of residues 301–440 in both ΔN279 and ΔN279^{2p} are indicative of well-ordered backbone segments, except in regions such as the HI-1/HI-2 and H2/H3 loops, as discussed in detail for ΔN301[8] Conversely, as shown by NOE ratios <0.6, the SRR* in both ΔN279 and ΔN279^{2p} exhibits flexibility on the sub-nanosecond timescale. This motion is not totally unrestricted, as the NOE values are mostly >0.2. Furthermore, positive ΔNOE values for residues 279–285 indicate that phosphorylation marginally dampens this fast timescale motion. Filled circles indicate the phosphoacceptor serines, and missing data correspond to prolines (*) or amides with weak or overlapping NMR signals.

{^{15}N}-NOE values of 645±66 ms, 113±39 ms, and 0.34±0.20, respectively (Fig. 5a). These parameters corresponded to isotropic Lipari-Szabo model-free S^2 values of 0.97±0.06 for the regulatable unit and 0.49±0.16 for the SRR*. In particular, the longer T_2 lifetimes and lower ^{1}H{^{15}N}-NOE values indicated substantially greater, but importantly not unrestricted, conformational mobility on a sub-nanosecond timescale for the truncated SRR* than for the structured ETS domain and inhibitory module. Upon phosphorylation, the SRR* residues of ΔN279^{2p} remained conformationally flexible relative to the regulatable unit (Fig. 5b and c). However, the ^{1}H{^{15}N}-NOE values of these residues increased slightly to 0.39±0.17, and the T_2 values decreased to 82±27 ms, whereas the rest of the protein was not measurably perturbed. Thus, phosphorylation of S282 and S285 partially dampens the fast timescale mobility of the truncated SRR*.

SRR* and phosphorylation-dependent changes in the regulatable unit

The SRR* is dynamic and lacks any predominant structure, yet this region stabilizes the regulatable unit against global unfolding in a phosphorylation-dependent manner. Insights into the mechanism of this stabilization were provided by a comparison of the amide $^1H^N$ and ^{15}N chemical shifts of ΔN301, ΔN279, and ΔN279^{2p} (Fig. 6a) Although not inducing any persistent, regular structure within the SRR*, phosphorylation altered the amide chemical shifts of S282 and S285, as well as those of adjacent residues (Fig. 6b). Such local changes are expected, at least in part, from inductive and electric field effects.[25] More interestingly, whereas the majority of the peaks displayed in the ^{1}H-^{15}N HSQC spectra of ΔN301 and ΔN279 were superimposable, clear perturbations due to the presence of the SRR* occurred for corresponding residues within the inhibitory module, H1, and the DNA-recognition helix H3 of the ETS domain (Fig. 6a). These perturbations increased upon phosphorylation to form ΔN279^{2p} (Fig. 6a and b; Supplementary Data Fig. S5). Amide chemical shifts are highly sensitive to subtle local environmental changes, and thus these results indicated that structural alterations occur in a region of the regulatable unit by the unmodified and, even more so, the phosphorylated SRR*. This region includes residues in the inhibitory module and the DNA-binding interface, bridged via a hydrophobic network involving helix H1 (Fig. 6c).[6] Importantly, as observed previously in the longer ΔN244, mutants with varying phosphorylation levels exhibited chemical shift perturbations that followed a co-linear relationship between

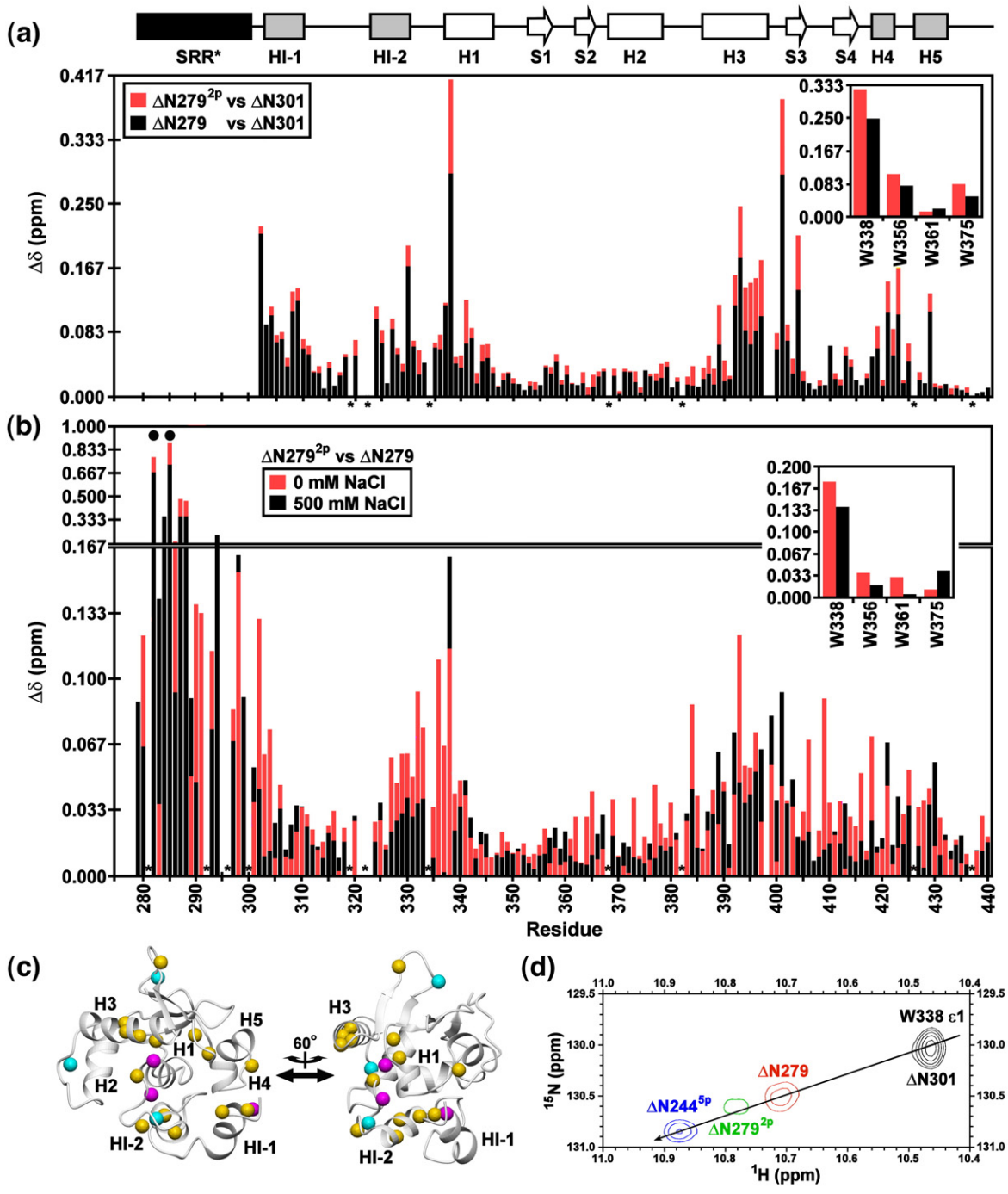

Fig. 6. Amide $^{1}H^{N}$ and ^{15}N chemical shift perturbations of the inhibitory module and DNA-binding interface by the SRR* are enhanced by phosphorylation and partially reduced with increasing ionic strength. (a) The combined backbone amide and tryptophan indole (insert) chemical shift perturbations (Δδ) for corresponding residues in ΔN279 (black) and $\Delta N279^{2p}$ (red) *versus* ΔN301 at 500 mM NaCl, and (b) $\Delta N279^{2p}$ versus ΔN279 in 0 mM (red) and 500 mM (black) NaCl are shown. A difference plot of the data in (b) is provided as Supplementary Data Fig. S5. The histogram bar for the smaller change is shown in front of that for the larger change. The absence of a bar indicates that the Δδ could not be measured unambiguously for a given residue due to spectral overlap or weak signals in at least one species or condition. Filled circles and asterisks represent the phosphoacceptor serines and prolines, respectively. (c) As expected, S282 and S285 underwent the largest chemical shift changes upon phosphorylation, with smaller effects occurring for adjacent amides within the SRR*. However, spectral perturbations also occurred in the inhibitory module, H1, and the DNA-binding interface, as shown by mapping the amide shift difference between $\Delta N279^{2p}$ and ΔN279 at 0 mM NaCl onto the ΔN301 structure (magenta, Δδ >0.15 ppm; cyan, 0.10–0.15 ppm; yellow, 0.05–0.10 ppm). The two views are rotated by 60° about the vertical axis. The orientation of the left ribbon diagram is equivalent to Fig. 1d. (d) A co-linear relationship is observed between chemical shift and increasing autoinhibition, indicating an allosteric shift in the conformational equilibrium of the regulatable core.[6] This is illustrated by an overlay of the sidechain indole signals of W338 in four constructs at 500 mM NaCl (ΔN301, black; ΔN279, red; $\Delta N279^{2p}$, green; $\Delta N244^{5p}$, blue). ΔN301 is poorly soluble in low ionic strength buffers, thus precluding comparisons at reduced concentrations of salt.

chemical shift and DNA-binding affinity (Fig. 6d).[6] This correlation confirms an allosteric shift in the conformational equilibrium of the regulatable unit with increasing autoinhibition.

HX measurements were also used to monitor the effects of the SRR* on the local and global stability of the regulatable unit in ΔN279. As summarized in Fig. 4a, HI-1 and HI-2 are marginally stable with HX protection factors only ~10-fold greater that those of the unstructured SRR*. Furthermore, amides within H3 of the ETS domain also exhibited modest protection factors of ~1000, indicative of significant local conformational fluctuations of the DNA recognition helix. In contrast, amides in helices H1 and H2 and β-strands S1, S2, and S4 of ΔN279 underwent HX at rates near six orders of magnitude slower than expected for a random coil polypeptide, demonstrating that they form the stable core of the ETS domain and likely exchange via a global unfolding pathway. Qualitatively, the HX profile of ΔN279 is similar to that measured earlier for ΔN301.[8] Quantitatively, however, amides throughout the regulatable unit exchanged by up to ~4-fold slower in ΔN279 than in ΔN301, demonstrating that the SRR* stabilizes the regulatable unit against fluctuations leading to HX by ~−0.8 kcal/mol (Fig. 4b). This parallels the increased autoinhibition of ΔN279 relative to ΔN301. Notably, the largest measurable increase in HX protection (sixfold) occurred for L422, a residue that is important for the integrity of the autoinhibitory module because it is located at the C terminus of H4, which abuts tail-to-head with HI-1.[8,10] Phosphorylation of S282 and S285 further reduced the HX rates of the regulatable unit. A clear trend for this is observed at the termini of HI-1 and within HI-1/HI-2 loop, for which protection factors increased progressively by at least sixfold in the order ΔN301, ΔN279, and $\Delta N279^{2P}$ (Fig. 4c). Thus, as observed in an earlier study of $\Delta N244^{5P}$, both amide HX and ^{15}N relaxation measurements (Fig. 5) revealed an increased damping of internal motions of the regulatable unit with increasing autoinhibition.

SRR* transiently interacts with the regulatable unit

Previously, we postulated that the structural and dynamic properties of the regulatable unit are allosterically modulated through transient interactions with the SRR. However, such interactions were not observed through NOESY measurements (not shown). The lack of detectable intramolecular ^{1}H-^{1}H NOEs between the SSR* and the regulatable unit, which typically arise from protons within ~5 Å of one another in well ordered proteins, may be due to many factors. These include low populations and/or an ensemble of conformations with the SRR* contacting the remainder of the protein, unfavorable correlation times for these interactions, and/or spectral degeneracy.

In contrast to ^{1}H-^{1}H NOE measurements, PRE experiments are sensitive to longer-range, as well as transient short-range, interactions.[26] Therefore, we utilized the amino-terminal copper and nickel-binding (ATCUN) motif engineered into the N terminus of ΔN279 to help localize the SRR* with respect to the regulatable unit by PRE. This motif, formed by the N-terminal Gly-Ser-His tripeptide remaining after thrombin cleavage of the His_6 tag, binds Cu^{2+} with high affinity ($K_D \sim 10^{-15}$ M).[27,28] In the case of an ordered ATCUN motif, proton–Cu^{2+} distances of ~10–20 Å can be measured from enhanced ^{1}H relaxation due to the unpaired electron in the paramagnetic metal ion. The signals from protons closer than this lower limit are generally broadened beyond detection. However, conformational averaging will attenuate this $1/r^6$-dependent effect.[26] Thus, we have used this approach as a qualitative indicator of the proximity of amide and methyl protons in ΔN279 and $\Delta N279^{2P}$ to the bound Cu^{2+} probe.

PRE measurements revealed a preferred localization of the ATCUN motif in ΔN279 with respect to the regulatable unit. As expected, ^{1}H-^{15}N and ^{1}H-^{13}C HSQC signals from SRR* residues immediately adjacent to this motif, such as V280 and S282, became undetectable upon formation of a 1:1 Cu^{2+}:protein complex (Fig. 7a). However, significant PREs were observed for residues located in the loop preceding H1 (notably, L337 and W338), in H3, in the loop between H3 and S3 (I401 and I402), and within and adjacent to H4 (D417 and L422). When mapped onto the structure of ΔN301, residues most affected by the ATCUN-bound Cu^{2+} lie along a region on one face extending from HI-1 of

Fig. 7. The SRR* is localized to a region of the regulatable unit spanning from the inhibitory helix HI-1 to the DNA recognition helix H3, and phosphorylation enhances this localization. (a) Paramagnetic relaxation enhancements (PRE) observed for the backbone amides and tryptophan indoles (inset) of ΔN279 (black) and $\Delta N279^{2P}$ (red) in 500 mM NaCl, as reflected by a linear regression analysis of the plots of ^{1}H-^{15}N HSQC signal intensities *versus* equivalents of Cu^{2+} added. Resonances that completely broaden upon addition of ~1 equivalent of $CuSO_4$ have slopes approaching −1.0. The absence of a bar indicates that data could not be measured unambiguously for a given residue due to spectral overlap or a weak signal. Filled circles and asterisks represent the phosphoacceptor serines and prolines, respectively. The PRE slope values of ΔN279 (b) and $\Delta N279^{2P}$ (c) are mapped onto the ΔN301 structure (rotated about the vertical axis as indicated). The upper and lower views are the ribbon and corresponding surface diagrams, respectively. The smaller balls represent backbone amides, while the larger balls indicate either Asn/Gln sidechain NH_2 or aliphatic methyl groups. The color scheme is red, slope <−0.4 (i.e. largest PRE); orange, −0.4↔−0.325; yellow, −0.325↔−0.25. Residues for which data were unavailable are shaded in gray. (d) Insights into enhanced DNA-binding inhibition may be derived from the surface diagram of ΔN301, showing negatively-charged (Asp, Glu; red), positively-charged (Arg, Lys, His; blue), hydrophobic (green), and neutral polar/Gly (white) residues. The orientations match those in (c). A cylinder model of the regulatable unit, colored and positioned as in Fig. 1e, is provided for orientation of the leftmost structures in (b–d).

the inhibitory module to the recognition helix H3 of the DNA-binding interface (Fig. 7b).

Phosphorylation of ΔN279 caused a similar, but stronger PRE effect (Fig. 7a and c). Once again, relaxation enhancement was observed within the inhibitory module, H1, and H3. However, in the case of $\Delta N279^{2P}$, a larger number of residues at this interface were affected by paramagnetic relaxation. Together, these data indicated that the SRR* interacts with one face of the regulatable unit, and that this effect is enhanced upon the phosphorylation of S282 and S285. Residues within the same region also displayed chemical shift perturbations due to the presence of the SRR* (Fig. 6). We postulate that these

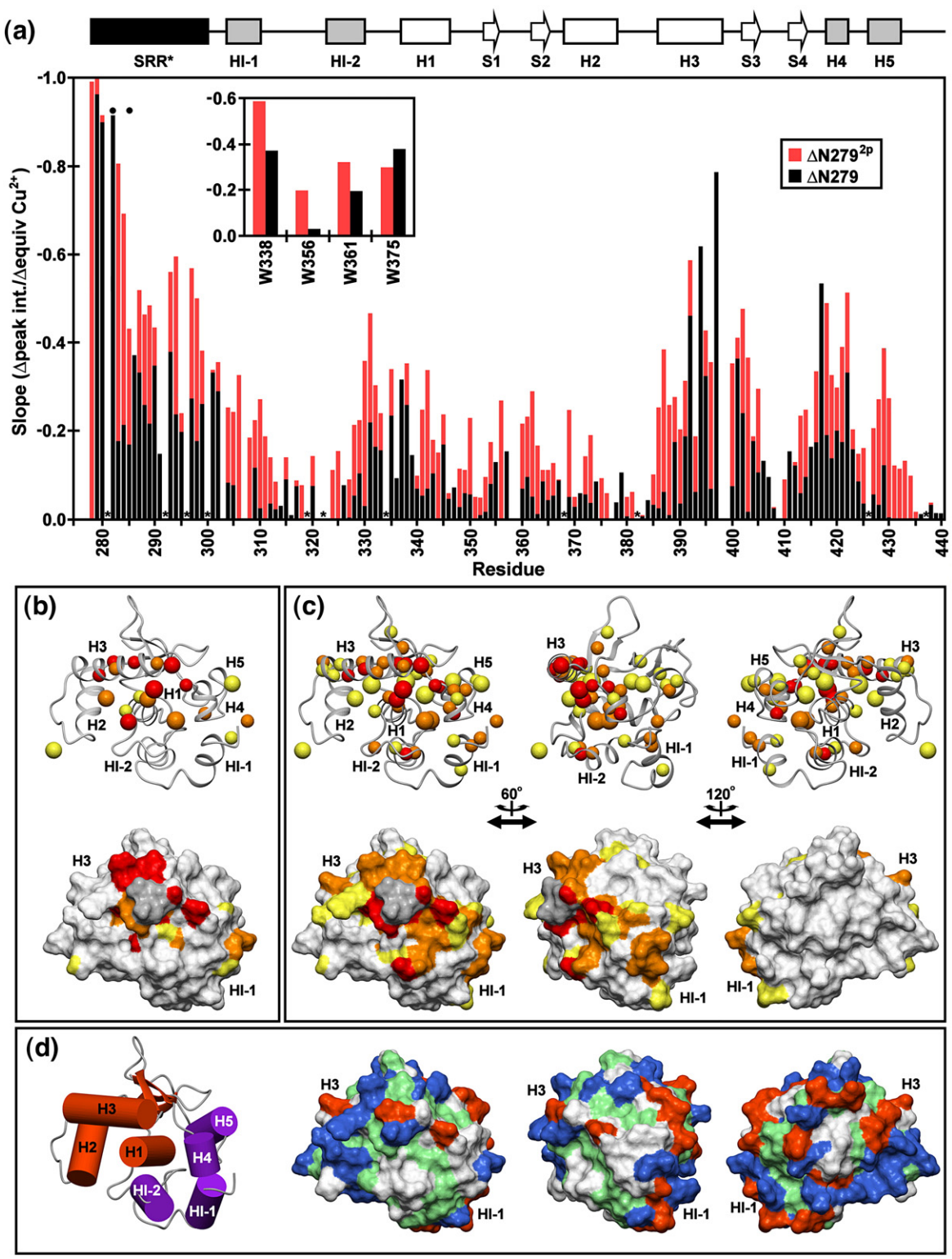

Fig. 7 (*legend on previous page*)

PREs and spectral shift changes reflect direct interactions of the SRR* to allosterically modulate the structure and dynamics of the regulatable unit. This correspondence indicates also that phosphorylation contributes to autoinhibition by reinforcing these interactions.

SRR* interactions are not predominantly electrostatic

The SRR* is net negatively-charged due to four asparate/glutamate residues, and this charge is increased upon phosphorylation of S282 and S285 (Fig. 1b). These observations prompted the hypothesis that electrostatic forces might mediate the interactions between the SRR and the regulatable unit. To test this possibility, urea denaturation assays were done with $\Delta N244^{5P}$ under conditions of varying ionic strength. Surprisingly, there was little change in the stability of $\Delta N244^{5P}$ upon increasing the concentration of KCl from 50 mM to 500 mM (Fig. 2c). In contrast, the mid-point of the denaturation profile of ΔN244 remained similar at 50 mM and 100 mM KCl, yet showed a loss of cooperativity at 500 mM KCl. These data argue against a major role of electrostatic interactions in the global stabilization of ΔN244 by SRR phosphorylation. To explore this phenomenon further, we also compared the amide chemical shifts of ΔN279 and $\Delta N279^{2P}$ under native conditions at varying ionic strengths (Fig. 6a and b; Supplementary Data Fig. S5). For most (~2/3) residues, the magnitude of shift perturbations resulting from phosphorylation increased when the concentration of NaCl was lowered from 500 mM to 0 mM. Thus, the effect of SRR* phosphorylation on the regulatable unit is partially ionic strength-dependent. However, the observation of clear spectral differences between ΔN279 and $\Delta N279^{2P}$ at even 500 mM NaCl suggests that electrostatic interactions are not the dominant driving force for phosphorylation-dependent autoinhibition.

Discussion

Allosteric model of autoinhibition

Here, we describe new insights into the mechanism of phosphorylation-dependent autoinhibition of Ets-1 DNA binding. Our previous allosteric model for autoinhibition was developed from two major lines of evidence; namely, the labile nature of helix HI-1, including its unfolding upon DNA binding, and the impact of both the SRR and its phosphorylation on the dynamic character of the ETS domain and flanking inhibitory module.[6–10,19] The model proposes that a conformational equilibrium exists for the ETS domain and associated inhibitory module in the absence of DNA, and that this equilibrium can be the target of regulation by the flanking SRR, as well as by its phosphorylation (Fig. 1c). This study expands the evidence for the allosteric mechanism by showing direct evidence for the phosphorylation-dependent dampening of the fast timescale mobility of the predominantly unstructured SRR* in ΔN279, along with dampening of the internal dynamics (ΔN279) and enhanced stability (ΔN279 and ΔN244) of the regulatable unit. In addition, new mechanistic insights come from mapping the intramolecular interactions between SRR* and the regulatable unit, including the recognition helix, via chemical shift and PRE analyses. Importantly, the analyses were performed on ΔN279, a more easily manipulatable deletion fragment containing a truncated SRR* with two phosphoacceptor serines. The presence of residues 279–300 from the SRR increases the autoinhibition of ΔN279 by ~15-fold, from the modest level exhibited by the regulatable unit (ΔN301) to a level similar to that observed with native Ets-1 and ΔN244.[6,8,9] Phosphorylation of S282 and S285 reinforces this effect by an additional ~100-fold (Fig. 1e), again, to levels observed with native Ets-1 and ΔN244.[6,12]

Surprisingly, although required for autoinhibition, the truncated SRR* lacks any predominant structure in ΔN279 or $\Delta N279^{2P}$, as evidenced by random coil chemical shifts, the absence of detectable ^{1}H-^{1}H NOE interactions to the regulatable unit, and minimal protection from amide HX (Figs. 3 and 4; Supplementary Data Fig. S2). However, the conformational disorder of the SRR* is not completely unrestricted, as ^{15}N relaxation measurements revealed that the SRR* exhibits nanosecond to picosecond timescale mobility greater than that of the well-ordered regions of the regulatable unit, yet dampened relative to the highly flexible residues at the termini of a deletion fragment such as ΔN244 (Fig. 5; Supplementary Data Fig. S1). The availability of ΔN279 in both its unphosphorylated and phosphorylated state also enabled analysis that demonstrated the mobility of the SRR* was further, albeit modestly, dampened upon phosphorylation. These observations support the original allosteric model of autoinhibition by correlating phosphorylation effects on reducing SRR* dynamics with increasing effectiveness of the SRR* in inhibiting DNA binding.

The role of the truncated SRR* in mediating autoinhibition was investigated thermodynamically and spectroscopically by analyzing the effects of its presence and its phosphorylation on the regulatable unit. The SRR* stabilizes the regulatable unit against fluctuations that lead to amide HX (Fig. 4). Phosphorylation of S282 and S285 enhances this effect, as observed most notably for the labile helix HI-1, which had been shown to be unfolded in the DNA-bound state.[9,10] Within the context of ΔN244, phosphorylation also dramatically stabilizes the regulatable unit against thermal- and denaturant-induced global unfolding (Fig. 2) and dampens millisecond to microsecond timescale motions detected by relaxation dispersion experiments.[6] Detailed chemical shift comparisons between ΔN301, ΔN279, and $\Delta N279^{2P}$ indicate that the truncated SRR* either directly or indirectly perturbs the structure of a contiguous region of the

regulatable unit encompassing the inhibitory module and helices H1 and H3 of the ETS domain, and that the perturbations increase with phosphorylation (Fig. 6). Interestingly, a comparison of SSP scores, which predict secondary structure from chemical shift information, shows small but distinct patterns of increased α-helical and β-strand values for several regions of $\Delta N279^{2P}$ *versus* ΔN279, including the N-terminus of HI-1 and H4 in the inhibitory module and S1, S2, and the DNA-recognition helix H3 in the ETS domain (Fig. 3c). Although it is unclear how to interpret SSP scores for folded regions of proteins,[24] based on the correlation of secondary chemical shifts and dynamics noted by Wishart and co-workers,[22] this suggests that the spectral changes occurring upon phosphorylation also reflect the stabilization of the regulatable unit into a more rigid conformation.

In our previous work on Ets-1 DNA binding, we used similar data to propose an allosteric mechanism of regulation. According to this model, the ETS domain and inhibitory module pack together to form a regulatable unit that is conformationally flexible, as shown by amide HX, ^{15}N and ^{13}C relaxation, and proteolysis measurements.[6,8] The presence of the SRR and increasing levels of phosphorylation progressively shift the equilibrium structure and dynamics of the regulatable unit to a more rigid state with reduced DNA affinity. A co-linear change in the amide chemical shifts of residues in the inhibitory module and DNA-binding interface that correlates with increasing autoinhibition provided clear evidence for an equilibrium between dynamic-active and rigid-inactive states.[6] Such a diagnostic co-linear change was also exhibited by ΔN279 and $\Delta N279^{2P}$ (Fig. 6d). Note that this mechanism is allosteric from two complementary perspectives: DNA binding via the ETS domain is coupled to a conformational change in the inhibitory module that is highlighted by the unfolding of HI-1, a helix distal to the "DNA effector", and the phosphorylatable SRR serves as an "intramolecular effector", shifting the conformation, dynamic properties, and stability of the regulatable unit to a more rigid inactive state, refractory to DNA binding.

To explore the mechanism by which the SRR, a predominantly unstructured and conformationally flexible element, could be an intramolecular allosteric effector, we sought experimental evidence for its direct interaction with the regulatable unit. PRE effects, measured using Cu^{2+} bound to the ATCUN motif of ΔN279 (Fig. 7), revealed transient interactions consistent with the flexible, yet not unrestricted, dynamic properties of the SRR. Phosphorylation enhanced the magnitude or lifetime of these interactions. These PRE effects correlate with the partially dampened fast timescale mobility and reduced HX of the SRR* in $\Delta N279^{2P}$ *versus* ΔN279 (Figs. 3–6). In addition, PRE mapping demonstrated that the truncated SRR* interacts with both the inhibitory module and the DNA recognition helix H3 (Figs. 6 and 7) along one contiguous surface of the regulatable unit. Many of these same residues displayed chemical shift perturbations upon addition of the SRR* and further upon phosphorylation. As noted previously, these elements are linked by a dynamic, hydrophobic network that includes the intervening helix H1 of the ETS domain.[6] Thus, we speculate that transient surface contacts made by the SRR allosterically transduce effects broadly through the regulatable unit.

Electrostatic forces are not dominant for allosteric regulation

We next considered the possible physicochemical nature of the transient interactions leading to allosteric control of Ets-1 DNA binding. The SRR* has four negatively-charged residues (D284, D287, E289, and D290) in segments required for autoinhibition, as demonstrated through deletion analysis (Fig. 1e). Phosphorylation of S282 and S285 increases further the net negative charge of the SRR*. Also, many of the residues most affected by the presence of the SRR*, as shown by PRE measurements, lie along the positively-charged DNA-binding interface of the ETS domain. Accordingly, we asked whether electrostatic interactions might have a role in mediating the transient interactions of the SRR* with the regulatable unit. Previously, we observed that the millisecond to microsecond timescale motions of ΔN279 and $\Delta N279^{2P}$ detected by NMR relaxation-dispersion measurements were dampened in buffers of reduced salt concentration (data not shown).[6] Also, the phosphorylation-dependent chemical shift perturbations of the regulatable unit by the SRR* generally decreased with increasing ionic strength (Fig. 6a and b; Supplementary Data Fig. S5), suggesting some electrostatic contributions to autoinhibition. However, even in 500 mM NaCl, clear differences existed between the ^{1}H-^{15}N HSQC spectra of $\Delta N279^{2P}$ and ΔN279. More dramatically, the stability of $\Delta N244^{5P}$ against urea-induced denaturation showed no change between measurements made in 50 mM and 500 mM KCl (Fig. 2). It is difficult to gauge the extent of screening expected for the intramolecular association of the phosphorylated SRR* with the regulatory unit. Nevertheless, persistent NMR spectral perturbations and the lack of a significant difference in the $[urea]_{1/2}$ of $\Delta N244^{5P}$ over this large range of ionic strength argues strongly against a dominant role of electrostatic interactions in mediating the phosphorylation-dependent stabilization of the regulatable unit, and by inference, in DNA-binding autoinhibition.

Alternatively, we note that the truncated SRR* contains several hydrophobic amino acids (V280, Y283, F286, Y288, Y291, and L295) immediately adjacent to negatively-charged Asp or Glu residues and the phosphoacceptor serines. Perhaps the association of the SRR* with the regulatable unit involves hydrophobic contacts to that neutral side-chains on a surface patch between HI-1 and H3 that also show PRE effects upon addition of Cu^{2+} to ΔN279 (Fig. 7d). A mechanistic model for this could involve phosphorylation-dependent changes in

some fluctuating aromatic/hydrophobic clustering within the SRR to enable greater aromatic/hydrophobic interaction with the regulatable unit. All known Ets-1 vertebrate orthologs display overall >95% identity at the amino acid level, and thus the importance of these hydrophobic residues is not predictable from homology arguments. However, we note that the above residues lie in a region of Ets-1 that shares >80% amino acid sequence conservation relative to highly related Ets-2, which also displays autoinhibitory properties. Five of the six hydrophobic residues are conserved in 16 Ets-1 and Ets-2 vertebrate orthologs, with the sixth being a variant only in mouse Ets-1. Site-directed mutational studies of these individual residues within the SRR* should help define the relative roles of electrostatic and hydrophobic interactions in autoinhibition.

A possible steric component to regulation of DNA binding

One feature of our findings suggests additional possible mechanistic contributions to the inhibition of DNA binding. PRE measurements demonstrated that the SRR* transiently interacts with the DNA-binding interface of the ETS domain. Such localization of the negatively-charged phosphorylated SRR near the recognition helix H3 could reinforce autoinhibition by sterically blocking and/or electrostatically repelling DNA. Previous kinetic studies revealed that autoinhibition results mainly from a reduction in the lifetime of the bound Ets-1/DNA complex.[19] However, a small reduction in association rates, as would be expected for steric blockage mechanism, was also observed. Note that a global electrostatic repulsion mechanism is unlikely as disruption of the inhibitory module through mutation of its hydrophobic core leads to loss of autoinhibition and insensitivity to phosphorylation effects without changing the net charge of the Ets-1 fragments studied.[10–12] That is, the simple presence of the SRR and phosphorylated serine residues does not attenuate DNA binding affinity. Together, these data indicate that the allosteric and any possible steric contributions to autoinhibition are likely intimately linked. That is, the integrity of the inhibitory module is thermodynamically and structurally coupled to the proper juxtaposition of the SRR with respect to regulatory unit, as required for both modulating the equilibrium populations of dynamic-active and rigid-inactive states and for possible blockage of the DNA-binding interface. Although the allosteric component of this mechanism is well established, dissecting the nature and magnitude of the steric contribution requires more detailed mutational and kinetic analysis.

Adoption of structure is not required for SRR regulation of Ets-1 autoinhibition

Most studies of intrinsically disordered protein segments report a transition to a stable conformation in order to function (however, see Ref. 29).[1] In contrast, our previous work and the new results presented here show that the multiply phosphorylated SRR of Ets-1 is able to inhibit binding by over two orders of magnitude in K_D despite its predominantly unstructured and flexible character. A similar example of a functionally important regulator that retains disorder both before and after multiple phosphorylation events is found with the yeast cyclin-dependent kinase inhibitor Sic1.[30] However, Sic1 displays a switch-like behavior, in that it associates with the WD40 domain of the SCF ubiquitin ligase subunit Cdc4 only after any six of its nine possible sites have been phosphorylated.[31] Each of the phosphorylation sites is a sub-optimal binding motif for the WD40 domain, and the switch has been proposed to result from a threshold level of cumulative "polyelectrostatic" interactions necessary for net binding of Sic1 to Cdc4.[30] In the case of Ets-1, however, electrostatic forces do not appear to be crucial to the autoinhibitory mechanism and variable or "rheostat-type" regulation, rather than an all-or-none switch, is accomplished by progressive addition/removal of phosphates to the flexible SRR segment.[6] As part of this rheostatic mechanism, a correlation between dampened nanosecond to picosecond timescale dynamics of the SRR, but not adoption of a predominant structure, and reduced millisecond to microsecond conformational flexibility of the regulatable ETS domain and inhibitory module are observed. A link between changes in the fast motions of flexible segments to regulation of intermediate timescale dynamics has been documented recently for enzymatic catalysis.[32,33] Further characterization of such dynamic mechanisms in biological processes is of great importance due to the preponderance of unstructured protein segments encoded by the genome.

Flexible SRR allows for rapid response to cell signals

The properties of Ets-1 are ideal for rapid and sensitive integration of signals. Intrinsically disordered regions, such as the SRR, are frequent targets of post-translational modification. In their unstructured forms, they allow unfettered access to the chemical moieties of the sidechains, and have low energy barriers to adopting the conformation required for rapid binding and modification via signal transduction machinery. For example, in response to Ca^{2+} release, Ca^{2+} dependent kinases, such as CamKII, are activated and, in turn, phosphorylate multiple serines within the flexible SRR. However, as noted above, phosphorylation does not induce and persistent structure within the SRR, nor does it cause stable binding of this region to the regulatable unit of Ets-1. Instead, the phosphorylated SRR region stays available for modification by other kinases or, importantly, phosphatases such as calcineurin, which can also become activated depending on the nature and length of Ca^{2+} stimulation.[34] Furthermore, we showed earlier that

increasing the phosphorylation level of the SRR progressively attenuates the affinity of Ets-1 for DNA. Thus, by maintaining flexibility, regardless of the modification state, the SRR can be modified rapidly and the DNA-binding affinity of Ets-1 fine-tuned by the kinase/phosphatase balance in the cell. On the basis of these structural and biochemical properties, the SRR of Ets-1 can serve as an integrator for Ca^{2+} signaling, thereby modulating gene expression at the level of DNA binding with exquisite sensitivity.

Methods

Sample expression, purification, and phosphorylation

Expression and purification of Ets-1 fragments were performed according to previous methods.[6] Genes encoding ΔN244, ΔN280, ΔN286, ΔN292, ΔN296, and ΔN301 were sub-cloned into the pET22b vector (Invitrogen), expressed in *E. coli* BL29(λDE3) cells, and purified by conventional ion-exchange and gel-filtration chromatography. The gene encoding ΔN279 with an N-terminal His_6 tag was cloned into the pET28a vector, followed by mutation of the codon from the vector encoding a methionine to the native R279 by the QuikChange method (Stratagene). ΔN279 was expressed in *E. coli* BL29(λDE3) cells. After lysis by sonication into 50 mM Tris, pH 7.5, 500 mM NaCl, 1 mM PMSF, 1 mM DTT, 20 mM imidazole, and centrifugation at 40,000 rpm for 40 min, the supernatant was loaded onto a 5 mL nickel Sepharose column (GE Biosciences), and eluted in the same buffer with a gradient of 20 mM–500 mM imidazole. Peak fractions were combined with thrombin (5 units/mg ΔN279; Sigma) and 2.5 mM $CaCl_2$, dialyzed overnight against 20 mM sodium citrate, pH 5.3, 100 mM NaCl, 1 mM DTT, and purified as described above for non-tagged constructs. After thrombin cleavage, the resulting ΔN279 contains three additional, non-native N-terminal residues (Gly-Ser-His). [U-^{15}N]-, [U-^{13}C,^{15}N]-, and [U-^{15}N]-selectively [*methyl*-^{13}C] Ile/Val/Leu labeled samples of ΔN244 and ΔN279 were prepared as described.[6,8] Sample concentrations were quantified by measuring absorbance at 280 nm using a predicted ε_{280} of 38120 M^{-1} cm^{-1} (ExPASy Protparam‡).

All Ets-1 fragments were phosphorylated using the same published protocol.[6] Samples at a final concentration of ~25 μM were incubated for 1 h at 30 °C in 50 mM Hepes, pH 7.5, 10 mM magnesium acetate, 0.5 mM $CaCl_2$, 2 mM DTT, 1 μM calmodulin, 200 nM calmodulin kinase II, 1 mM ATP. The reaction mixtures were then diluted 1:10 with 25 mM Tris, pH 7.9, 10% (v/v) glycerol, 1 mM EDTA, loaded onto a strong anion-exchange column (MonoQ, Pharmacia), and eluted with a 50 mM–400 mM KCl gradient. Peak fractions were pooled, analyzed by electrospray ionization mass spectrometry, and stored at 4 °C.

Electrophoretic mobility-shift assays

EMSAs were performed on Ets-1 fragments as described,[6,12] using a high-affinity ETS binding site composed of a 9 bp consensus site (underlined) embedded in the following complimentary 27-mers that include 4 bp overhangs:

5′-TCGACGGCCAAGCCGGAAGTGAGTGCC-3′ (top strand);
5′-TCGAGGCACTCACTTCCGGCTTGGCCG-3′ (bottom strand).

Circular dichroism and denaturation measurements

Circular dichroism (CD) spectra of 30 μM protein samples, dialyzed into 25 mM potassium phosphate, pH 7.9, 100 mM KCl, 1 mM β-mercaptoethanol, 0.1 mM EDTA, were recorded using a Jasco J-720 spectropolarimeter with a 0.1 cm pathlength cuvette. The final spectra represent the average of six scans at 25 °C. Thermal denaturation measurements were performed using a water-circulating temperature-controlled 0.5 cm pathlength cuvette. The water temperature was regulated by a Neslab RET-110. Samples were allowed to equilibrate for 10 min between temperature changes, and the final spectra represent the average of three scans at each temperature. Urea denaturation measurements were carried out with a series of protein samples in 0–8 M urea. A 10 M urea stock was prepared with 0.2 μM filtered dialysis buffer, and then samples were added to a fixed volume of protein solution to generate equimolar samples at the desired concentrations of urea. The CD signal θ_{obs} of each sample was measured at 222 nm and 25 °C with an AVIV 62DS spectropolarimeter. The value reported represents the average of readings acquired at a rate of 1 s^{-1} for 100 s. Data were analyzed by normalizing the blank-corrected CD signal *versus* the most negative signal recorded (θ_{min}):

$$y_{obs} = 1 - \theta_{obs}/\theta_{min}$$

followed by fitting to a standard two-state equation for urea-induced protein unfolding:[35]

$$y_{obs} = \frac{y_F + y_U(e^{-(m([urea]_{1/2}-[urea])/RT)}}{1 + e^{-(m([urea]_{1/2}-[urea])/RT)}}$$

with $y_F = y_F^o + b_F[urea]$ and $y_U = y_U^o + b_U[urea]$. In this equation, y_F^o and y_U^o are the folded and unfolded baseline intercepts, b_f and b_u are the folded and unfolded baseline slopes, m is the linear dependence of free energy of unfolding on [urea], and $[urea]_{1/2}$ is the midpoint concentration of denaturant for unfolding.

Spectral assignments

All NMR spectra were recorded on a cryoprobe-equipped Varian Inova 600 MHz spectrometer at 28 °C. A typical NMR sample consisted of 0.1–0.3 mM protein in 0.35–0.50 mL of 20 mM phosphate buffer (pH 6.5) containing 0.02% (w/v) NaN_3, 5 mM DTT, 10% (v/v) ^2H_2O, and either 0, 50, or 500 mM NaCl. The sample conditions were adjusted by dialysis or by concentration and buffer exchange using MicroSep 3K (Pall Life Sciences) or Amicon Ultra 5K Centrifugal Filter Devices (Millipore Corp.). Spectral processing and analysis were performed with NMRpipe[36] and Sparky§.

‡ http://ca.expasy.org/tools/protparam.html

§ http://www.cgl.ucsf.edu/home/sparky/

Assignments for the backbone and selected sidechain ^{1}H, ^{15}N, and ^{13}C resonances of ΔN279 and ΔN279^{2P} were obtained using multidimensional NMR experiments acquired on a series of [U-^{15}N]-, [U-^{13}C,^{15}N]-, or [U-^{15}N]-selectively [*methyl* ^{13}C]-Ile/Val/Leu-labeled proteins, as described.[8] Simultaneous 3D ^{15}N,^{13}C-NOESY-HSQC, centered on the methyl (τ_m = 140 ms), aliphatic (τ_m = 150 ms), and aromatic (τ_m = 150 ms) ^{13}C regions, as well as 3D ^{15}N NOESY-HSQC (τ_m = 150 ms) spectra were acquired for both ΔN279 and ΔN279^{2P}. The first three residues (Gly-Ser-His) were not assignable due to rapid amide HX. Ionic strength-dependent chemical shifts were obtained from ^{1}H-^{15}N HSQC spectra recorded with ~0.5 mL samples of ~0.1–0.3 mM [^{15}N]protein, initially in 0 mM NaCl, to which samples of sample buffer containing 5 M NaCl were added. Chemical shift perturbations were calculated from the combined ^{1}H and ^{15}N shift differences as:

$$\Delta\delta = \sqrt{(\Delta\delta_H)^2 + (0.1 * \Delta\delta_N)^2}$$

and mapped onto the NMR-derived structure of ΔN301 (PDB accession code *1R36*.pdb) using MolMol.[37]

Backbone amide hydrogen exchange

Slow amide proton-deuterium HX rates, k_{ex}, for ΔN279 were measured from a series of ^{1}H-^{15}N HSQC spectra recorded after rapid transfer of the $^{[15N]}$protein into $^{2}H_2O$ buffer (28 °C, pH* 6.5, 500 mM NaCl), as described for ΔN301.[8] Rapid amide proton–proton HX rates were acquired for both ΔN279 and ΔN279^{2P} (28 °C, 500 mM NaCl, pH 7.5 and pH 8.25) using the CLEANEX-PM method.[38] Predicted exchange rates, k_{pred}, for an unstructured protein containing the ΔN279 sequence were calculated with the program SPHERE[39] using poly-D,L-alanine reference data corrected for amino acid type, pH, temperature, and isotope effects.[40,41] In the case of ΔN279^{2P}, reference k_{pred} values for phosphorylated serines were estimated by replacing S282 and S285 in the sequence with aspartates. Amide-specific protection factors were calculated as the ratio k_{pred}/k_{ex}. As such, a protection factor can be interpreted as the inverse of an equilibrium constant describing fluctuations between a closed, non-exchangeable state and a transiently exposed, exchange-competent state, and thus provides a measure of the residue-specific free energy changes, $\Delta G^{o}_{HX} = RT \ln(k_{pred}/k_{ex})$, governing local or global conformational equilibria detected by HX.

Backbone amide relaxation

Backbone amide ^{15}N relaxation parameters of the ^{15}N-labeled ΔN279 and ΔN279^{2P} samples in both 50 mM and 500 mM NaCl were acquired at 28 °C, as described.[42] Curve fitting and relaxation rate calculations were performed with either Sparky or a Matlab (The MathWorks, Inc.) macro supplied by W.-Y. Choy (University of Toronto). Error analysis was facilitated by a 200-step Monte Carlo routine. Due to the dynamic nature of residues 279–300, only per-residue Lipari-Szabo model-free fits[20] were obtained using a Matlab macro provided by L.E. Kay (University of Toronto).

ATCUN paramagnetic relaxation enhancement measurements

Immediately before Cu^{2+} titrations, ΔN279 and ΔN279^{2P} samples were exchanged into 20 mM Bis-Tris (pH 6.5), 0.02% NaN_3, 500 mM NaCl with no reducing agent. These conditions were necessary to avoid the formation of insoluble Cu^{2+} complexes and the reduction of paramagnetic Cu^{2+} to diamagnetic Cu^{2+}. The Cu^{2+} titrations were performed by adding samples of a stock solution of 5 mM $CuSO_4$ in this buffer to ~0.5 mL of a solution containing 0.1–0.2 mM protein. Relatively low concentrations of protein were used to limit the possible effects of non-specific Cu^{2+} binding or intermolecular paramagnetic relaxation. The titrations were monitored with ^{1}H-^{15}N and/or ^{1}H-^{13}C HSQC spectra. An approximate 1:1 ratio of Cu^{2+}:protein was ascertained when the normalized intensities of the methyl and amide peaks of V280 approached a baseline value, typically 0–5% of the original value.

^{1}H-^{15}N HSQC-detected amide $^{1}H^{N}$ T_2 (=$1/R_2$) relaxation measurements[28] of ΔN279 and ΔN279^{2P} with 0 and ~1 equivalent of $CuSO_4$ were recorded at 28 °C. Residue-specific amide PRE values were calculated as:

$$\Delta R_2 = R_2(Cu^{2+}\text{bound}) - R_2(Cu^{2+}\text{free})$$

Alternatively, PRE values were evaluated qualitatively during the Cu^{2+} titration by plotting the normalized ^{1}H-^{15}N and/or ^{1}H-^{13}C-HSQC peak intensities *versus* the equivalents of Cu^{2+} added. Since a linear relationship between the reduction of peak intensities and added equivalents of Cu^{2+} was observed due to tight binding, linear regression analyses were performed using data points ranging from 0:1 ~1:1 Cu^{2+} to protein ratios. Slopes decreasing from 0 to −1.0 represent HSQC peaks are increasingly affected by high-affinity Cu^{2+} binding to the limit of being broadened beyond detection upon complete saturation of the ATCUN motif.

Acknowledgements

We are grateful to Lewis Kay, Algirdas Velyvis, Wing-Yiu (James) Choy, and Oscar Millet for providing data analysis programs, and to Mark Okon for assistance with NMR spectroscopy. This research was supported by grants from the National Cancer Institute of Canada with funds from the Canadian Cancer Society (to L.P.M.) and the National Institutes of Health grants GM38663 (to B.J.G.) and CA42014-I (to the Huntsman Cancer Institute for support of core facilities). B.J.G. acknowledges funding from the Huntsman Cancer Institute/Huntsman Cancer Foundation. Instrument support was provided by the Canadian Institutes for Health Research, the Protein Engineering Network of Centres of Excellence, the Canadian Foundation for Innovation, the British Columbia Knowledge Development Fund, the UBC Blusson Fund, and the Michael Smith Foundation for Health Research. The work done by M.A.P. was performed under NIH grants T32-CA93247 and GM08537, and he is currently a fellow of the Leukemia and Lymphoma Society (5416-07).

Supplementary Data

Supplementary data associated with this article can be found, in the online version, at doi:10.1016/j.jmb.2008.07.064

References

1. Dyson, H. J. & Wright, P. E. (2005). Intrinsically unstructured proteins and their functions. *Nature Rev. Mol. Cell Biol.* **6**, 197–208.
2. Mittag, T. & Forman-Kay, J. D. (2007). Atomic-level characterization of disordered protein ensembles. *Curr. Opin. Struct. Biol.* **17**, 3–14.
3. Iakoucheva, L. M., Radivojac, P., Brown, C. J., O'Connor, T. R., Sikes, J. G., Obradovic, Z. & Dunker, A. K. (2004). The importance of intrinsic disorder for protein phosphorylation. *Nucleic Acids Res.* **32**, 1037–1049.
4. Steinmetz, M. O. (2007). Structure and thermodynamics of the tubulin-stathmin interaction. *J. Struct. Biol.* **158**, 137–147.
5. Sugase, K., Dyson, H. J. & Wright, P. E. (2007). Mechanism of coupled folding and binding of an intrinsically disordered protein. *Nature*, **447**, 1021–1025.
6. Pufall, M. A., Lee, G. M., Nelson, M. L., Kang, H.-S., Velyvis, A., Kay, L. E. *et al.* (2005). Variable control of Ets-1 DNA binding by multiple phosphates in an unstructured region. *Science*, **309**, 142–145.
7. Pufall, M. A. & Graves, B. J. (2002). Autoinhibitory domains: modular effectors of cellular regulation. *Ann. Rev. Cell Dev. Biol.* **18**, 421–462.
8. Lee, G. M., Donaldson, L. W., Pufall, M. A., Kang, H.-S., Pot, I., Graves, B. J. & McIntosh, L. P. (2005). The structural and dynamic basis of Ets-1 DNA binding autoinhibition. *J. Biol. Chem.* **280**, 7088–7099.
9. Petersen, J. M., Skalicky, J. J., Donaldson, L. W., McIntosh, L. P., Alber, T. & Graves, B. J. (1995). Modulation of transcription factor Ets-1 DNA-binding: DNA-induced unfolding of an alpha-helix. *Science*, **269**, 1866–1869.
10. Garvie, C. W., Pufall, M. A., Graves, B. J. & Wolberger, C. (2002). Structural analysis of the autoinhibition of Ets-1 and its role in protein partnerships. *J. Biol. Chem.* **277**, 45529–45536.
11. Wang, H., McIntosh, L. P. & Graves, B. J. (2002). Inhibitory module of Ets-1 allosterically regulates DNA binding through a dipole-facilitated phosphate contact. *J. Biol. Chem.* **277**, 2225–2233.
12. Cowley, D. O. & Graves, B. J. (2000). Phosphorylation represses Ets-1 DNA binding by reinforcing autoinhibition. *Genes Dev.* **14**, 366–376.
13. Goetz, T. L., Gu, T. L., Speck, N. A. & Graves, B. J. (2000). Auto-inhibition of Ets-1 is counteracted by DNA binding cooperativity with core-binding factor alpha 2. *Mol. Cell. Biol.* **20**, 81–90.
14. Baillat, D., Bègue, A., Stéhelin, D. & Aumercier, M. (2002). Ets-1 transcription factor binds cooperatively to the palindromic head to head Ets-binding sites of the stromelysin-1 promoter by counteracting autoinhibition. *J. Biol. Chem.* **277**, 29386–29398.
15. Lamber, E. P., Vanhille, L., Textor, L. C., Kachalova, G. S., Sieweke, M. H. & Wilmanns, M. (2008). Regulation of the transcription factor Ets-1 by DNA-mediated homo-dimerization. *EMBO J.* **27**, 2006–2017.
16. Kern, D. & Zuiderweg, E. R. P. (2003). The role of dynamics in allosteric regulation. *Curr. Opin. Struct. Biol.* **13**, 748–757.
17. Liu, H. & Grundstrom, T. (2002). Calcium regulation of GM-SCF by calmodulin-dependent kinase II phosphorylation of Ets1. *Mol. Biol. Cell*, **13**, 4497–4507.
18. Skalicky, J. J., Donaldson, L. W., Petersen, J. M., Graves, B. J. & McIntosh, L. P. (1996). Structural coupling of the inhibitory regions flanking the Ets domain of murine Ets-1. *Protein Sci.* **5**, 296–309.
19. Jonsen, M. D., Petersen, J. M., Xu, Q. & Graves, B. J. (1996). Characterization of the cooperative function of inhibitory sequences of Ets-1. *Mol. Cell. Biol.* **16**, 2065–2073.
20. Lipari, G. & Szabo, A. (1982). Model-free approach to the interpretation of nuclear magnetic-resonance relaxation in macromolecules. 1. Theory and range of validity. *J. Am. Chem. Soc.* **104**, 4546–4559.
21. Wishart, D. S. & Sykes, B. D. (1994). The C-13 chemical-shift index — a simple method for the identification of protein secondary structure using C-13 chemical-shift data. *J. Biomol. NMR*, **4**, 171–180.
22. Berjanskii, M. V. & Wishart, D. S. (2005). A simple method to predict protein flexibility using secondary chemical shifts. *J. Am. Chem. Soc.* **127**, 14970–14971.
23. Cornilescu, G., Delaglio, F. & Bax, A. (1999). Protein backbone angle restraints from searching a database for chemical shift and sequence homology. *J. Biomol. NMR*, **13**, 289–302.
24. Marsh, J. A., Singh, V. K., Jia, Z. & Forman-Kay, J. D. (2006). Sensitivity of secondary structure propensities to sequence differences between alpha- and gamma-synuclein: Implications for fibrillation. *Protein Sci.* **15**, 2795–2804.
25. Bienkiewicz, E. A. & Lumb, K. J. (1999). Random-coil chemical shifts of phosphorylated amino acids. *J. Biomol. NMR*, **15**, 203–206.
26. Clore, G. M., Tang, C. & Iwahara, J. (2007). Elucidating transient macromolecular interactions using paramagnetic relaxation enhancement. *Curr. Opin. Struct. Biol.* **17**, 603–616.
27. Harford, C. & Sarkar, B. (1997). Amino terminal Cu (ii)- and Ni(ii)-binding (ATCUN) motif of proteins and peptides: Metal binding, DNA cleavage, and other properties. *Acc. Chem. Res.* **30**, 123–130.
28. Donaldson, L. W., Skrynnikov, N. R., Choy, W. Y., Muhandiram, D. R., Sarkar, B., Forman-Kay, J. D. & Kay, L. E. (2001). Structural characterization of proteins with an attached ATCUN motif by paramagnetic relaxation enhancement NMR spectroscopy. *J. Am. Chem. Soc.* **123**, 9843–9847.
29. Tompa, P. & Fuxreiter, M. (2008). Fuzzy complexes: polymorphism and structural disorder in protein-protein interactions. *Trends. Biochem. Sci.* **33**, 2–8.
30. Borg, M., Mittag, T., Pawson, T., Tyers, M., Forman-Kay, J. D. & Chan, H. S. (2007). Polyelectrostatic interactions of disordered ligands suggest a physical basis for ultrasensitivity. *Proc. Natl Acad. Sci. USA*, **104**, 9650–9655.
31. Nash, P., Tang, X. J., Orlicky, S., Chen, Q. H., Gertler, F. B., Mendenhall, M. D. *et al.* (2001). Multisite phosphorylation of a CDK inhibitor sets a threshold for the onset of DNA replication. *Nature*, **414**, 514–521.
32. Henzler-Wildman, K. A., Lei, M., Thai, V., Kerns, S. J., Karplus, M. & Kern, D. (2007). A hierarchy of timescales in protein dynamics is linked to enzyme catalysis. *Nature*, **450**, 913–927.
33. Henzler-Wildman, K. A., Thai, V., Lei, M., Ott, M., Wolf-Watz, M., Fenn, T. *et al.* (2007). Intrinsic motions along an enzymatic reaction trajectory. *Nature*, **450**, 838–913.
34. Salazar, C., Politi, A. Z. & Hofer, T. (2008). Decoding of calcium oscillations by phosphorylation cycles: analytic results. *Biophys. J.* **94**, 1203–1215.

35. Pace, C. N., Shirley, B. A. & Thomson, J. A. (1989). Measuring the conformational stability of a protein. In Protein Structure – a Practical Approach (Creighton, T. E., ed.), pp. 311–330, IRL Press, Oxford.
36. Delaglio, F., Grzesiek, S., Vuister, G. W., Zhu, G., Pfeifer, J. & Bax, A. (1995). NMRpipe: A multi-dimensional spectral processing system based on UNIX pipes. *J. Biomol. NMR*, **6**, 277–293.
37. Koradi, R., Billeter, M. & Wuthrich, K. (1996). MolMol: a program for display and analysis of macromolecular structures. *J. Mol. Graph.* **14**, 51.
38. Hwang, T. L., van Zijl, P. C. & Mori, S. (1998). Accurate quantitation of water-amide proton exchange rates using the phase-modulated clean chemical exchange (CLEANX-PM) approach with a fast-hsqc (fhsqc) detection scheme. *J. Biomol. NMR*, **11**, 221–226.
39. Zhang, Y.-Z. (1995). Protein and peptide structure and interactions studied by hydrogen exchange and NMR. PhD. thesis, University of Pennsylvania.
40. Bai, Y. W., Milne, J. S., Mayne, L. & Englander, S. W. (1993). Primary structure effects on peptide group hydrogen-exchange. *Protein Struct. Funct. Genet.* **17**, 75–86.
41. Connelly, G. P., Bai, Y. W., Jeng, M. F. & Englander, S. W. (1993). Isotope effects in peptide group hydrogen-exchange. *Protein: Struct. Funct. Genet.* **17**, 87–92.
42. Farrow, N. A., Muhandiram, R., Singer, A. U., Pascal, S. M., Kay, C. M., Gish, G., Shoelson, S. E., Pawson, T., Formankay, J. D. & Kay, L. E. (1994). Backbone dynamics of a free and a phosphopeptide-complexed Src homology-2 domain studied by N-15 NMR relaxation. *Biochemistry*, **33**, 5984–6003.

CHAPTER 3

PHOSPHORYLATION FUNCTIONS WITH AROMATIC RESIDUES IN AN UNSTRUCTURED REGION TO MODULATE THE AUTOINHIBITION OF ETS-1 DNA BINDING

Introduction

According to the long-accepted structure-function paradigm, amino acid sequence determines the three-dimensional structure of a protein, which structure determines its function (Dunker et al., 2008b; Radivojac et al., 2007; Uversky and Dunker, 2010). Advances in experimental characterization and computational prediction of unstructured proteins and protein regions, however, have challenged this well-established dogma (Boehr et al., 2006; Dunker et al., 2002; Dunker et al., 2008a; Dyson and Wright, 2005; Wright and Dyson, 1999). Recent reports predict that over half of the eukaryotic proteome can be classified as intrinsically unstructured, having at least one region, >30 residues in length, displaying an unstructured or disordered profile, and that 25-30% of these proteins are mostly disordered (Dunker et al., 2000; Oldfield et al., 2005; Uversky, 2002). Furthermore, there is an overrepresentation of these intrinsically unstructured proteins (IUPs) in disease-related and biological regulatory processes. For example, close to 75% of known cancer-related proteins, 70% of signaling proteins, and 94% of transcription factors are predicted to have one or more regions of intrinsic disorder (Iakoucheva et al., 2002; Liu et al., 2006; Midic et al., 2009).

The role of conformational disorder has been recognized for its importance in providing flexible linkers between structural domains within modular protein, in bearing sites of posttranslational modification, and ligand binding (Iakoucheva et al., 2004; Uversky and Dunker, 2010). Often, these regions undergo disorder-to-order transitions upon ligand binding (Dyson and Wright, 2005). In contrast, the role of functional IUP regions has only recently been recognized and reported (Wright and Dyson, 1999). Examples have been reported in which these regions have a direct role in regulatory

processes while remaining in an unstructured state (Mittag et al., 2010). The biochemical mechanisms employed by these functional IUPs have yet to be elucidated.

The autoregulation of DNA binding in the transcription factor Ets-1 employs one such region of intrinsic disorder. The serine-rich region (SRR) lacks any predominant structure yet plays an essential role in both constitutive and reinforced autoinhibition of DNA binding (Lee et al., 2008; Pufall et al., 2005). The SRR is positioned N-terminal to the regulatable unit of Ets-1, which consists of the DNA-binding ETS domain as well as four flanking inhibitory helices, which fold into a tertiary structure, termed the *inhibitory module* (Hagman and Grosschedl, 1992; Jonsen et al., 1996; Lim et al., 1992; Skalicky et al., 1996). Together, the SRR, inhibitory module and ETS domain have a DNA-binding affinity comparable to the full-length protein; approximately 10- to 20-fold lower than the full binding potential of the ETS domain (Figure 3.1 A) (Lee et al., 2008; Pufall et al., 2005). Phosphorylation of the SRR by Ca^{2+}/calmodulin-dependent protein kinase II (CaMKII) causes a further one 100-fold decrease in DNA-binding affinity (Figure 3.1 A) (Lee et al., 2008; Pufall et al., 2005).

According to the current model for Ets-1 autoinhibition, a conformational equilibrium of the regulatable unit exists between a flexible-active and a rigid-inactive state. Regulation of this equilibrium affects DNA binding. Though a fixed location is not observed, the SRR makes transient interactions with the regulatable unit and, thus, shifts the equilibrium (Figure 3.1 B) (Lee et al., 2008). Phosphorylation of the SRR enhances the transient localization (Figure 3.1 B) (Lee et al., 2008). The chemical nature of this transient interaction, which allows the SRR to function as an intramolecular effector of DNA-binding affinity over three orders of magnitude, has yet to be

Figure 3.1 Autoinhibition in Ets-1. (A) Schematic representation of Ets-1 and Ets-1 truncations (with and without SRR phosphorylation, P) with corresponding values for equilibrium dissociation constant (K_D) and relative DNA binding affinity. Structural organization of the C-terminal domains; including the serine-rich region (SRR, yellow) and the regulatable unit, comprising the DNA-binding ETS domain (red) and autoinhibitory module (purple). Also shown are the secondary structural elements of ΔN279 (α-helix, cylinder [H]; β-sheet, arrow [S]; and unstructured, rectangle) and primary sequence of amino acid residues 279-300 of the truncated SRR, with a Gly-Ser-His motif remaining after thrombin cleavage of an N-terminal His_6-tag and sites of Ca^{2+}-dependant kinase phosphorylation (S282 and S285; dots). (B) Structural model of autoinhibition in Ets-1 depicting a dynamic, two-state conformational equilibrium (within brackets) between the flexible-active state (center-right), which is competent to bind DNA (far right) and is characterized by a disrupted autoinhibitory module (as indicated by the obvious unfolding of helix HI-1), and the rigid-inactive state (center-left), which is refractory to binding and which is stabilized by phosphorylation and the observed increase in localization of the SRR to the regulatable unit (far left) (adapted from Lee et al., 2008). The Protein Data Bank (PDB) structures displayed are that of DNA-bound ΔN280 (center-right and far-right, 1MDM.pdb) and isolated ΔN301 (center-left and far-left, 1R36.pdb), with SRR and phosphorylated SRR (yellow) added to emphasize the effects of phosphorylation on structural dynamics and localization of the SRR to the regulatable unit.

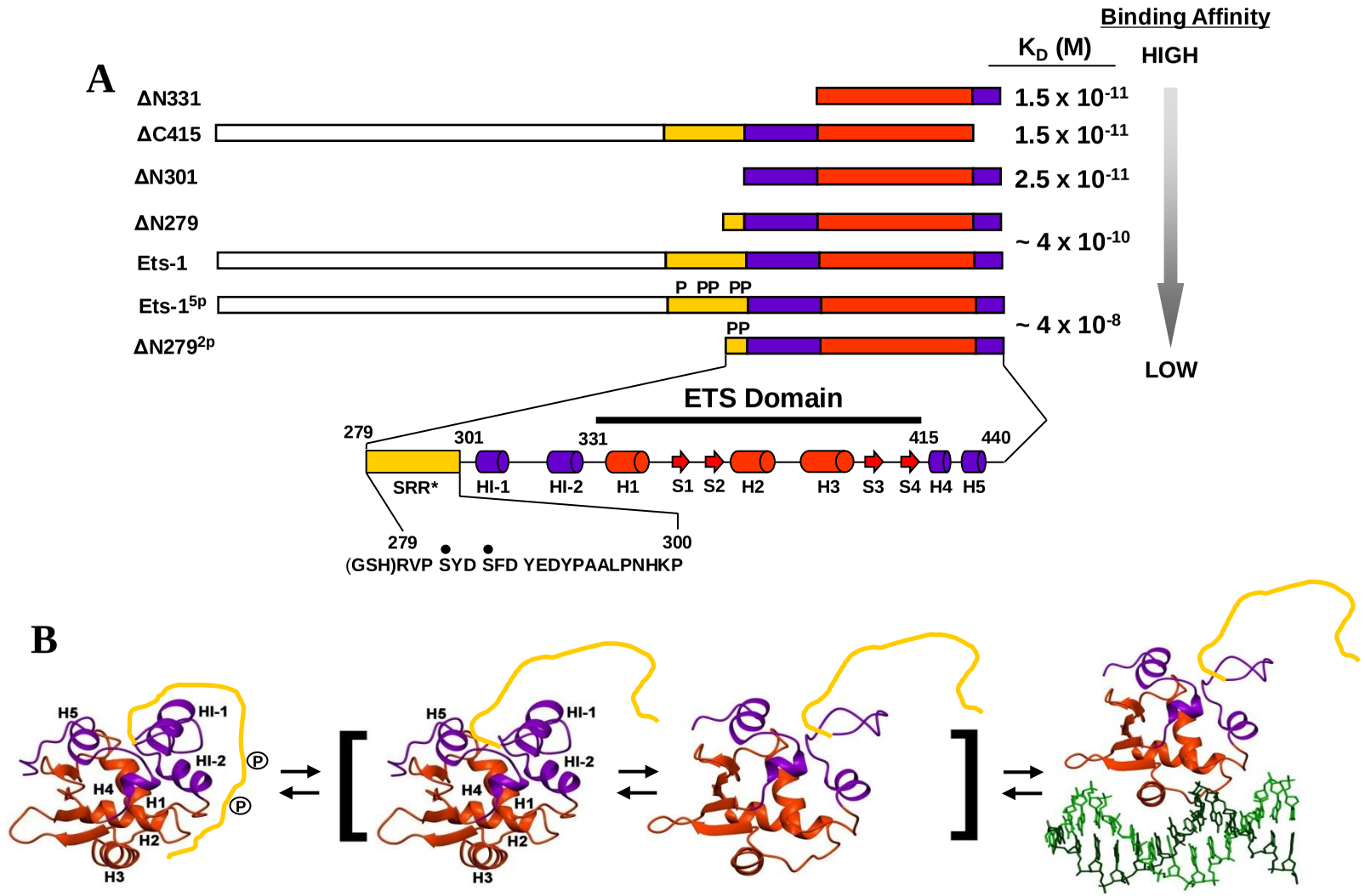
A
Binding Affinity
K_D (M)
HIGH
LOW
ΔN331
ΔC415
ΔN301
ΔN279
Ets-1
Ets-1^{5p}
ΔN279^{2p}
1.5 x 10^{-11}
1.5 x 10^{-11}
2.5 x 10^{-11}
~ 4 x 10^{-10}
~ 4 x 10^{-8}
P PP PP
PP
ETS Domain
279
301
331
415
440
SRR*
HI-1
HI-2
H1
S1
S2
H2
H3
S3
S4
H4
H5
279
300
(GSH)RVP SYD SFD YEDYPAALPNHKP
B
H5
HI-1
HI-2
H4
H1
H2
H3
Ⓟ
Ⓟ

determined. One clue to mechanism derives from analysis of the dynamic character of the SRR (Lee et al., 2008; Pufall et al., 2005). NMR-based experiments have shown that the SRR is unstructured and flexible on the sub-nanosecond timescale (Figure 3.1 A). Upon phosphorylation, internal motions of the SRR are decreased partially without adopting secondary structure. Addition of the SRR, especially in its phosphorylated state dampens the dynamic motions within the regulatable unit as well. Thus, the mechanism of action of the SRR exploits its disordered state to affect the dynamics of a more structured region.

In this report, we demonstrate that aromatic residues in the SRR, though not required for serine phosphorylation, are required for phosphorylation-dependent reduction in Ets-1 DNA-binding affinity. We further present an allelic series of Ets-1 variants that display progressive inhibition. Each mutant bears a different number of tandemly repeated phospho-acceptor units with the required adjacent aromatic residue. Finally, we observed that phosphorylation-induced structural changes, previously correlated with Ets-1 autoinhibition, are altered by the loss of four aromatic residues in the SRR, thus providing a structural correlate to the functional data. We conclude that aromatic residues in the unstructured SRR are essential for the phosphorylation-induced, inhibitory effects on DNA binding that function through conformational alterations. The integration of phosphorylation-dependent charge effects and hydrophobic forces within a disordered region represents a novel regulatory pathway for IUPs.

Results

The phospho-acceptor SRR is highly conserved in Ets-1

Conservation of Ets-1 protein sequences from 16 vertebrate species provides insight into a potential functional role for the unstructured SRR. While the entire Ets-1 protein sequence displayed 63% homology across all 16 species, the highly conserved DNA-binding domain was 79% identical (data not shown). The 22 amino acids SRR, which bares the phospho-acceptor sites, displays 78% identity, emphasizing the potential functional importance of this unstructured protein region (Figure 3.2). The prevalence of highly conserved acidic and aromatic amino acid residues, particularly adjacent to the sites of phosphorylation, suggested a possible mechanistic role for these residues in Ets-1 autoinhibition and phosphorylation effects. We investigated the functional importance of these residues through a combination of charge reversal and alanine replacement via site-directed mutagenesis.

Electrostatic forces do not drive Ets-1 Autoinhibition

Due to the negative charge of ~ -2 at neutral pH held by phosphate moieties, it is common for electrostatic forces to play a major role in the mechanism of phosphorylation-induced changes to protein structure and function. To understand the role of electrostatic forces in constitutive and phospho-enhanced autoinhibition of Ets-1, we made single- and multi-site substitutions at the two phospho-acceptor sites (serines 282 and 285) as well as the four adjacent acidic residues (aspartic acids 284, 287, and 290, and glutamic acid 289). The resulting effect on inhibition of DNA binding, as

Figure 3.2 Amino acid sequence conservation of residues 279-300 of the unstructured SRR of Ets-1 ΔN279. (A) Weblogo displaying sequence conservation among 16 vertebrate species (human, mouse, rat, horse, cow, pig, dog, marmoset, opossum, platypus, armadillo, chicken, Xenopus, zebrafish, stickleback, and pufferfish). Coloring scheme is used to emphasize chemical character of residues; basic (blue), acidic (red), hydrophobic (green), neutral (purple), and serine (black), with letter height directly proportional to the degree of conservation. Inhibitory phosphorylation sites (●) within CamKII recognition motifs [S-F/Y-E/D] are indicated. (B) ClustalW sequence alignment of 16 vertebrate species with identical residues (*), and similar residues (.) indicated. Inhibitory phosphorylation sites (●) within CamKII recognition motifs [S-F/Y-E/D] are also indicated.

A

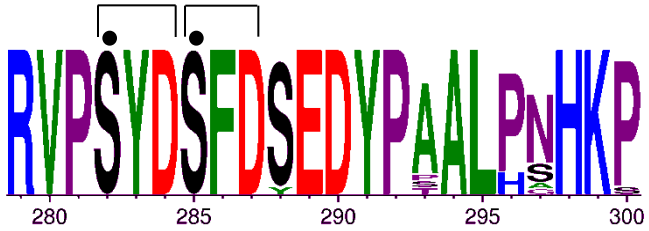

B

```
                    ..  ..
Human               RVPSYDSFDSEDYPAALPNHKP
Mouse               RVPSYDSFDYEDYPAALPNHKP
Rat                 RVPSYDSFDSEDYPAALPNHKP
Horse               RVPSYDSFDSEDYPAALPNHKP
Cow                 RVPSYDSFDSEDYPAALPNHKP
Pig                 RVPSYDSFDSEDYPAALPNHKP
Dog                 RVPSYDSFDSEDYPAALPNHKP
Marmoset            RVPSYDSFDSEDYPAALPNHKP
Opossum             RVPSYDSFDSEDYPAALPNHKP
Platypus            RVPSYDSFDSEDYPAALPSHKP
Armadillo           RVPSYDSFDSEDYPAALPNHKP
Chicken             RVPSYDSFDSEDYPAALPNHKP
Xenopus             RVPSYDSFDSEDYPPALPSHKS
Zebrafish           RVPSYDSFDSEDYPSALHAHKP
Stickleback         RVPSYDSFDSEDYPTALHSHKP
Pufferfish          RVPSYDSFDSEDYPAALHGHKP
                    ********* ****.**  **.
```

indicated by the equilibrium dissociation constant (Kd) of Ets-1, was determined by electrophoretic mobility shift assay (EMSA).

Substitution of positively-charged amino acid residues at the two sites of phosphorylation had no measurable effect on binding affinity, indicating that a simple introduction of positive charge is not sufficient to activate DNA binding in ΔN279 Ets-1 (Table 3.1). Mutagenesis of the four Asp/Glu residues to alanine likewise had no significant effect on DNA-binding affinity. However, mutation of these residues, or loss of the negative-charge they provide, abolished the Ca^{2+}/calmodulin-dependent protein kinase II (CaMKII) consensus site for phosphorylation. Therefore, the effect of these mutations on phosphorylation-induced inhibition could not be explored directly. Attempts to mimic the phosphates through amino acid substitution of serine 282 and 285 with either aspartic acid or glutamic acid did not yield a potent, inhibited species, indicating that the negative charge provided by these residues, at the site of phosphorylation, was not sufficient to observe the 100-fold decrease in DNA-binding affinity. It is also interesting to note that loss of electrostatic interaction potential in the SRR did not affect the level of basal autoinhibition. These results suggested that phosphorylation-induced inhibition of Ets-1 DNA binding may not result from a direct charge-charge interface between the SRR and the regulatable unit.

Phosphorylation-induced inhibition of Ets1 is dependent upon aromatic residue

To determine to role of hydrophobic or van der Waals interactions in Ets-1 autoinhibition and phosphorylation effects, we mutated the aromatic residues (Φ) adjacent to the phospho-acceptor sites. Mutagenesis of four aromatic residues (tyrosine

Table 3.1

Electrostatic mutational analysis of the SRR

Name	SRR Sequence	Kd (x10^{-11} M)	Fold Inhibition
ΔN301	(ΔSRR)	2.5 ± 0.5	——
ΔN279wt	RVP**S** Y**D**S F**D**Y**E**D**E**YPAALPNHKP	44 ± 4.4	18 ± 2.7
ΔN279^{2p}	RVP**S**$^{\cdot}$Y**D**S$^{\cdot}$F**D**Y**E**D**E**YPAALPNHKP	4700 ± 580	1900 ± 320
M1	RVP**R**$^{+}$Y**D**R^{+}F**D**Y**E**D**E**YPAALPNHKP	45 ± 4.9	18 ± 2.7
M2	RVP**S** Y**AS** F**A**Y**AA**YPAALPNHKP	71 ± 16	28 ± 8.5
M3	RVP**E**$^{-}$Y**D**E^{-}F**D**Y**E**D**E**YPAALPNHKP	180 ± 50	73 ± 27
M4	RVP**D**$^{-}$Y**D**D^{-}F**D**Y**E**D**E**YPAALPNHKP	190 ± 7.8	77 ± 9.8

Summary of EMSA binding data for ΔN279 proteins containing SRR mutations in phospho-acceptor serine 282 and 285, and four adjacent acidic residues (D284, D287, E289, D290). K_D and fold inhibition, relative to ΔN301 (ΔSRR), for wild-type ΔN279 and the SRR mutants indicated (M1: S282/285R, M2: D284/287/290A; E289A, M3: S282/285E, M4: S282/285D). For each protein, K_D values represent the mean ± standard error for at least two experiments. Fold inhibition ± propagated error is the ratio of mean experimental K_D and the reported K_D for Ets-1 ΔN301, with error bars representing standard error of the ratio of the mean K_D values of the tested species compared to ΔN301.

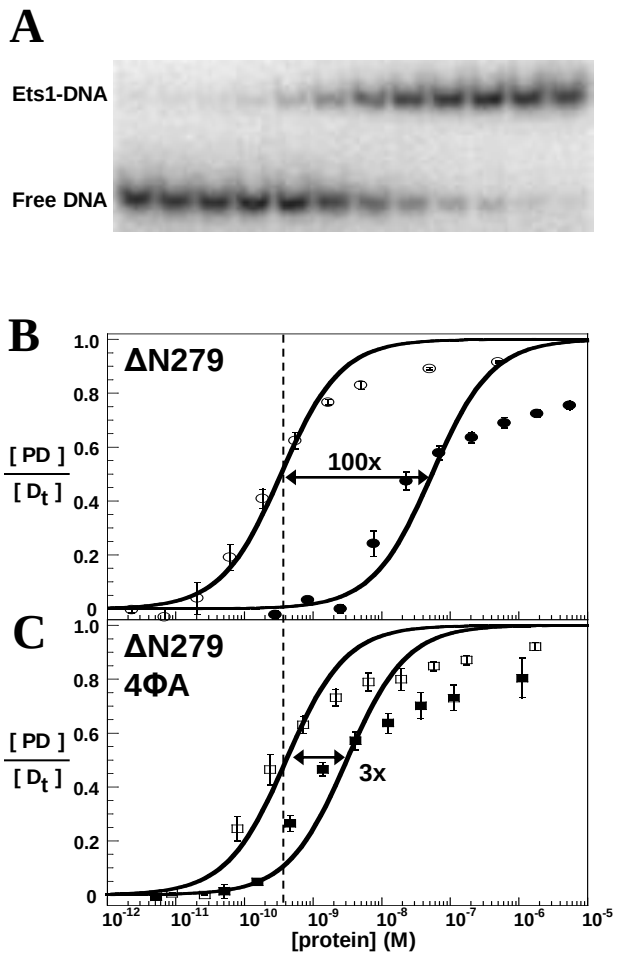

Figure 3.3 Aromatic residues are essential for phosphorylation effects. (A) Phosphorimage of a representative Electrophoretic Mobility Shift Assay (EMSA) gel used in equilibrium binding studies. For each binding experiment, a constant amount of radiolabeled DNA duplex containing a high affinity ETS binding site was mixed with an Ets-1 protein under varying concentrations between 10^{-13} and 10^{-6} M, with each lane representing a 3-fold increase. Bound vs. unbound DNA was detected on a native gel and visualized by phosphorimaging and quantified. (B,C) Equilibrium binding analysis performed without phosphorylation (open symbols) or with phosphorylation (closed symbols) of ΔN279 (B, circles) and ΔN279 with four aromatic SRR residues mutated to alanine (ΔN279 4ΦA) (C, squares). DNA binding isotherms were generated, as described under "Materials and Methods," with fraction bound DNA ([PD] / [Dt]) plotted against free protein concentration ([protein]). Data points with error bars represent the average ± standard deviation for three independent experiments.

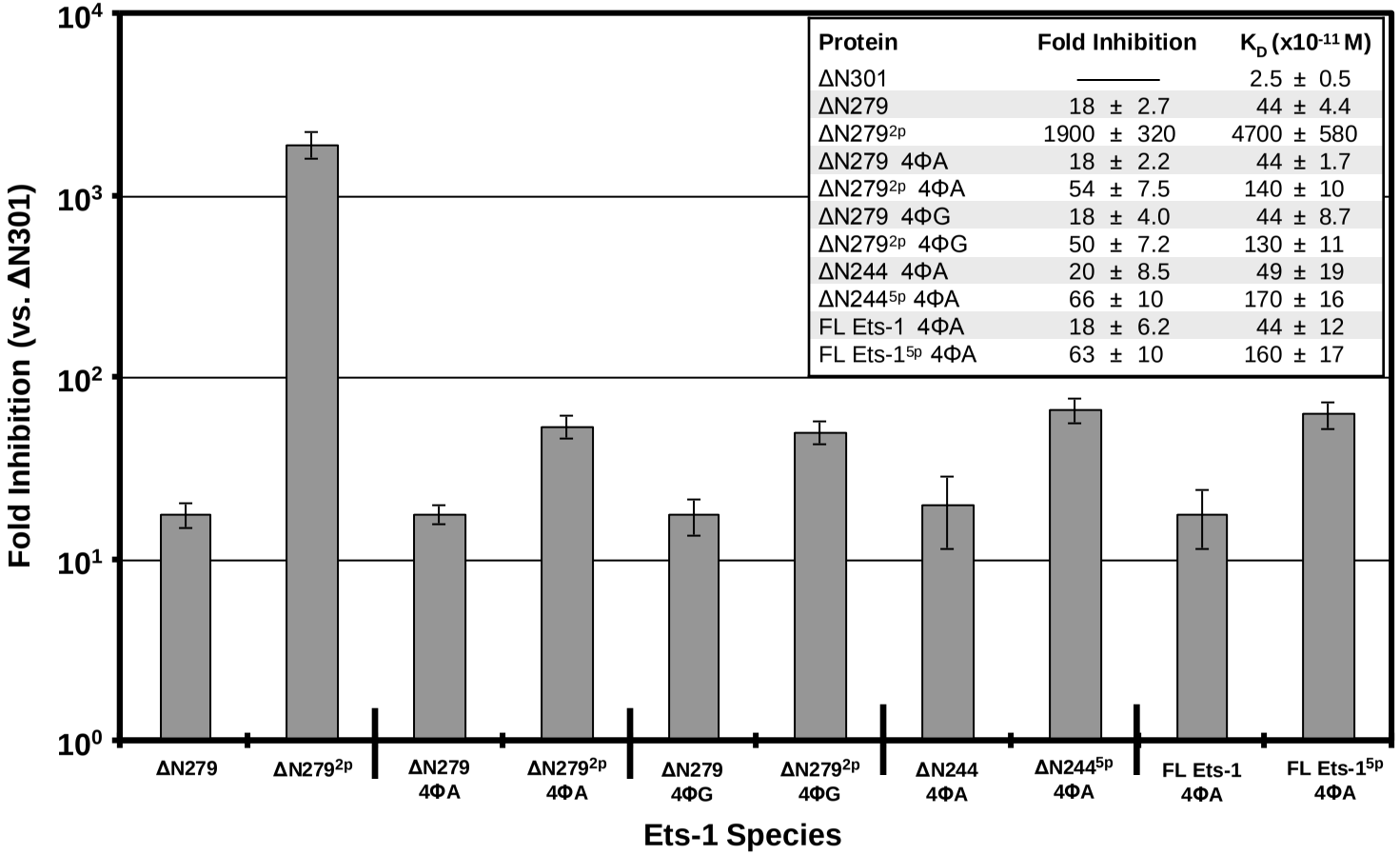

Figure 3.4 Phosphorylation-induced enhancement of autoinhibition requires aromatic residues located in the SRR. A summary and logarithmic comparison of EMSA binding data for Ets-1 proteins, showing the K_D and fold inhibition, relative to ΔN301 (ΔSRR), for the Ets-1 species indicated in the absence and presence of phosphorylation. For each protein, K_D values represent the mean ± standard error for at least three independent experiments. Fold inhibition ± propagated error is the ratio of mean experimental K_D and the reported K_D for Ets-1 ΔN301.

283, 288, and 291, and phenylalanine 286) to alanine had no effect on the DNA-binding affinity of Ets-1 (Figure 3.3 C; Figure 3.4). Thus, the basal level of auto-inhibition was not dependent upon the SRR aromatic residues. However, though complete phosphorylation was observed in the four aromatic residue-mutant (4ΦA), there was a dramatic loss of phosphorylation-induced inhibition. Whereas the affinity of wild-type Ets1 ΔN279 was reduced 100-fold upon phosphorylation (Figure 3.3 B), only a modest, 3-fold decrease was observed for the 4ΦA mutant (Figure 3.3 C). Substitution of these four aromatic residues with glycine produced a similar effect on ΔN279 before and after phosphorylation (Figure 3.4). Thus, the hydrophobicity of alanine was not playing a residual role in the observed 3-fold effect.

The previously-studied full-length Ets-1 and ΔN244 fragment, which also display a 50-100 fold phosphorylation-induced decrease in binding affinity (Cowley and Graves, 2000; Pufall et al., 2005), likewise lost the ability to be fully phospho-regulated upon introduction of the aromatics-to-alanine mutations (Figure 3.4). These results suggest a mechanistic interdependence between phosphorylation effects and adjacent aromatic residues in the phosphorylation-induced inhibition of Ets-1 DNA binding. We proposed that the phospho-acceptor / aromatic combination formed the functional unit of the SRR.

Variable phospho-regulation of Ets1 requires adjacent aromatic residues

A previous report demonstrated the graded effect of individual phosphate additions on the binding affinity of Ets-1 (Pufall et al., 2005). We hypothesized that this type of variable control could be recapitulated in the smaller ΔN279 fragment by creating variable numbers of phospho-acceptor / aromatic units (Ser-Φ-Asp). Indeed, a graded increase in the level of phosphorylation-induced inhibition was observed following

substitution of native residues with increasing numbers of phospho-acceptor / aromatic units (Figure 3.5). As with ΔN279, loss of the aromatic residues within these units abrogated the effects of phosphorylation on DNA binding. These results demonstrated that phosphorylation-induced inhibition in Ets-1 could be graded across a wider range than is currently observed in a biological context and supports the proposal that phosphate moieties with adjacent aromatic amino acid residues are a functional unit of the SRR.

Loss of aromatic residues effects phosphorylation-induced structural changes

Phosphorylation-induced structural changes in the regulatable unit, which function through shifts in the conformational equilibrium, have been linked with reinforcement of Ets-1 autoinhibition, i.e., reduced DNA-binding affinity (Lee et al., 2008; Pufall et al., 2005). These structural changes were detected by observing chemical shift changes (or perturbations) in ^{1}H- ^{15}N heteronuclear single quantum correlation (HSQC) spectra. Based on the reduction in phosphorylation induced-decrease of DNA-binding affinity for the aromatic mutant (Figure 3.3 B, C), we predicted a dampening of phosphorylation-induced chemical shift perturbations would be observed. We recorded and compared HSQC spectra under identical conditions for ΔN279 and ΔN279^{2p} as well as ΔN279 4ΦA and ΔN279 4ΦA^{2p}. As amide chemical shifts are extremely sensitive to changes in chemical environment, some mild aromatic mutation-induced chemical shift perturbations were observed for residues within the regulatable units of the unphosphorylated proteins (Figure 3.6 - green spacers). More importantly, the magnitude and directionality of the phosphorylation-induced chemical shift perturbations for these

Figure 3.5 Variable numbers of aromatic / phosphorylated serine units lead to variable DNA binding affinity. (A) summary of EMSA binding data for ΔN279 proteins containing a variable number of the CaMKII phospho-acceptor motif [S-Y/F-D] replacing native sequence. K_D and fold inhibition, relative to ΔN301 (ΔSRR), for ΔN279 and the SRR mutants indicated, in the absence and presence of phosphorylation. +2p, +3p, +4p and +5p phosphorylation states were verified by ESI mass spectrometry. (B) Logarithmic comparison of fold inhibition, relative to ΔN301 for ΔN279 and the SRR mutants indicated, in the absence and presence of phosphorylation. For each protein, K_D values represent the mean ± standard error for at least two experiments. Fold inhibition ± propagated error is the ratio of mean experimental K_D and the reported K_D for Ets-1 ΔN301, with error bars representing standard error of the ratio of the mean K_D values of the tested species compared to ΔN301.

A

Protein name	SRR sequence	Fold Inhibition	K_D ($\times 10^{-11}$ M)
ΔN301	(ΔSRR)	———	2.5 ± 0.5
ΔN279	RVP[S YD][S FD] Y ED Y PA A LP N HK	18 ± 2.7	44 ± 4.4
ΔN279^{2p}	RVP[S•YD][S•FD] Y ED Y PA A LP N HK	1,900 ± 320	4,700 ± 580
3-unit SRR	RVP[S YD][S FD][S YD] Y PA A LP N HK	18 ± 2.2	44 ± 3.8
3-unit SRR^{3p}	RVP[S•YD][S•FD][S•YD] Y PA A LP N HK	2,400 ± 1200	5,900 ± 2700
4-unit SRR	RVP[S YD][S FD][S YD][S FD] A LP N HK	20 ± 2.5	51 ± 1.7
4-unit SRR^{4p}	RVP[S•YD][S•FD][S•YD][S•FD] A LP N HK	13,000 ± 5700	33,000 ± 17000
6-unit SRR	RVP[S YD][S FD][S YD][S FD][S YD][S FD]	23 ± 7.0	58 ± 17
6-unit SRR^{5p}	RVP[S•YD][S•FD][S•YD][S•FD][S•YD][S FD]	> 100,000	> 200,000
6-unit 6ΦA	RVP[S AD][S AD][S AD][S AD][S AD][S AD]	16 ± 2.6	40 ± 4.4
6-unit 6ΦA^{5p}	RVP[S•AD][S•AD][S•AD][S•AD][S•AD][S AD]	84 ± 21	210 ± 46

B

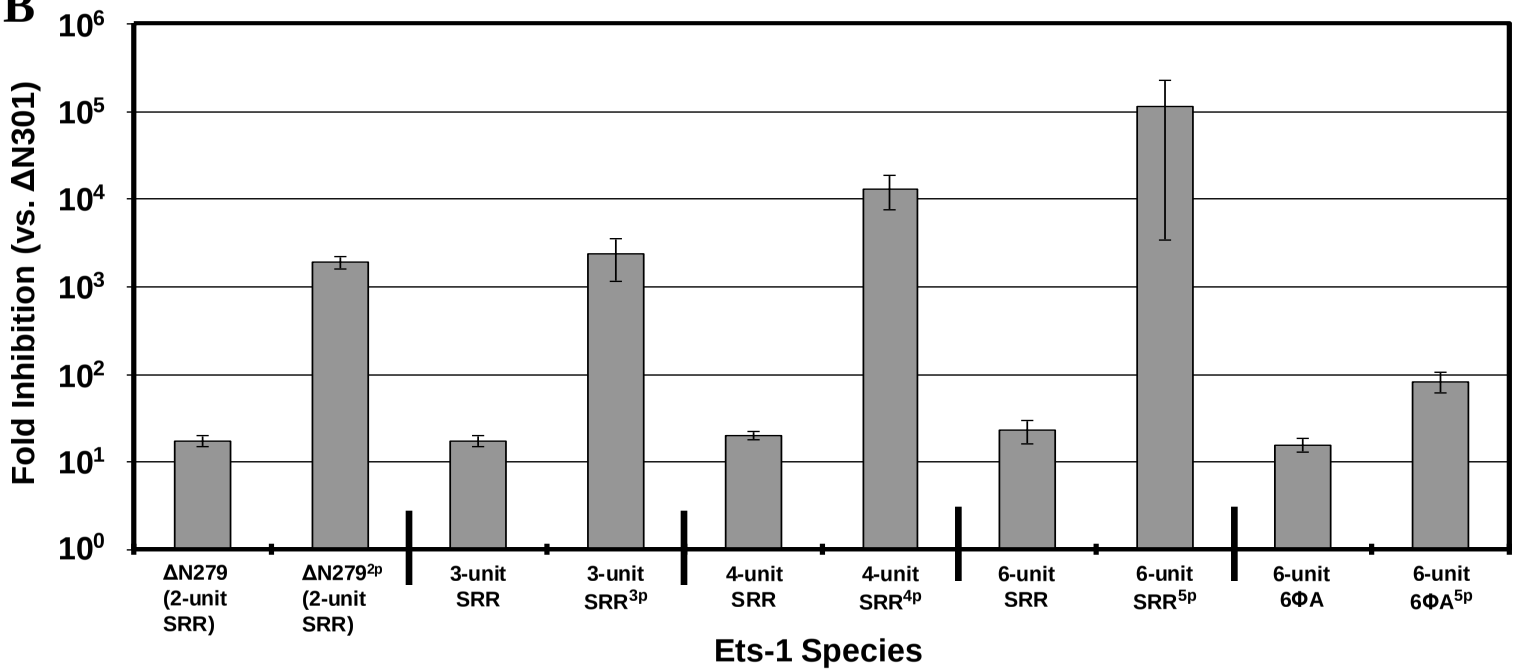

Figure 3.6 Individual changes in phosphorylation-induced chemical shift perturbations. (A) Changes to backbone amide ^{1}H and ^{15}N chemical shifts (Δshift) of the indicated amino acid residue upon phosphorylation of Ets-1 ΔN279 (red), ΔN279^{2p} (blue), ΔN279 4ΦA (cyan), and ΔN279^{2p} 4ΦA (gold). A relationship between the magnitude of chemical shift perturbation (Δshift) and degree of inhibition has been reported previously (Pufall et al., 2005; Lee et al., 2008). The directionality and magnitude of the phosphorylation-induced Δshift for key residues is readily observed for ΔN279 (red → blue, solid arrow). In the case of the 4ΦA aromatic mutant, however, not only has the magnitude of the Δshift been significantly reduced, but the direction has also been altered (cyan → gold, dashed arrow), indicating a change in the way the conformational equilibrium is affected by phosphorylation in the aromatic mutant compared to wild-type. Extreme ends of arrow heads and tails represent the center of shift peaks for phosphorylated and unphosphorylated samples, respectively. Green spacers indicate aromatic mutation-induced chemical shift perturbation of the unphosphorylated protein.

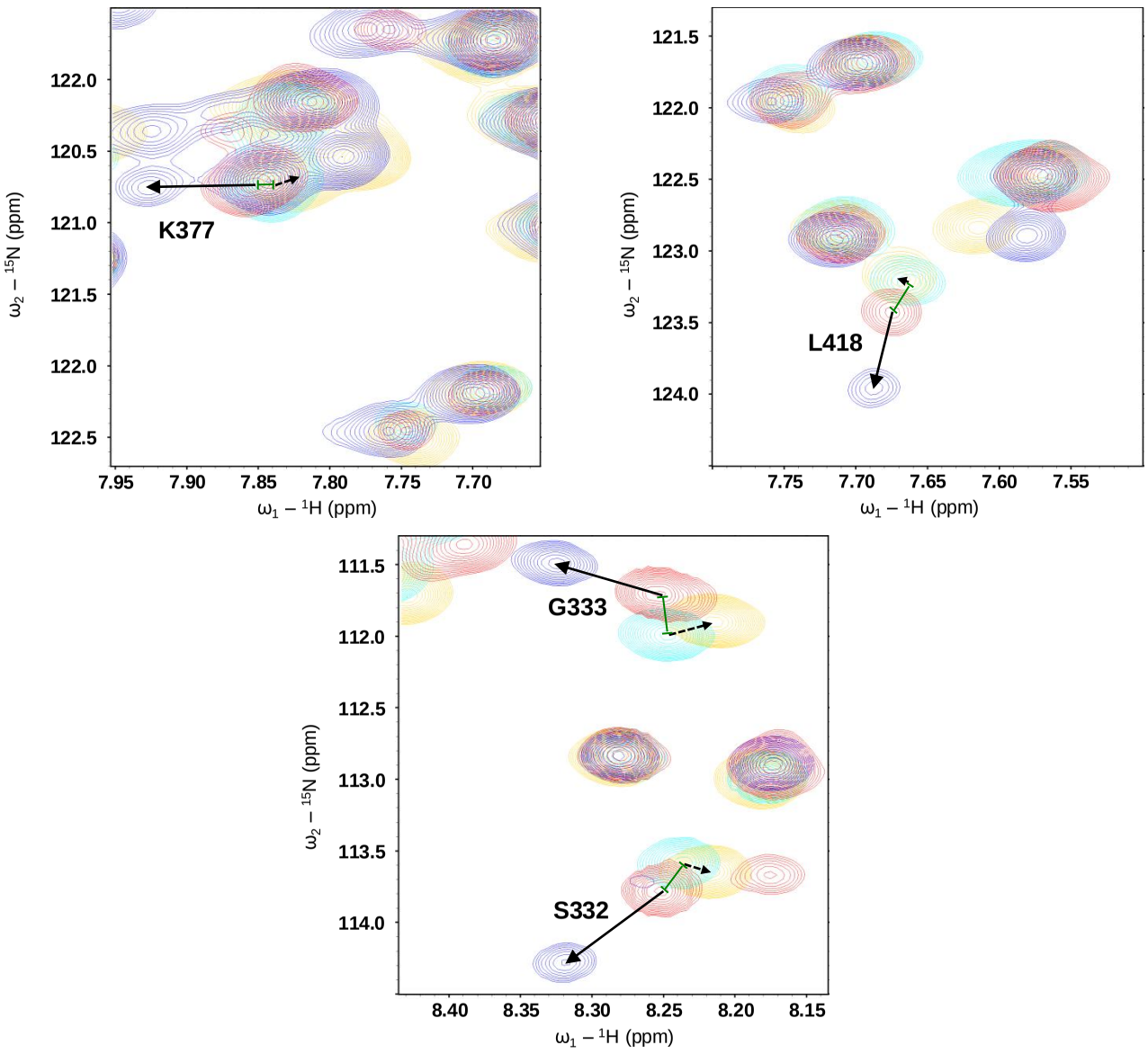
K377
L418
G333
S332
ω2 – 15N (ppm)
ω1 – 1H (ppm)

same residues in wild-type ΔN279 were noticeably diminished in the aromatic mutant following phosphorylation (Figure 3.6 - arrows). These results provide independent evidence that the aromatic mutations are disrupting the established autoinhibitory mechanism of Ets-1.

The regions of ΔN279 in which the pattern of phosphorylation-induced chemical shift perturbations was most altered included the SRR, the area spanning inhibitory helix HI-2 and helix H1 of the ETS domain, the region containing the DNA-contacting helix H3, and inhibitory helix H4 (Figure 3.7 A). Phosphorylation-induced chemical shift perturbations for ΔN279 4ΦA, however, were markedly reduced in all of these areas relative to ΔN279 (Figure 3.7 B). Two SRR aromatic residues (F286 and Y288) in particular, were significantly less affected by phosphorylation following mutation to alanine. In summary, structural alterations observed within the regulatable unit upon phosphorylation of the aromatic mutant SRR were dampened compared to wild-type.

Discussion

The focus of this study has been the biochemical basis for the transient interaction and inhibitory effects observed between the evolutionarily conserved, unstructured SRR and the regulatable unit of Ets-1. We have demonstrated the absence of a major role for direct charge-charge interactions in the autoinhibitory mechanism of Ets-1, and the requirement for aromatic residues in the phosphorylation-induced inhibition of DNA binding. We have also provided supporting evidence for the variable control of binding affinity through graded addition of phosphates within the context of the aromatic residue-containing, CaMKII phospho-acceptor motif. Finally, structural effects of phosphorylation of Ets-1 were also shown to be aromatic residue-dependent. These

Figure 3.7 Global view of phosphorylation-induced chemical shift perturbations. Changes to backbone amide ^{1}H and ^{15}N chemical shifts (Δshift) upon phosphorylation of Ets-1 ΔN279 (A) and ΔN279 4ΦA (B). Structural organization of ΔN279 is provided (above) for reference. Δshift bars reaching above the shaded box are considered to be perturbed by phosphorylation (see Materials and Methods). The absence of a bar indicates that the Δshift could not be measured unambiguously for a given residue due to spectral overlap or weak signals in at least one of the directly compared species. Filled circles and asterisks represent the phospho-acceptor serines and prolines, respectively. Two SRR aromatic residues (F286 and Y288) are marked as previously indicated (Φ). Example residues from Figure 3.6 (S332, G333, K377, and L418) are also marked (red arrows).

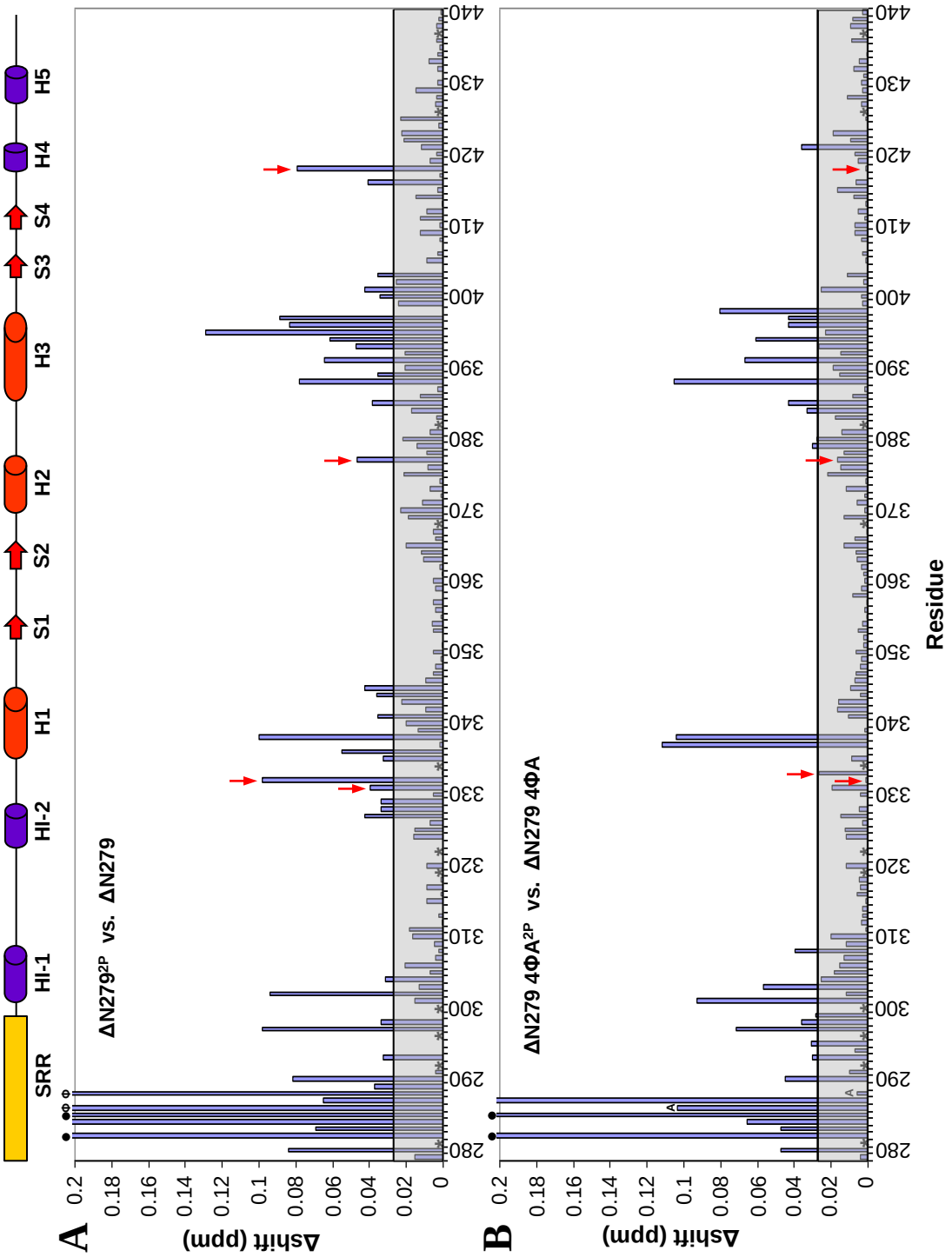
SRR
HI-1
HI-2
H1
S1
S2
H2
H3
S3
S4
H4
H5
A
ΔN279^{2P} vs. ΔN279
Δshift (ppm)
B
ΔN279 4ΦA^{2P} vs. ΔN279 4ΦA
Δshift (ppm)
Residue

findings provide evidence for a mechanistic interdependence between phosphates and adjacent aromatic residues in the phosphorylation-induced inhibition of Ets-1 DNA binding.

The structural model for autoinhibition in Ets-1 involves shifting the two-state conformational equilibrium of the regulatable unit from a dynamic-active to a rigid-inactive state. Phosphorylation of the flexible, unstructured SRR has been shown to promote the inactive state by stabilizing the inhibitory module and dampening the dynamics of the hydrophobic core (Pufall et al., 2005; Lee et al., 2008). Mechanistically, this is achieved as the fast timescale motion of the SRR is decreased and the transient localization of the SRR to the regulatable unit is enhanced, whereby allosteric effects on regulatable unit dynamics occur. This study provides insight into the chemical nature of the phosphorylation-enhanced autoinhibitory mechanism. Though the negative charge of a phosphate moiety can certainly enhance electrostatic interactions (Gorbunoff, 1984), in the case of Ets-1 autoinhibition there does not appear to be a positively charged interface to which the net negatively-charged, phosphorylated SRR binds in a "lock-and-key"-type interaction. This is evidenced by the relative insensitivity of phosphorylation-induced chemical shift perturbations to changes in salt concentration (Lee et al., 2008). The phospho-enhanced stability of the regulatable unit against urea denaturation is also insensitive to changes in salt concentration (Lee et al., 2008). Additionally, mutational analysis of the phospho-acceptor serines, reported in this work, indicates that positively-charged amino acid substitution at those positions does not have an activating effect on DNA binding and that negatively-charged amino acid substitutions are not sufficiently strong to mimic the effects of phosphorylation (Table 3.1). Loss of electrostatic

interaction potential through substitution of the four Asp/Glu SRR residues with alanine was also unable to activate DNA binding, suggesting that phosphate addition does not simply enhance those negative charges already dispersed throughout the SRR. Unfortunately, the position of acidic residues adjacent to the phospho-acceptor site is absolutely required for in vitro CaMKII phosphorylation. Without effective phospho-mimetic mutants, we could not test the effects of acidic residue loss on phosphorylation-induced inhibition.

The under-representation of evolutionarily conserved aromatic residues in disordered, unstructured protein regions continues to be observed and predicted (Obradovic et al., 2003; Romero et al., 2001). The surprising presence of four bulky, hydrophobic, aromatic residues in the unstructured SRR of murine Ets-1 led to our investigation of their possible role in the autoinhibitory mechanism (Figure 3.2). Similar to the mutation of the four Asp/Glu residues, mutation of the four aromatic SRR residues to either alanine or glycine did not activate DNA binding in the unphosphorylated state (Figure 3.4). However, upon phosphorylation of the two phospho-acceptor serines, the 100-fold inhibitory effect observed for wild-type ΔN279 was almost completely lost in the ΔN279 4ΦA mutant (Figure 3.3 B, C). Importantly, we were able to recapitulate the loss of inhibitory phosphorylation effects in full-length Ets-1, as well as the ΔN244 truncation, by introducing the 4ΦA mutation (Figure 3.4). Phosphorylation-induced perturbation of NMR chemical shifts for residues in ΔN279 was also diminished in overall effect and altered in pattern in ΔN279 4ΦA, indicating that phosphorylation-induced, inhibitory structural changes to the regulatable unit are also dampened in the

aromatic mutant (Figure 3.6; 3.7). This correlation between structural alterations and DNA-binding affinity is a hallmark of Ets-1 autoinhibition.

The SRR of full-length Ets-1 extends from residue 244-300 (Cowley and Graves, 2000). Within this larger region, a total of seven potentially modified Ca^{2+}-dependent phosphorylation sites have been observed (Pufall et al., 2005). However, of these, only three have been shown to contribute to the graded, inhibitory effects of phosphorylation on the DNA binding affinity of Ets-1 (Pufall et al., 2005). All three of these phospho-acceptor sites exist within the context of the conserved, CaMKII recognition motif [S-Y/F-D/E]. We showed that artificial amplification of the phospho-serine / aromatic unit further inhibits Ets-1 DNA binding. As the length of the SRR has proven to be an important contributing factor to the level of autoinhibition in Ets-1 (Lee et al., 2008), addition of phospho-acceptor motifs were engineered as substitutions for native amino acid residues, rather than insertions. Interestingly, and consistent with other data presented in this work, phospho-acceptor motif-substitution within the SRR had no effect on the basal levels of DNA binding inhibition in ΔN279. Upon full phosphorylation of the altered SRRs, however, a proportional increase in the level of inhibition is observed (Figure 3.5). Moreover, these hyper-phosphorylation effects remain dependent upon the presence of the aromatic residue adjacent to the phospho-acceptor site.

Taken together, these data suggest that the phosphorylation-induced changes to the SRR and regulatable unit are driven by transient hydrophobic or van der Waals intramolecular interactions, which are enhanced following covalent modification of the SRR by Ca^{2+}-dependent kinase. These interactions may exist between aromatic / hydrophobic residues in the SRR and the regulatable unit, or be confined to within the

SRR (Figure 3.8). Further experimentation designed to observe structural alterations within an isolated SRR, as well as more precise paramagnetic relaxation enhancing (PRE) site-direct spin labeling (SDSL) experiments are already under way to elucidate the nature of the aromatic-dependent intramolecular interaction.

Previous reports have described intrinsically unstructured domains that modulate the activity of a structured core through intramolecular interactions, as well as phosphorylation-mediated control of intrinsically disordered proteins (Honnappa et al., 2006; Jonker et al., 2006). Proposed mechanisms of action for the IUP regions have included participation as a ligand or other factor binding site, adopting structure / order upon modification, and even remaining functionally unstructured while masking a binding interface or making polyelectrostatic interactions (Borg et al., 2007; Dunker et al., 2005; Iakoucheva et al., 2004; Mittag et al., 2010; Oldfield et al., 2008; Serber and Ferrell, 2007). We have discovered a new mechanism in Ets-1, whereby phosphorylation of an IUP region enhances a transient hydrophobic interaction, modulating the activity of a structured unit without adopting a structured conformation.

Materials and methods

Expression plasmids

Mutation of acidic, aromatic, and phospho-acceptor serine residues within the SRR were performed by QuikChange site-directed mutagenesis (Statagene), and confirmed by DNA sequencing (University of Utah HCS Core DNA Sequencing Facility). Substitution of native sequence for tandem repeats of the phospho-acceptor motif [S-Y/F-D] was accomplished by engineering unique restriction sites at the 5' (Bsu36I) and 3' (AvrII) end of the SRR coding sequence. Restriction double digest was

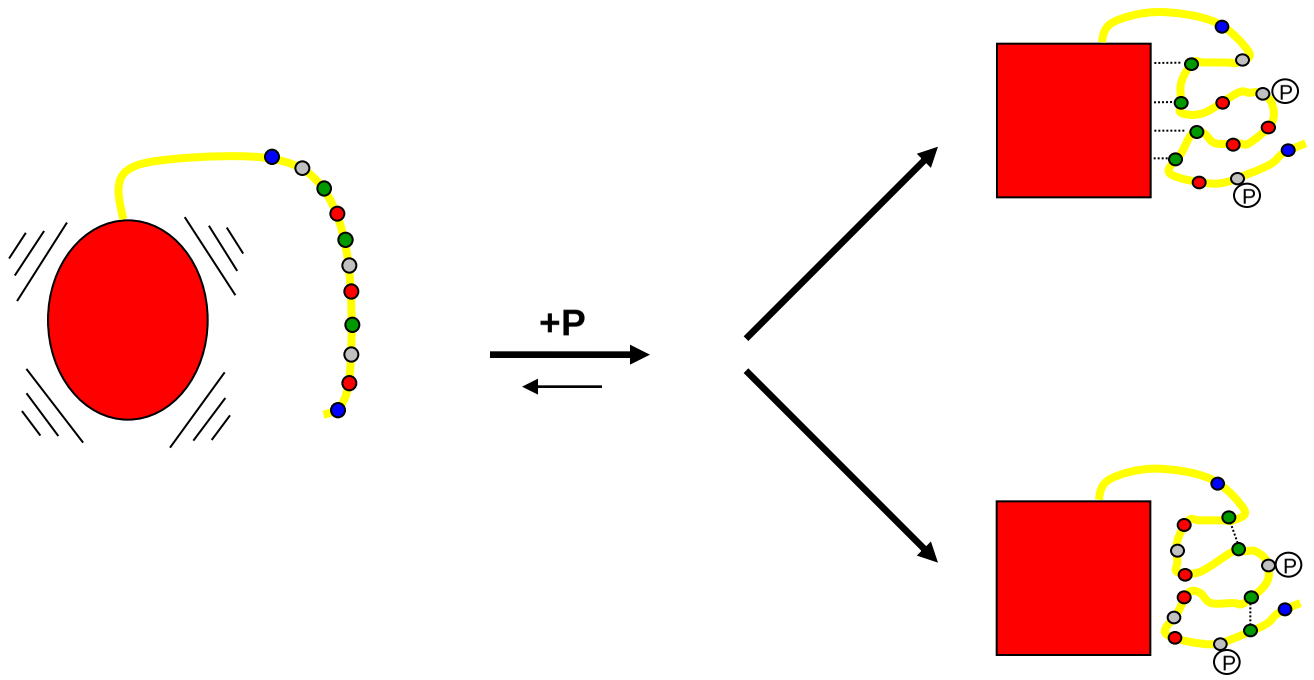

Figure 3.8 Model of Ets-1 autoinhibition. The regulatable unit of Ets-1 (red oval) exists in a dynamic-active conformation (motion lines) in the absence of Ca^{2+}-dependent phosphorylation. The unphosphorylated SRR (yellow - left) is flexible and unstructured, without a fixed location. Amino acid residues within the SRR (colored circles) make transient interactions with the regulatable unit. We propose two alternative models for the mechanism of phosphorylation-enhanced autoinhibition. Phosphorylation may enhance transient hydrophobic interactions (dotted lines) between aromatic residues in the SRR (green circles) and the regulatable unit (red square – top). Alternatively, transient hydrophobic interactions within the SRR may be enhanced upon phosphorylation (bottom). Either aromatic residue-dependent phosphorylation effect results in a decrease of SRR mobility (Lee et al., 2008), enhanced localization of the SRR to the regulatable unit (Lee et al., 2008), dampening of regulatable unit dynamics (Pufall et al., 2005), and a 50- to 100-fold decrease in Ets-1 DNA-binding affinity.

used to excise the coding sequence for the SRR. Parental vector was treated with Calf Intestinal Phosphatase (CIP), resolved on a 1% Agarose gel, and purified by gel extraction (Qiagen). Complimentary 5'-phosphorylated oligonucleotides encoding mutant version of the SRR were ordered from the University of Utah HCS Core DNA/Peptide Facility, dissolved in water, and annealed by boiling for 5 minutes and cooling slowly over 6 - 8 hours. Oligonucleotide duplexes were ligated into purified, open parental vector using T4 DNA ligase (Invitrogen). Positive clones were screened by DNA sequencing and artificial restriction sites were reverted to native sequence through QuikChange.

Sample expression, purification, and phosphorylation

Expression and purification of Ets-1 ΔN279 proteins from the pET28a vector (Invitrogen) were performed according to previous methods (Lee et al., 2008). Proteins were expressed in *E. coli* BL21(λDE3) cells with cultures grown at 37 °C and induced at OD_{600} = 0.9 with 1 mM IPTG. After continued growth for 3 hours at 30 °C, cultures were harvested by centrifugation at 7000 x g for 10 minutes, and resuspended in 25 ml extraction buffer (25 mM Tris, pH 7.5, 1 M NaCl, 0.1 mM EDTA, 10 mM imidizole, 2 mM β-mercaptoethanol (BME), and 1 mM phenylmethylsulfonyl fluoride (PMSF). Following lysis by sonication, and ultra-centrifugation at 42,000 rpm for 45 minutes, soluble supernatant was bound to a 5 mL HisTrap Nickel Sepharose column (GE Biosciences) with the use of the ÄKTA FPLC system (Amersham Pharmacia Biotech). Purified proteins were eluted with a gradient of 10 mM-250 mM imidizole and peak fractions were detection by monitoring UV absorbance at 280 nm. Like fractions were determined by resolving peak fractions on a 15% SDS polyacrylamide gel and visualized

by Coomassie staining. Fractions were combined, treated with 5 units thrombin (Sigma) per mg ΔN279 protein and 2.5 mM $CaCl_2$ to remove the His_6-tag, and dialyzed overnight against 25 mM Tris, pH 7.9, 50 mM KCl, 1 mM ETDA, 2.5 mM $CaCl_2$, 1 mM DTT, and 10% (v/v) glycerol. Following thrombin cleavage of the His_6-tag, ΔN279 proteins contain a non-native, N-terminal tri-peptide motif (Gly-Ser-His). The buffer exchanged, cleaved samples were submitted to ultra-centrifugation at 40,000 rpm for 40 minutes and soluble protein was loaded onto a 5 mL HiTrap S-Sepharose ion exchange chromatography column (GE Biosciences). Purified proteins were eluted with a gradient of 50 mM-300 mM KCl, concentrated to < 13 ml, and loaded onto a HiLoad 26/60 Superdex 75 gel filtration column (Pharmacia) for size exclusion chromatography. Unphosphorylated protein was eluted in storage buffer (25 mM Tris, pH 7.9, 300 mM NaCl, 1 mM EDTA, 1mM DTT, and 10% (v/v) glycerol), concentrated to between 20 µM-50 µM and 25 µl aliquots were snap frozen in liquid nitrogen and stored at -80 °C for use in assay. Protein identities were confirmed by intact molecular weight confirmation through electrospray ionization mass spectrometry (ESI-MS) (University of Utah HCS Core Mass Spectrometry Facility) Protein concentrations were determined by two independent measurements; absorbance at 280 nm using the predicted ε_{280} of 38360 M-1 cm-1 (Protein Properties Calculator - www.basic.northwestern.edu/biotools/proteincalc.html) and Bio-Rad protein assay compared to BSA standards.

Concentrated proteins were phosphorylated for 1 - 2 hours at 30 °C in storage buffer plus 10 mM MgAcetate, 0.5 mM $CaCl_2$, 1 µM Calmodulin (Sigma), 200 nM Ca^{2+}/calmodulin-dependent protein kinase II (CaMKII), and 1 mM ATP (Sigma). The

reaction was dialyzed overnight against 25 mM Tris, pH 7.9, 40 mM KCl, 1 mM ETDA, 2.5 mM $CaCl_2$, 1 mM DTT, and 10% (v/v) glycerol, followed by ultra-centrifugation at 40,000 rpm for 40 minutes. Soluble, phosphorylated proteins were then loaded onto a 10/10 MonoQ FPLC column (Pharamcia) for strong ion-exchange chromatography and eluted with a gradient of 40 mM-300 mM KCl. Purified, phosphorylated proteins were concentrated to > 20 µM and snap frozen in liquid nitrogen for storage at -80 °C. Homogeneity of phosphorylated proteins was verified by ESI-MS.

Full length Ets-1 and ΔN244 proteins were purified as above, except without a His_6-tag and Nickel Sepharose chromatography.

Expression and purification of CaMKII

Murine CaMKIIα was expressed from a baculovirus. Sf9 cells were grown in serum-free medium to a density of $2e10^6$ cells/mL, and infected with a P3 viral solution. The cells were harvested by centrifugation at >20% lysis, as observed by trypan blue staining, and resuspended in CaMKII buffer containing 10 mM Tris (pH 7.5), 1 mM ethylene glycol-bis-(2-aminoethyl) N,N,N',N'-tetraacetic acid (EGTA), 1 mM EDTA, 5 mM DTT, and a mix of protease inhibitors. Cells were then lysed using a Dounce homogenizer and centrifuged to remove insoluble material. CaMKII was precipitated by the addition of 60% w/w $(NH_4)_2SO_4$ to the supernatant, resuspended, and bound to a calmodulin column (CaM Sepharose, Amersham Biosciences). The column was washed with CamKII buffer containing 1 M NaCl, and CaMKII was eluted with 50 mM 4-(2-hydroxyethyl)-1-piperazineethanesulfonic acid (HEPES) (pH 7.5), 50 mM NaCl, 2 mM EDTA, 2 mM EGTA, 1 mM DTT, and 1 mM benzamidine. Fractions containing protein were dialyzed into 100 mM HEPES (pH 7.5), 50% (v/v) glycerol, 10% (v/v) ethylene

glycol, 1 mM EDTA, 1 mM benzamidine, and 5 mM DTT, concentrated to ~30 µM, and stored at -20°C.

Electrophoretic Mobility-Shift Assay (EMSA)

EMSAs of Ets-1 proteins were performed as previously described (Pufall et al., 2005). Equilibrium binding conditions were established between a single Ets-1 protein and a duplex of radio-labeled, 27-mer oligonucleotides containing a high affinity ETS binding site, termed SC1:

5'- TCGACGGCCAAGCCGGAAGTGAGTGCC -3' (top strand);

5'- TCGAGGCACTCACTTCCGGCTTGGCCG -3' (bottom strand).

Oligos were labeled with [γ^{32}-P] ATP using T4 polynucleotide kinase (Invitrogen) and annealed by boiling for 5 minutes and slowly cooling over 6 - 8 hours. DNA concentration was kept constant at $2.5e^{-12}$ M, while Ets-1 protein concentrations ranged over six orders of magnitude. Reactions were incubated for 3 - 4 hours in a buffer containing 25 mM Tris, ph 8.0, 0.1 mM EDTA, 60 mM KCl, 6 mM $MgCl_2$, 200 µg/mL BSA, 10 mM DTT, 2.5 ng/µl poly dIdC, and 10% (v/v) glycerol, and resolved on an 8% native polyacrylamide gel. Gels were dried using a Bio-Rad gel dryer and exposed to a blank phosphorimage screen overnight. Binding reactions were visualized and quantified by phosphorimaging on a STORM scanner. Equilibrium dissociation constants (K_D) were measured by non-linear least squares fitting of the free protein concentration [P] versus fraction of DNA bound ($[PD]/[D]_t$) to the equation $[PD]/[D]_t = 1/(1 + (K_D/[P]))$ using Kaleidagraph (v 3.51, Synergy Software). DNA concentration is kept constant at 10 - 100 fold lower that the predicted and confirmed K_D to create conditions under which

unbound protein [P] is in excess for all reactions. These conditions allow for the assumption the [P] is equal to total protein [P_t].

Preparation of protein samples for NMR

E. coli were freshly transformed and grown in M9 minimal medium supplemented with vitamins. ^{15}N labeling was accomplished by the addition of 1 g 99% $^{15}NH_4Cl$, 10 g glucose, and 10 mg Celtone-N (Cambridge Isotopes) per liter of media. Cultures were induced at OD_{600} = 0.9 with 1 mM IPTG, growth for 4 hours at 30 °C, and harvested, purified, and phosphorylated as described above. Samples were dialyzed against 20 mM sodium phosphate (pH 6.5), 0.1 mM EDTA, 1 mM DTT and 50 mM NaCl for spectral data collection and comparisons with other Ets-1 fragments. Final sample concentrations were 0.3 to 0.5 mM for ΔN279 proteins.

Calculation of chemical shift perturbations

^{15}N labeled versions of wild type ΔN279 and ΔN279 4ΦA with and without phosphorylation were expressed and purified as described above. ^{1}H-^{15}N HSQC spectra were recorded under identical conditions: 20 mM sodium phosphate (pH 6.5), 0.1 mM EDTA, 1 mM DTT, 50 mM NaCl, at 25°C. A linear change in chemical shifts (Δδ) was calculated as follows: $[(\Delta\delta_{1H})^2 + (\Delta\delta_{15N}/(6.5))^2]^{1/2}$. Δδ values greater than 5-fold over the estimated background were considered significant. All NMR spectra were recorded on a cryoprobe-equipped Varian Inova 600 MHz spectrometer at 25 °C. A typical NMR sample consisted of 0.3–0.5 mM protein in 0.35–0.50 mL of NMR buffer (listed above). The sample conditions were adjusted by dialysis and concentration using Amicon Ultra

3K Centrifugal Filter Devices (Millipore Corp.). Spectral processing and analysis were performed with NMRpipe and Sparky.

References

Baillat D, Begue A, Stehelin D, Aumercier M. 2002. ETS-1 transcription factor binds cooperatively to the palindromic head to head ETS-binding sites of the stromelysin-1 promoter by counteracting autoinhibition. The Journal of biological chemistry 277(33):29386-29398.

Boehr DD, Dyson HJ, Wright PE. 2006. An NMR perspective on enzyme dynamics. Chemical reviews 106(8):3055-3079.

Borg M, Mittag T, Pawson T, Tyers M, Forman-Kay JD, Chan HS. 2007. Polyelectrostatic interactions of disordered ligands suggest a physical basis for ultrasensitivity. Proceedings of the National Academy of Sciences of the United States of America 104(23):9650-9655.

Cowley DO, Graves BJ. 2000. Phosphorylation represses Ets-1 DNA binding by reinforcing autoinhibition. Genes Dev 14(3):366-376.

Dunker AK, Brown CJ, Lawson JD, Iakoucheva LM, Obradovic Z. 2002. Intrinsic disorder and protein function. Biochemistry 41(21):6573-6582.

Dunker AK, Cortese MS, Romero P, Iakoucheva LM, Uversky VN. 2005. Flexible nets. The roles of intrinsic disorder in protein interaction networks. The FEBS journal 272(20):5129-5148.

Dunker AK, Obradovic Z, Romero P, Garner EC, Brown CJ. 2000. Intrinsic protein disorder in complete genomes. Genome informatics 11:161-171.

Dunker AK, Oldfield CJ, Meng J, Romero P, Yang JY, Chen JW, Vacic V, Obradovic Z, Uversky VN. 2008a. The unfoldomics decade: an update on intrinsically disordered proteins. BMC genomics 9 Suppl 2:S1.

Dunker AK, Silman I, Uversky VN, Sussman JL. 2008b. Function and structure of inherently disordered proteins. Current opinion in structural biology 18(6):756-764.

Dyson HJ, Wright PE. 2005. Intrinsically unstructured proteins and their functions. Nat Rev Mol Cell Biol 6(3):197-208.

Fitzsimmons D, Hodsdon W, Wheat W, Sauveur-Michel M, Wasylyk B, Hagman J. 1996. Pax-5 (BSAP) recruits Ets proto-oncogene family proteins to form functional ternary complexes on a B-cell-specific promoter. Genes Dev 10:2198-2211.

Garvie CW, Hagman J, Wolberger C. 2001. Structural studies of Ets-1/Pax5 complex formation on DNA. Molecular cell 8(6):1267-1276.

Goetz TL, Gu TL, Speck NA, Graves BJ. 2000. Auto-inhibition of Ets-1 is counteracted by DNA binding cooperativity with core-binding factor alpha2. Mol Cell Biol 20(1):81-90.

Gorbunoff MJ. 1984. The interaction of proteins with hydroxyapatite. II. Role of acidic and basic groups. Analytical biochemistry 136(2):433-439.

Gu TL, Goetz TL, Graves BJ, Speck NA. 2000. Auto-inhibition and partner proteins, core-binding factor beta (CBFbeta) and Ets-1, modulate DNA binding by CBFalpha2 (AML1). Mol Cell Biol 20(1):91-103.

Hagman J, Grosschedl R. 1992. An inhibitory carboxyl terminal domain in Ets-1 and Ets-2 mediates differential binding of ETS family factors to promoter sequences of the *mb-1* gene. Proc Natl Acad Sci USA 89:8889-8893.

Honnappa S, Jahnke W, Seelig J, Steinmetz MO. 2006. Control of intrinsically disordered stathmin by multisite phosphorylation. The Journal of biological chemistry 281(23):16078-16083.

Iakoucheva LM, Brown CJ, Lawson JD, Obradovic Z, Dunker AK. 2002. Intrinsic disorder in cell-signaling and cancer-associated proteins. Journal of molecular biology 323(3):573-584.

Iakoucheva LM, Radivojac P, Brown CJ, O'Connor TR, Sikes JG, Obradovic Z, Dunker AK. 2004. The importance of intrinsic disorder for protein phosphorylation. Nucleic acids research 32(3):1037-1049.

Jonker HR, Wechselberger RW, Boelens R, Kaptein R, Folkers GE. 2006. The intrinsically unstructured domain of PC4 modulates the activity of the structured core through inter- and intramolecular interactions. Biochemistry 45(15):5067-5081.

Jonsen MD, Petersen JM, Xu Q, Graves BJ. 1996. Characterization of the cooperative function of inhibitory sequences of Ets-1. Mol Cell Biol 16(5):2065-2073.

Lamber EP, Vanhille L, Textor LC, Kachalova GS, Sieweke MH, Wilmanns M. 2008. Regulation of the transcription factor Ets-1 by DNA-mediated homo-dimerization. The EMBO journal 27(14):2006-20017.

Lee GM, Pufall MA, Meeker CA, Kang HS, Graves BJ, McIntosh LP. 2008. The affinity of Ets-1 for DNA is modulated by phosphorylation through transient interactions of an unstructured region. J Mol Biol 382(4):1014-1030.

Lim F, Kraut N, Frampton J, Graf T. 1992. DNA binding by c-Ets-1, but not v-Ets, is repressed by an intramolecular mechanism. EMBO J 11:643-652.

Liu H, Grundstrom T. 2002. Calcium regulation of GM-CSF by calmodulin-dependent kinase II phosphorylation of Ets1. Mol Biol Cell 13(12):4497-4507.

Liu J, Perumal NB, Oldfield CJ, Su EW, Uversky VN, Dunker AK. 2006. Intrinsic disorder in transcription factors. Biochemistry 45(22):6873-6888.

Midic U, Oldfield CJ, Dunker AK, Obradovic Z, Uversky VN. 2009. Protein disorder in the human diseasome: unfoldomics of human genetic diseases. BMC genomics 10 Suppl 1:S12.

Mittag T, Kay LE, Forman-Kay JD. 2010. Protein dynamics and conformational disorder in molecular recognition. J Mol Recognit 23(2):105-116.

Obradovic Z, Peng K, Vucetic S, Radivojac P, Brown CJ, Dunker AK. 2003. Predicting intrinsic disorder from amino acid sequence. Proteins 53 Suppl 6:566-572.

Oldfield CJ, Cheng Y, Cortese MS, Brown CJ, Uversky VN, Dunker AK. 2005. Comparing and combining predictors of mostly disordered proteins. Biochemistry 44(6):1989-2000.

Oldfield CJ, Meng J, Yang JY, Yang MQ, Uversky VN, Dunker AK. 2008. Flexible nets: disorder and induced fit in the associations of p53 and 14-3-3 with their partners. BMC genomics 9 Suppl 1:S1.

Petersen JM, Skalicky JJ, Donaldson LW, McIntosh LP, Alber T, Graves BJ. 1995. Modulation of transcription factor Ets-1 DNA binding: DNA-induced unfolding of an alpha helix. Science (New York, NY 269(5232):1866-1869.

Pufall MA, Lee GM, Nelson ML, Kang HS, Velyvis A, Kay LE, McIntosh LP, Graves BJ. 2005. Variable control of Ets-1 DNA binding by multiple phosphates in an unstructured region. Science (New York, NY 309(5731):142-145.

Rabault B, Ghysdael J. 1994. Calcium-induced phosphorylation of ETS1 inhibits its specific DNA binding activity. J Biol Chem 269:28143-28151.

Radivojac P, Iakoucheva LM, Oldfield CJ, Obradovic Z, Uversky VN, Dunker AK. 2007. Intrinsic disorder and functional proteomics. Biophysical journal 92(5):1439-1456.

Romero P, Obradovic Z, Li X, Garner EC, Brown CJ, Dunker AK. 2001. Sequence complexity of disordered protein. Proteins 42(1):38-48.

Serber Z, Ferrell JE, Jr. 2007. Tuning bulk electrostatics to regulate protein function. Cell 128(3):441-444.

Skalicky JJ, Donaldson LW, Petersen JM, Graves BJ, McIntosh LP. 1996. Structural coupling of the inhibitory regions flanking the ETS domain of murine Ets-1. Prot Science 5:296-309.

Uversky VN. 2002. What does it mean to be natively unfolded? European journal of biochemistry / FEBS 269(1):2-12.

Uversky VN, Dunker AK. 2010. Understanding protein non-folding. Biochimica et biophysica acta 1804(6):1231-1264.

Volkman BF, Lipson D, Wemmer DE, Kern D. 2001. Two-state allosteric behavior in a single-domain signaling protein. Science (New York, NY 291(5512):2429-2433.

Wright PE, Dyson HJ. 1999. Intrinsically unstructured proteins: re-assessing the protein structure-function paradigm. J Mol Biol 293(2):321-331.

CHAPTER 4

SUMMARY, DISCUSSION, AND FUTURE DIRECTIONS

Cell signaling and transcriptional regulation of gene expression

Proper biological growth and development is dependent upon the cells ability to respond to the need for changes in gene expression. Cell signaling pathways, often culminating in posttranslational modification of target proteins, are a common means of relaying information about cellular needs. Transcription factors that bind DNA in a sequence-specific manner are vital for this kind of regulation. Ets-1 is a sequence-specific DNA-binding protein which responds to at least two distinct signaling pathways, resulting in transcriptional responses. Autoinhibition of Ets-1 controls its DNA-binding ability and can be alleviated by protein partnership, or enhanced by Ca^{2+} signaling-induced phosphorylation of specific serine residues located in a disordered region adjacent to the DNA-binding and autoinhibitory domains. The mechanistic role of phosphorylation in this unstructured serine-rich region (SRR) is the scope of this project.

Summary

This dissertation describes an advance in our understanding of how Ets-1 autoinhibition is regulated in a structural manner and how an intrinsically unstructured protein (IUP) region functions in biology. Prior to this work, a connection between changes in DNA binding affinity and structural alterations was reported for Ets-1 (Pufall et al., 2005). To investigate the relationship between these changes, we fully characterized a minimal C-terminal fragment of Ets-1 (ΔN279), which recapitulates the DNA-binding affinity of the full length protein before, and after Ca^{2+}-dependent phosphorylation (Chapter 2). Having done this, we were able to monitor and report the direct effects of phosphorylation on the unstructured SRR and structured regulatable unit of the same Ets-1 protein. Our next goal was to elucidate the chemical forces responsible for these phosphorylation effects in an effort to understand how the flexible,

unstructured SRR performs its function (Chapter 3). We found no evidence for a dominant electrostatic interaction affecting the affinity of ΔN279. However, the 100-fold decrease in DNA-binding affinity observed upon phosphorylation of ΔN279 was almost completely lost following mutation of four SRR aromatic residues to alanine (4ΦA) or glycine (4ΦG). This loss of phosphorylation effect was also observed upon mutation of the same aromatic residues in the longer ΔN244 fragment, the full length Ets-1 protein, and a hyper-phosphorylated ΔN279 mutant. A comparable reduction in phosphorylation-induced structural alterations was also observed, once again connecting inhibitory structural changes with the DNA-binding affinity of Ets-1.

Discussion

A model for autoinhibition in Ets-1

The ability of Ets-1 to bind DNA with high affinity is controlled by autoinhibition (Jonsen et al., 1996). Biochemical and structural studies of Ets-1 have led to the development of the following model. In the absence of DNA, the regulatable unit (ETS domain and inhibitory module) exists in a conformational equilibrium between an active state, which is competent to bind DNA, and an inactive state, which is refractory to binding (Lee et al., 2008). The active state is characterized by an unfolded inhibitory helix HI-1 and a high degree of internal molecular motion. The inactive state, in contrast, displays a folded helix HI-1 and a reduced level of internal dynamic character. A single Ets-1 protein, therefore, exists in equilibrium between these two states, without adopting a steady, average conformation. Cellular events resulting in a change in DNA-binding affinity stabilize one conformation over the other, shifting the equilibrium towards the active or inactive state. Binding partners, such as RUNX1, have been shown to increase Ets-1 binding affinity in vitro, and are thought to stabilize the dynamic,

active conformation (Goetz et al., 2000). The unstructured SRR has been shown to promote the inactive state by partially stabilizing the inhibitory module and dampening the internal molecular motion of Ets-1 (Pufall et al., 2005). This, of course, causes a measurable reduction in DNA binding affinity. Ca^{2+}-dependent phosphorylation of the SRR further stabilizes the inhibitory module, reduces the internal dynamic motions, and dramatically decreases Ets-1 DNA-binding affinity. Insights into how an unstructured protein region can have such a profound effect come from studying the region itself (Lee et al., 2008). Though phosphorylation does not induce any predominant secondary structure, the fast timescale mobility of the SRR is partially reduced following phosphate addition. Accompanying this decrease in dynamic motion is an enhanced localization of the SRR to the regulatable unit. Phosphorylation-induced structural and binding effects can be disrupted by mutating four aromatic residues adjacent to the phospho-acceptor sites (Chapter 3). Therefore, we conclude that phosphorylation function with the aromatic residues to regulate autoinhibition and control Ets-1 binding affinity.

The phosphate-aromatic connection

IUP regions are commonly identified by observing a low content of bulky amino acid residues, including tyrosine, phenylalanine, and tryptophan (Obradovic et al., 2003; Romero et al., 2001). When aromatic residues are reported in unstructured regions, they are often shown to be near sites of posttranslational modification. These aromatic residues are frequently required for binding to the enzyme active site, as with the unstructured C-terminal tail of Ddc1, a subunit of the 9-1-1 checkpoint clamp (Navadgi-Patil and Burgers, 2009). Phospho-acceptor site-associated aromatic residues in Ddc1 are essential for Mec1/ATR activation because they are required for phosphorylation of the adjacent sites. Another commonly reported feature of aromatic residues in modified IUP regions is their requirement for binding-induced structure

formation, as with the intrinsically disordered KID domain of the transcription factor CREB (Sugase et al., 2007). In this case, the KID domain becomes phosphorylated and undergoes a disordered-to-ordered transition, forming two α-helices that interact with the KIX domain of the co-activator p300. The formation of the helices and subsequent intermolecular interaction are dependent upon three bulky, hydrophobic residues that lie on one face of helix α_B. The SRR of Ets-1, however, has not been shown to adopt any predominant secondary structure upon phosphorylation or inter/intramolecular interaction and is still efficiently bound and modified by Ca^{2+}-dependent kinase upon mutation of adjacent aromatic residues to alanine or glycine (Chapter 2; Chapter 3). The persistent disorder observed in the SRR of Ets-1 may be an essential part of its novel functional mechanism. In discussing Ets-1 autoinhibition, one research group noted that a disordered conformation may permit more fine-tuned regulation, as it permits rapid access to both kinase and phosphatase, allowing integration of multiple signaling pathways and the modulation of transcription at the level of DNA binding (Mittag et al., 2010). Additionally, because transient hydrophobic clustering is not highly specific, the enhanced interaction may be more sensitive to variable phosphorylation in both number and location of the modification. In this way, dynamic character is an evolutionary conserved mechanism for creating the observed "rheostat" behavior. This transient hydrophobic clustering may occur between residues within the SRR itself, causing the observed decrease in sub-nanosecond timescale motion (Figure 3.8). The partial restriction of mobility would result in an apparent enhancement of the intramolecular interaction, as both time of interaction and proximity may increase. Alternatively, phosphorylation may force aromatic residues in the SRR to cluster transiently with surface-exposed hydrophobic residues of the regulatable unit. Indeed, a large pocket of hydrophobic residues has been observed at the surface of transient interaction (Lee et al., 2008). This

interaction could also result in a dampening of SRR mobility and, of course, an enhanced localization to the regulatable unit.

The dynamic core of Ets-1

According to the allosteric model for Ets-1 autoinhibition, the inhibitory module is intramolecularly connected to the DNA-binding domain through a dynamic, hydrophobic core of amino acid residues (Figure 1.6). The magnitude of NMR chemical shift perturbations for these residues is proportional to the level of inhibition. Dampening of the internal molecular motion of this dynamic core is associated with a decrease in DNA-binding affinity and other inactive conformation indicators, while fragments displaying a higher degree of dynamic motion bind DNA with higher affinity (Cowley and Graves, 2000; Jonsen et al., 1996; Pufall et al., 2005). This pattern is reminiscent of the dynamic regulation of internal molecular motion for the bacterial *lac* repressor (Kalodimos et al., 2004). Only a highly dynamic form of the *lac* repressor protein is capable of scanning DNA sequences in search of a sequence-specific binding site. One might envision an evolutionarily conserved mechanism in which phosphorylation-induced dampening of Ets-1 dynamics leads to changes of sequence specificity, and/or the level of Ets-1 core dynamics changes in response to sequence-specific DNA binding. In this way, the dynamic character of Ets-1 allows the conformational sampling required for Ets-1 to actively bind DNA, while a less dynamic form of the protein displays reduced DNA-binding affinity. Phosphorylation of the unstructured SRR may enhance transient interactions between adjacent aromatic residues and partially exposed, dynamic core residues. Though a fixed interface may never be observed, multiple short-lived hydrophobic interactions could act to dampen the internal molecular motion of the core, decreasing the dynamic conformational sampling required for high affinity DNA binding.

Future directions

Aromatic residue-dependent SRR localization

Chapter 2 of this dissertation reports a transient interaction between the unstructured SRR and structured regulatable unit, observed by measuring NMR paramagnetic relaxation enhancement (PRE). This interaction is enhanced following phosphorylation of the SRR. In Chapter 3, the phosphorylation-induced decrease in Ets-1 DNA-binding affinity was shown to be aromatic residue-dependent. Our model predicts that the phosphorylation-induced enhancement of the transient interaction is also dependent upon the presence of aromatic residues adjacent to the phospho-acceptor sites. Recent improvements in the use of site-directed spin labels (SDSL) for measuring PRE have increased the utility and accuracy of this type of NMR spectroscopy. SDSL experiments comparing phosphorylation effects in ΔN279 with ΔN279 4ΦA are in progress.

Analysis of the SRR in isolation

Ca^{2+}-dependent phosphorylation has been shown to decrease the sub-nanosecond timescale mobility of the SRR (Lee et al., 2008). Phosphorylation effects have been shown to be aromatic residue-dependent (Chapter 3). Transient hydrophobic clustering has been implicated as the mechanism of phosphorylation-induced inhibition of Ets-1. This transient interaction may take place between the SRR and the regulatable unit or between residues located within the SRR. By studying the SRR in isolation (without the presence of the regulatable unit) we can determine whether the phosphorylation-induced decrease in fast timescale motion requires complimentary residues on the surface of the regulatable unit. If phosphorylation effects are observed in the isolated SRR, an isolated aromatic mutant SRR should be refractory to these effects. If the mobility of the isolated SRR is not affected by phosphorylation, and interaction with the

regulatable unit is required to detect these effects, the presence of phospho-specific NMR chemical shift perturbations would be observed only upon titration of the isolated, phosphorylated SRR onto the regulatable unit. We have already been successful in expressing and purifying the isolated SRR with and without phosphorylation. Though DNA-binding studies aimed at inhibiting the regulatable unit by adding the phosphorylated SRR in-trans were inconclusive (data not shown), NMR experiments exploring the effects of phosphorylation on an isolated SRR, as well as adding the phosphorylated SRR to the regulatable unit in-trans, are currently underway. As the transient nature of this intramolecular interaction may require the high local concentration brought about by a cis-acting SRR, the affinity of the phosphorylated SRR for the regulatable unit may be enhanced by the use of the hyper-phosphorylated SRR described in Chapter 3.

Binding-induced changes to Ets-1 dynamics

An evolutionarily-conserved mechanism, like that observed for the bacterial *lac* repressor, in which protein dynamics regulates binding affinity, has been suggested for Ets-1 (Kalodimos et al., 2004; Pufall et al., 2005). Accordingly, changes in the dynamic internal molecular motion of Ets-1 are predicted upon DNA binding. Determination of the dynamic character of Ets-1 ΔN279 bound to an optimized, high-affinity DNA sequence, and a low-affinity sequence will test whether this mechanistic model plays a role in binding tolerance to a range of biological sites. In addition, cooperative protein partnership, which has been shown to increase Ets-1 DNA-binding affinity in vitro, may also function by affecting protein dynamics. Monitoring the dynamic character of Ets-1 ΔN279 in the presence of cooperative binding partners, such as RUNX1, will contribute to a thorough understanding of how Ets-1 dynamics and DNA-binding affinity are connected.

References

Cowley DO, Graves BJ. 2000. Phosphorylation represses Ets-1 DNA binding by reinforcing autoinhibition. Genes Dev 14(3):366-376.

Garvie CW, Pufall MA, Graves BJ, Wolberger C. 2002. Structural analysis of the autoinhibition of Ets-1 and its role in protein partnerships. J Biol Chem 277(47):45529-45536.

Goetz TL, Gu TL, Speck NA, Graves BJ. 2000. Auto-inhibition of Ets-1 is counteracted by DNA binding cooperativity with core-binding factor alpha2. Mol Cell Biol 20(1):81-90.

Jonsen MD, Petersen JM, Xu Q, Graves BJ. 1996. Characterization of the cooperative function of inhibitory sequences of Ets-1. Mol Cell Biol 16(5):2065-2073.

Kalodimos CG, Biris N, Bonvin AM, Levandoski MM, Guennuegues M, Boelens R, Kaptein R. 2004. Structure and flexibility adaptation in nonspecific and specific protein-DNA complexes. Science (New York, NY 305(5682):386-389.

Lee GM, Pufall MA, Meeker CA, Kang HS, Graves BJ, McIntosh LP. 2008. The affinity of Ets-1 for DNA is modulated by phosphorylation through transient interactions of an unstructured region. J Mol Biol 382(4):1014-1030.

Mittag T, Kay LE, Forman-Kay JD. 2010. Protein dynamics and conformational disorder in molecular recognition. J Mol Recognit 23(2):105-116.

Navadgi-Patil VM, Burgers PM. 2009. The unstructured C-terminal tail of the 9-1-1 clamp subunit Ddc1 activates Mec1/ATR via two distinct mechanisms. Molecular cell 36(5):743-753.

Obradovic Z, Peng K, Vucetic S, Radivojac P, Brown CJ, Dunker AK. 2003. Predicting intrinsic disorder from amino acid sequence. Proteins 53 Suppl 6:566-572.

Petersen JM, Skalicky JJ, Donaldson LW, McIntosh LP, Alber T, Graves BJ. 1995. Modulation of transcription factor Ets-1 DNA binding: DNA-induced unfolding of an alpha helix. Science (New York, NY 269(5232):1866-1869.

Pufall MA, Lee GM, Nelson ML, Kang HS, Velyvis A, Kay LE, McIntosh LP, Graves BJ. 2005. Variable control of Ets-1 DNA binding by multiple phosphates in an unstructured region. Science (New York, NY 309(5731):142-145.

Romero P, Obradovic Z, Li X, Garner EC, Brown CJ, Dunker AK. 2001. Sequence complexity of disordered protein. Proteins 42(1):38-48.

Sugase K, Dyson HJ, Wright PE. 2007. Mechanism of coupled folding and binding of an intrinsically disordered protein. Nature 447(7147):1021-1025.